

# **VMC**

**Venus Monitoring Camera for Venus Express**

## **FS Calibration and Performance Report**

VMC-MPAE-RP-SS011-001

04.08.2008

---

## Document Change Record

Iss./Rev.	Date	Chapter	Description
1/1	30.03.2006		
1/2	04.08.2008		Brief description of the flat fielding and calibration procedure



## Table of contents

1	Introduction .....	6
2	VMC for the Venus Express Mission.....	7
2.1	Science goals .....	7
2.1.1	Dayside observations.....	7
2.1.2	Nightside observations .....	8
2.2	Instrument Summary .....	10
2.2.1	<b>Overview and accommodation</b> .....	10
2.2.2	<b>Optical Design</b> .....	13
2.3	Science Observations in Orbit.....	17
2.3.1	Pericenter mode .....	17
2.3.2	Monitoring mode .....	17
2.3.3	Limb sounding mode .....	17
3	Calibration and Performance .....	19
4	Setups for Laboratory Calibration .....	24
4.1	CCD characterization setup.....	24
4.2	Focus Set-up .....	27
4.3	Geometrical, Spectral and Radiometric Set-up for Camera Calibration .....	28
4.4	VMC Assembly under Calibration.....	32
4.5	VMC Image Header.....	33
5	Laboratory Activity .....	36
6	Data Archiving .....	38
7	Results of the Calibration and Performance Study.....	39
7.1	CCD Performance.....	39
7.1.1	CCD Quantum Efficiency.....	39
7.1.2	Performance Test.....	39
7.1.3	Functional Tests.....	45
7.2	Geometric Properties .....	48
7.2.1	Focus Measurements .....	48
7.2.2	Field of View (FOV).....	52
7.2.3	Channels co-alignment .....	59
7.2.4	Stray Light Characterization.....	59
7.3	Dark Signal Properties.....	60
7.3.1	Dark Signal Behavior with Temperature and Exposure.....	60

7.3.2	Dark Signal Noise.....	61
7.4	Radiometric Properties .....	62
7.5	Spectral Properties.....	69
7.6	Thermal Behavior .....	72
7.6.1	Simulation of science operations in orbit .....	72
7.6.2	Expected in-flight performance .....	80
7.6.3	Conclusions and recommendation for in-flight operations .....	82
8	Annex 1. Calibration activity Log-book.....	82
9	VMC performance during the near-Earth commissioning .....	83
9.1	In-flight focus check and channels misalignment .....	83
9.2	In-flight stray light characterization .....	84
10	Image calibration procedure .....	84

## 1 Introduction

The purpose of this document is to provide a final report on the analysis of data collected during the on-ground lab calibration of the Venus Monitoring Camera (VMC) FS. The calibration data used to obtain results presented here was collected in April and May 2005 at the calibration facility of the Max-Planck-Institute for the Solar System Research. While properties of the VMC instrument are described whenever necessary for an understanding of the instrument calibration, a full description of the instrument is beyond the scope of the present document. See VMC PID-B for details about the instrument and its operation.

Section 2 gives the description of the scientific objectives of VMC. Summary of the calibration study together with comparison with the required performance to achieve the scientific goals are given in section 3. Section 4 describes the laboratory setup used for obtaining the calibration data. Section 5 gives the history of the laboratory activity. The actual calibration results are provided in section 6, which treat the CCD- performance, the focus, flat fielding and absolute intensity calibration, the relative spectral responsivity and geometric distortion.

## 2 VMC for the Venus Express Mission

### 2.1 Science goals

Venus Monitoring Camera will observe both day and night side of Venus.

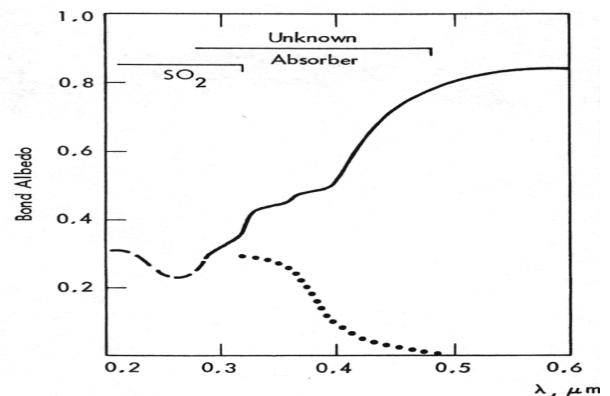
#### 2.1.1 Dayside observations

On the dayside VMC will take images of Venus in UV, visible and near-IR spectral channels that will correspond to the cloud tops (60-70 km). On the dayside the VMC will be detecting the solar light scattered back to space by the Venus clouds.

##### 2.1.1.1 UV-blue spectral range.

The spectrum of solar radiation reflected by Venus has broad absorption feature between 0.2 and 0.5  $\mu\text{m}$  (Fig. 2.1-1) (Moroz, 1985). The region between 0.2 and 0.32  $\mu\text{m}$  is well explained by the presence of  $\text{SO}_2$  at the cloud tops. The spectrum at longer wavelengths implies the presence of another absorber that has not been identified so far. The problem of the second UV-blue absorber at the cloud tops is one of the most important puzzles in the chemistry of the Venus atmosphere and cloud layer. Identification of the absorber is also important because due to this species Venus absorbs about 50% of solar radiation at the cloud top level. This has important implications for the energy balance and dynamics of the whole atmosphere.

**Figure 2.1** UV-visible spectrum of Venus' spherical albedo (solid) and contrasts (dots).



Inhomogeneity in spatial and/or vertical distribution of the unknown absorber produces the famous UV features on the Venusian disc (Fig. 2.1-2). Tracking their motions has been usually used to study the dynamics of the cloud tops, i.e. to measure the wind velocity and observe the wave phenomena. The typical size of the UV features does not exceed 100 km. Their motions mark the super-rotation of the Venus cloud tops at ~67 km altitude with zonal velocity of about 100 m/s and ten times slower meridional speed.

**Figure 2.2** Mariner-10 image of Venus in the UV.

The VMC imaging of Venus at 0.365  $\mu\text{m}$  has the following scientific objectives:

- Study of the atmospheric dynamics at cloud tops by tracing the motions of UV features;
- Study of spatial and vertical distribution of the UV-blue absorbers at the cloud tops;
- Study of correlation between  $\text{SO}_2$  and unknown absorber that would help to identify the latter;
- Study of the vertical distribution of haze above the main cloud layer.



### 2.1.1.2 Near IR spectral range

In two near-IR channels on the dayside VMC will investigate:

- Study of the H<sub>2</sub>O spatial distribution at the cloud tops;
- Study of the spatial distribution of clouds opacity.

### 2.1.2 Nightside observations

Night side observations by VMC will be mainly focused on recently discovered weak emissions (Allen and Crawford, 1984). Thermal radiation that originates in the deep atmosphere and at the surface can leak to space in the transparency windows between strong absorption bands of CO<sub>2</sub> and H<sub>2</sub>O thus providing a powerful tool to study the lower atmosphere of Venus from orbit.

#### 2.1.2.1 Near IR emissions

**Figure 2.3** Synthetic spectrum of the Venus night side (colored lines). Black subplot in the upper left-VIMS/Cassini measurements of the emission spectrum (Baines et al, 2000).

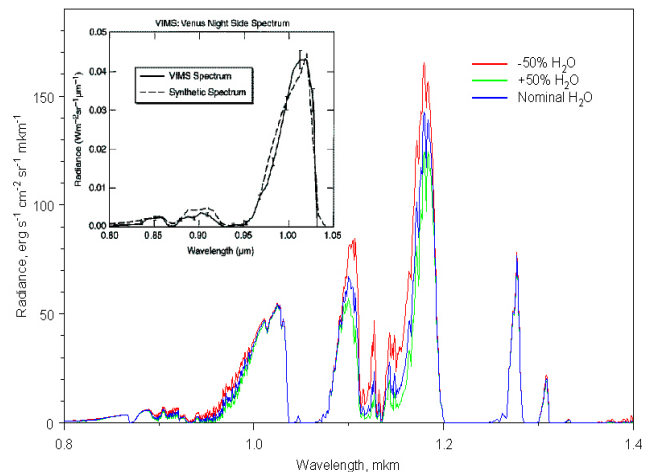
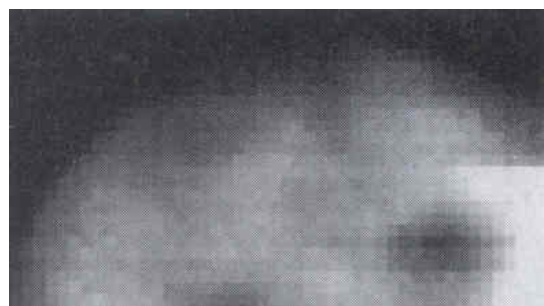


Figure 2.1-3 shows a synthetic spectrum of Venus night side. Ground-based imaging in 1 μm “window”(Fig. 2.1-4) shows weak (1-2%) contrasts that originate from surface temperature variations due to topography and inhomogeneity in cloud opacity. Track-

ing the motions of these features would characterize the wind speeds at ~50 km altitude. Moreover the 1 μm images could be effectively used to derive the lapse rate in the lower 6 km. Figure 2.1-3 also shows that the shortwavelength side of the 1μm emission peak is sensitive to the water vapour abundance in the lower atmosphere. In summary, the VMC night side observations will have the following scientific goals:

- Mapping the surface temperature distribution;
- Search for “hot spots” associated with volcanic activity;
- Search for emissivity anomalies and their correlation with radar images;
- Determination of the lapse rate in the lower 6-8 km of the atmosphere;
- Determination of the H<sub>2</sub>O global distribution in the lower 10 km;
- Study of the circulation of the main cloud deck;
- Monitoring the atmospheric column opacity and its variations.

**Figure 2.4** Ground-based observations of the Venus nightside in the 1 μm transparency “window” (Meadows and Crisp, 1996).



**2.1.2.2 O<sub>2</sub> airglow in the visible**

The spectrometer experiment onboard Venera-9 and -10 discovered night airglow in the visible (Fig. 2.1-5) that originates at 90-110 km altitude and results from recombination of O atoms produced on the day side and brought to the night side by thermospheric solar-antisolar flow.

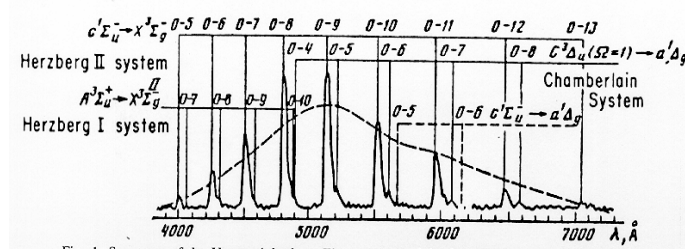


**Figure 2.5** Spectrum of the O<sub>2</sub> nightside airglow (Krasnopolsky, 1983).

The VMC observations in visible filter will aim at:

- Study of the airglow spatial distribution and its temporal variations to understand the circulation of the lower thermosphere.
- Search for lightning.

## 2.2 Instrument Summary

### 2.2.1 Overview and accommodation

The VMC camera consists of one unit that houses the optics, CCD and readout electronics (CRE), digital processing unit (DPU), and power converter (POC). Figure 2.2-1 shows the sketch of the VMC camera. Peltier element connected to the bottom of the CCD will cool the detector. In order to avoid moving parts (filter wheel) the camera is designed so that four objectives (channels) share a single CCD. The stray light protection is provided by external and internal baffles. The VMC will be mounted on the +Y wall inside the spacecraft (Fig 2.2-2).

A summary of the performance characteristics of the VMC components is given in the Table 2.2-1.

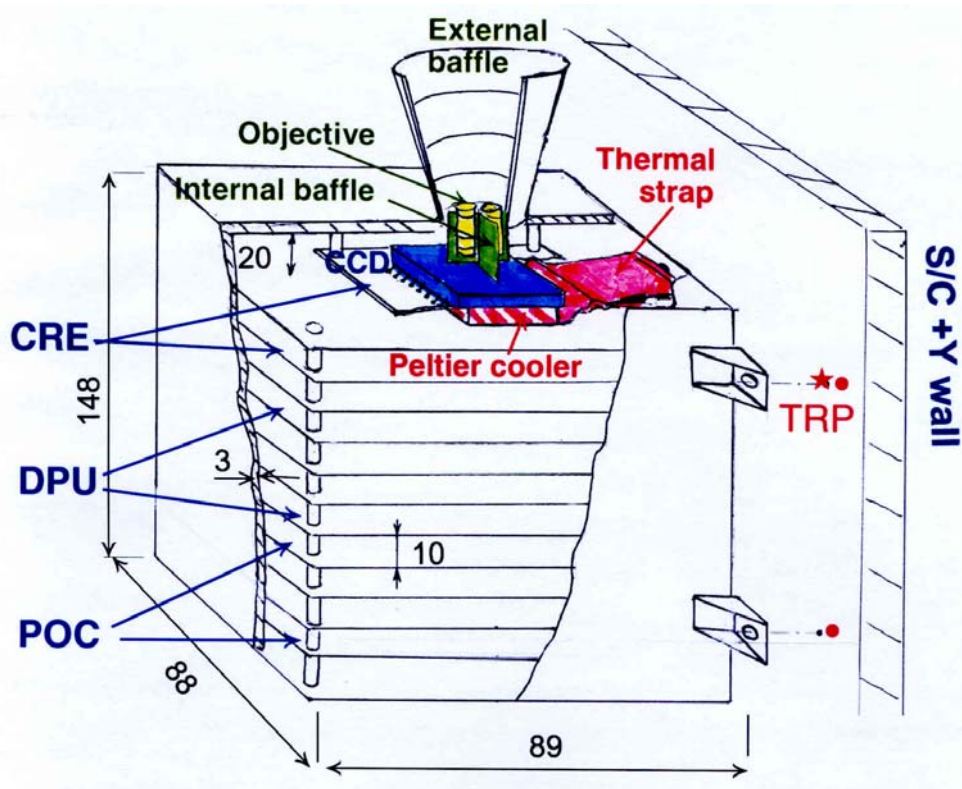
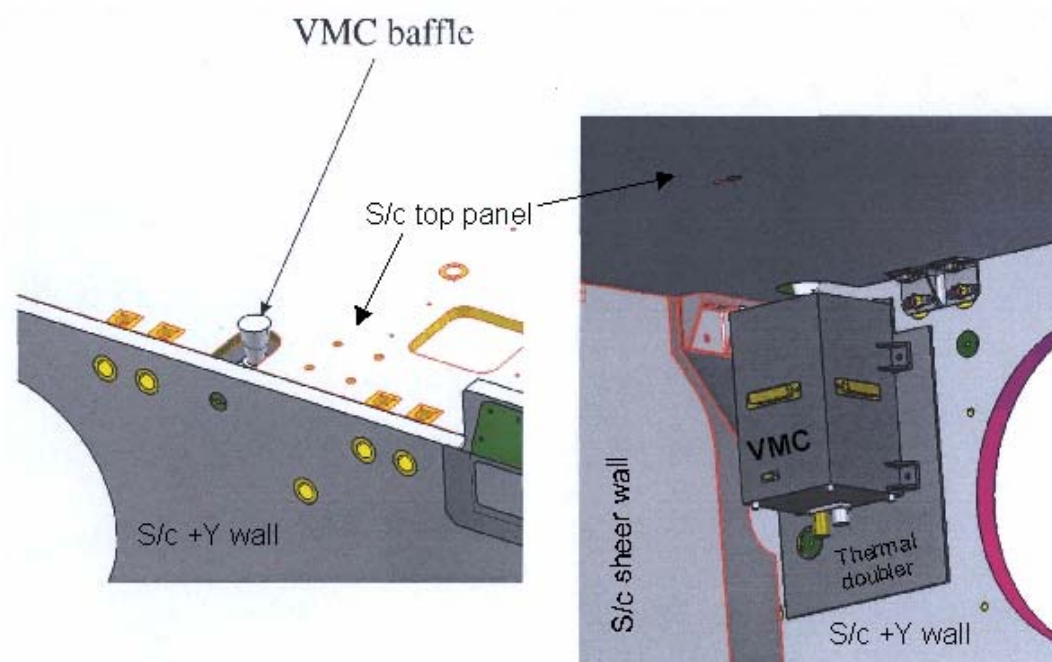


Figure 2.6 VMC sketch

**Table 2.2-1 Main performance parameters of the VMC instrument**

Item	Specification
<b>Optics</b>	
General concept	Four objectives sharing a single CCD
Total field of view	~ 17.5° (0.3 rad)
Image scale	~ 0.74 mrad/px
<b>Detector and CCD readout electronics (CRE)</b>	
Type	Kodak KAI-1010, front illuminated, interline architecture
Detector size	1032(H)x1024(V)
Pixel size	9.0x9.0 μm
Quantum efficiency	See 7.1.1 (TBD)
Full well	30,000 e
Total noise	~ 100 e @ +37 C
Sensitivity	~ 5 e <sup>-</sup> / DN
Antiblooming	Yes
Dark current	~ 3000*2**(-(40-t,C)/8), e/s/px
Readout frequency	2.08896 MHz
Integration time	N*0.504 ms, N=1,2,3...64449
Ops/non-ops temperature range	-30/-50... +50/+70C



**Figure 2.7** *VMC accommodation on the spacecraft*

## 2.2.2 Optical Design

General concept of the VMC is shown in the Figure 2.2-1. Four independent optical channels ( see Table 2.2-2) share one CCD. The optical design is presented in the Table 2.2-2. The figures 2.2-3 to 2.2-5 show pictures of VMC optics and of VMC on camera level.

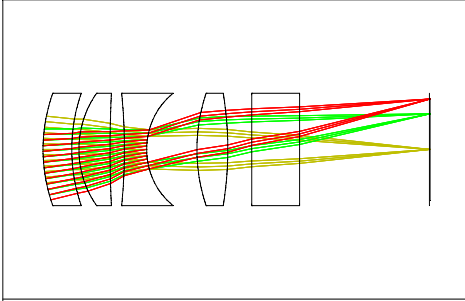
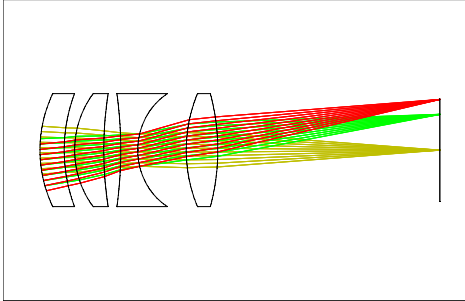
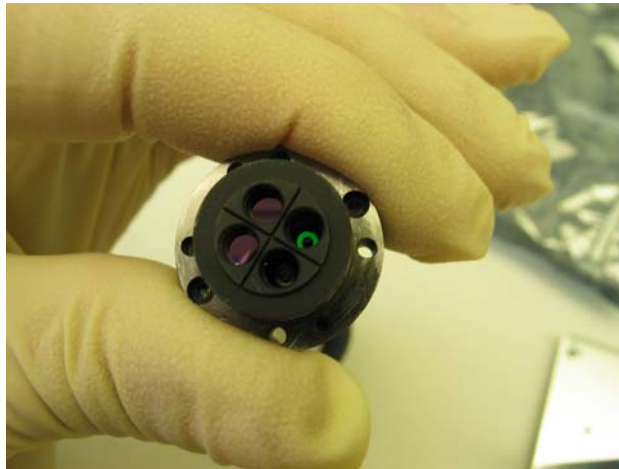
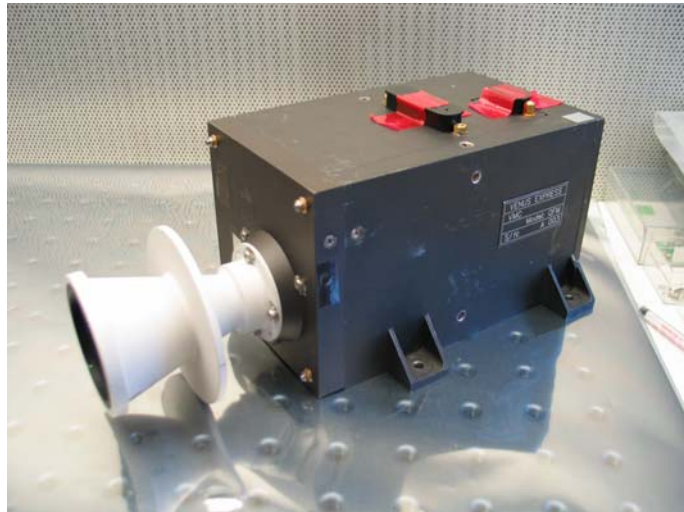
VMC Channel	VIS	NIR1	NIR2	UV
Spectral range	503 – 523 nm	900 – 970 nm	990 – 1030 nm	345 – 385 nm
Center wave-length	513 nm	935 nm	1.01 $\mu$ m	365 nm
Focal length	13 mm	13 mm	13 mm	13 mm
F-Number	5	5	5	7
Optics	3 Identical Cooke Triplets + curved front filter			Separate Cooke Triplet + curved front filter
Stop	Central obscuration			No obscuration
CCD	Kodak KAI-1010 Series, 1024 x 1024 pixel interline CCD, 9 $\mu$ m pixel pitch			
Used area for imaging	1. Quadrant of CCD	2. Quadrant of CCD	3. Quadrant of CCD	4. Quadrant of CCD
Optical Lay-out	 <p style="text-align: center;">LAYOUT</p> <p>COOKE TRIPLET F/5 F = 13 MM THU JUL 24 2003 SCALE: 13.0000 1.54 MILLIMETERS</p>			 <p style="text-align: center;">LAYOUT</p> <p>UV TRIPLET F/5 F=13 THU JUL 24 2003 SCALE: 13.0000 1.54 MILLIMETERS</p>

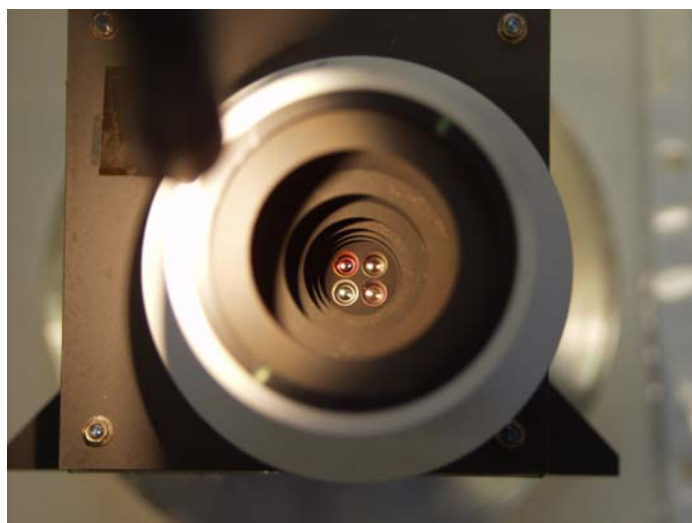
Table 2.2-2 Optical design of VMC



**Figure 2.8** Rear View of VMC Optics (green: VIS, purple: NIR channels)



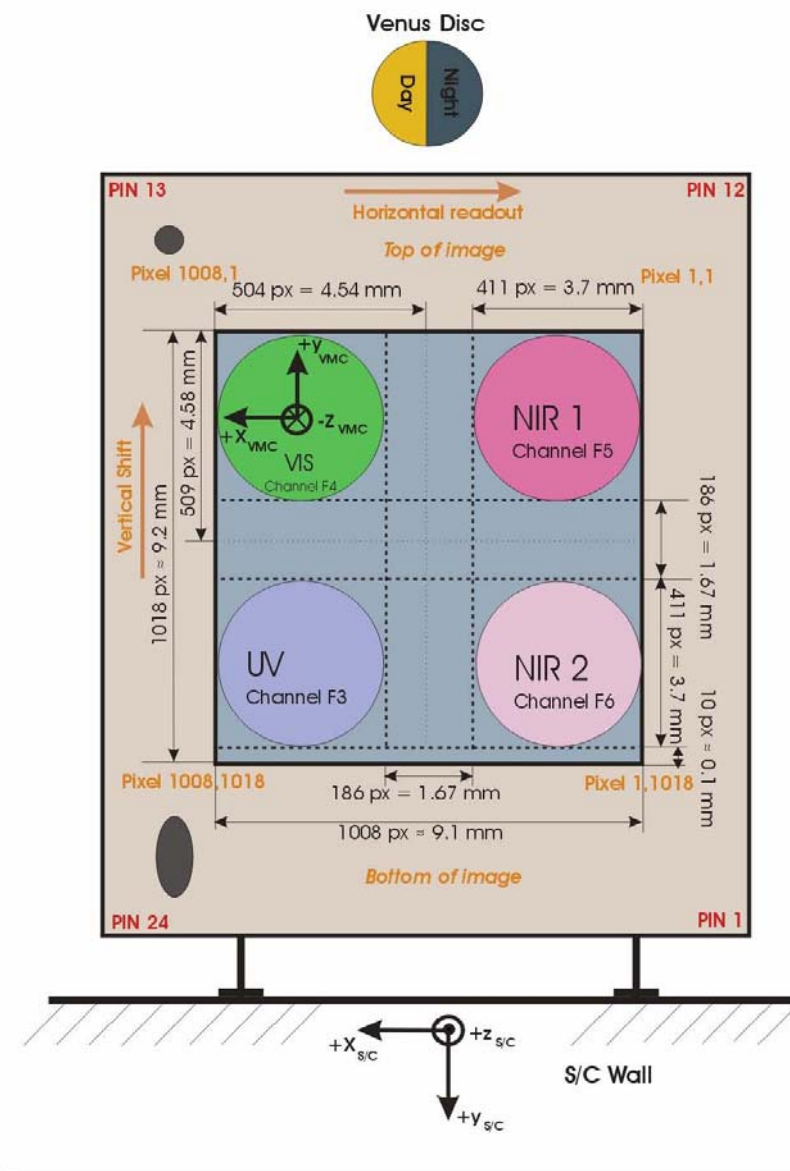
**Figure 2.9** VMC Side View (QFM)



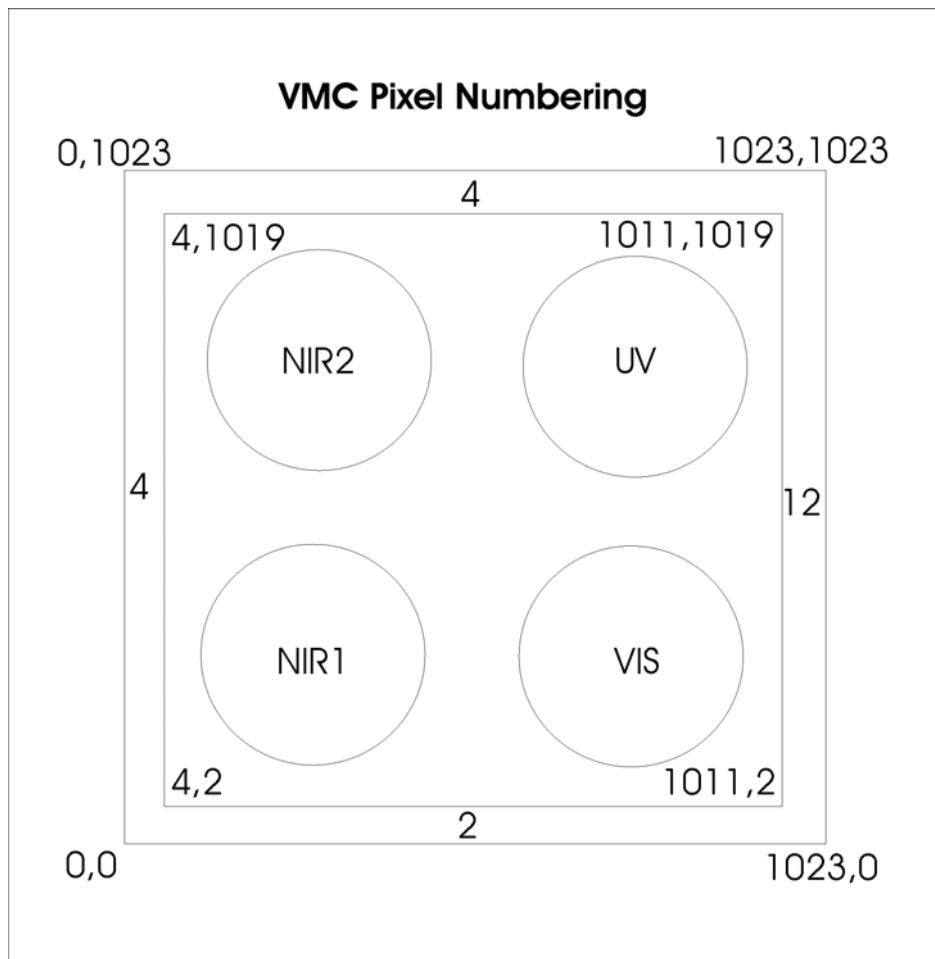
**Figure 2.10** VMC Front View (QFM)

Figure 2.2-6 shows the spot view on the CCD photosensitive area as well as the CCD orientation relative to spacecraft axes. Figure 2.2-7 shows the CCD pixel numbering in IDL presentation.

## VMC: Front View on CCD Photosensitive Area, Co-ordinate System and Pixel Numbering



**Figure 2.11** The spot view on the CCD photosensitive area and VMC and spacecraft coordinate system.

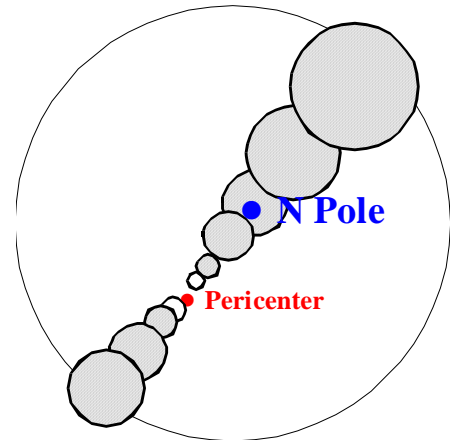


**Figure 2.12** *VMC Pixel Numbering usable in IDL®*

## 2.3 Science Observations in Orbit

In flight the VMC will have several operation modes to cover all possible observation goals and conditions. The modes are: *pericentre*, *transmission*, *monitoring*, and *limb*. Table 2.3-1 summarizes main parameters of the VMC modes.

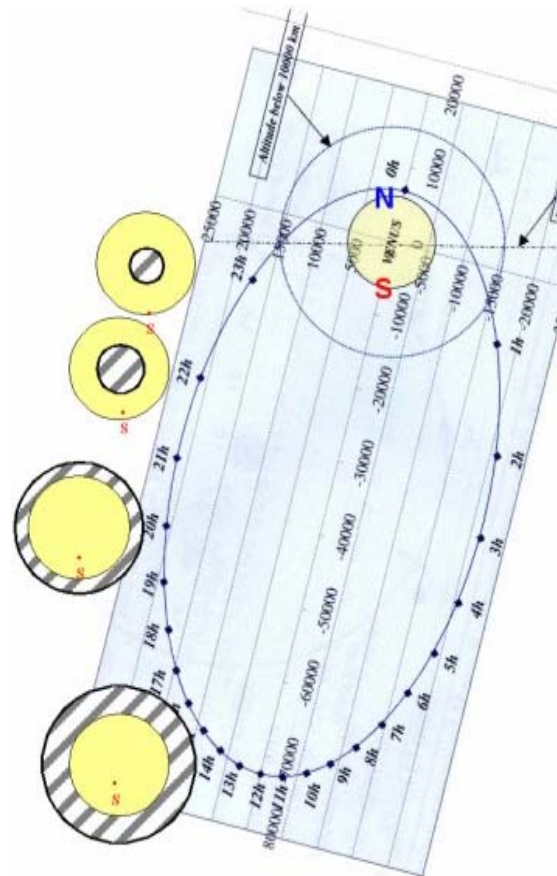
**Figure 2.13** Sketch of the projections of the VMC field of view on the Northern hemisphere of Venus in the pericentre mode.



### 2.3.1 Pericenter mode

The *pericenter* mode will be used to study small scale dynamics and the fine cloud structure with high spatial resolution. It will be used when the spacecraft is within ~10,000 km from the planet (Fig. 2.3-2). At such short distance VMC will be the only imaging instrument. Figure 2.3-1 shows a sketch of VMC fields of view covering the Northern hemisphere of Venus. The images collected during a pericentre pass will be stored in the VMC internal memory and send to the spacecraft afterwards in *transmission* mode.

**Figure 2.14** Sketch of the VMC observations in the monitoring mode. Yellow disc-Venus. Shaded area represents VMC FOV.



### 2.3.2 Monitoring mode

The *monitoring* mode will be used to study the global atmospheric dynamics from distance for relatively long time: ~8 hours in ascending arc of the orbit or ~2 hours in the vicinity of pericentre. In figure 2.3.2 hatched area shows the size of the VMC field of view relative to the Venus disc represented by a yellow circle.

### 2.3.3 Limb sounding mode

In the *Limb* mode, VMC will study vertical structure of atmospheric hazes above the clouds.

---

	<b>Pericenter</b>	<b>Monitoring</b>	<b>Limb</b>
<b>Distance</b>	250 – 10,000 km	10,000 – 66,000 km	~ 2,000 km
<b>Total FOV</b>	70 – 3,000 km	3,000 – 20,000 km	~ 500 km
<b>Spatial Resolution</b>	0.2 – 7 km	7 – 45 km	~ 1.5 km
<b>Time between Images</b>	5 – 300 s	~ 10 min	~ 10 s
<b>Data Volume</b>	~ 350 Mbits/orbit	~ 175 Mbits/orbit	~ 100 Mbits/orbit

**Table 2.3-1 VMC Modes and their parameters**

### 3 Calibration and Performance

This section contains brief description of the VMC properties and behavior that had been investigated during the on-ground instrument characterization, in particular

- Laboratory study of the CCD behavior
- Laboratory geometrical calibration
  - Focus measurements
  - FOV size
  - In-FOV distortions
  - Channels alignment
  - Stray light characterization
  - What else ?
- Laboratory radiometric calibration
  - Dark current
  - Flat field
  - Linearity
  - Absolute Calibration
- Spectral responsivity
- Thermal behaviour (i.e. summary of expected in-flight temperature behavior derived from the VMC TV tests and thermal modeling by Astrium and VMC )
- Planned in-flight characterization (i.e. brief description of in-flight activity that is planned additionally to characterize the VMC properties (pointing scenario, stray light test, focus check) )

The following table contains detailed description of the topics covered during the laboratory VMC calibration on camera level at MPS.

Purpose	Set-up	Proposed Activity	Data Product	CAL ID	VMC Mode
<b>VIS Focus</b>	Geometric set-up using small collimator  No external cooling,  No external heating,  Peltier cooling  Vacuum	<ul style="list-style-type: none"> <li>• Illumination of approximately 100 x 100 pixel of VIS channel by star target “Siemensstern” at infinity</li> <li>• Series of images vs. definitely defocused collimator</li> <li>• Evaluation of unresolved pixels in the “Siemensstar” images vs. defocus</li> <li>• Peltier is switched off/on</li> </ul>	Focus status of the VIS channel at infinity with CCD temperature 20°C  Changes of focus in VIS channel depended on CCD temperature changing to -20°C	<b>CAL1</b>	Limb  Cooling Limb
<b>All Channel Focus</b>	Geometric set-up using big collimator directly equipped with xenon lamp  No external cooling,  No external heating,  Peltier cooling  Vacuum	<ul style="list-style-type: none"> <li>• Single pixel illumination by a pinhole of pixel dimension simultaneously for all channels at infinity</li> <li>• Adjustment of the pinhole image centrally to the defined VIS center pixel (811,209) using turn table movement</li> <li>• Peltier is switched off/.</li> </ul>	Focus status of all channels with CCD temperature 20°C  Relative channel adjustment wrt. VIS channel  Changes of focus and of relative channel adjustment depended on CCD temperature changing to -20°C	<b>CAL 2</b>	Limb  Cooling Limb
<b>Purpose</b>	<b>Set-up</b>	<b>Proposed Activity</b>	<b>Data Product</b>	<b>CAL ID</b>	<b>VMC Mode</b>

<p><b>All Channel Focus with S/C thermal I/F simulation</b></p>	<p>Geometric set-up using big collimator directly equipped with xenon lamp  External cooling,  External heating,  Peltier cooling,  Vacuum</p>	<ul style="list-style-type: none"> <li>• Cooling via liquid nitrogen + heating via external heaters to simulate S/C thermal I/F temperature of <b>-10°C to +40°C</b></li> <li>• Single pixel illumination by a pinhole of pixel dimension simultaneously for all channels at infinity</li> <li>• Adjustment of pinhole image centrally to the defined VIS center pixel (<b>811,209</b>)</li> <li>• Peltier is switched on</li> <li>• Thermal I/F temperature of <b>-10°C</b> and cooling by Peltier shall be combined</li> </ul>	<p>Evaluation of focus status as in CAL2  Reachable optimum of Peltier operations under mission-like environment</p>	<p><b>CAL 3</b></p>	<p>Cooling Limb</p>
<p><b>Flat-field and Absolute calibration with S/C thermal I/F simulation</b></p>	<p>Radiometric set-up  External cooling,  External heating,  Peltier cooling,  Vacuum</p>	<ul style="list-style-type: none"> <li>• Cooling via liquid nitrogen + heating via external heaters to simulate S/C thermal I/F temperature of <b>-10°C to +40°C</b></li> <li>• Simultaneous flat-field illumination of all channels at same time vs. VMC exposure time</li> <li>• Peltier is switched on</li> </ul>	<p>Mission-like flat field per channel  Linearity vs. exposure time  Absolute values: DN/s per W/m<sup>2</sup> μm sr  Saturation level</p>	<p><b>CAL 4</b></p>	<p>Cooling Limb Monitoring</p>
<p><b>Dark signal with S/C thermal I/F simulation</b></p>	<p>External cooling,  External heating,  Peltier cooling,  Vacuum</p>	<ul style="list-style-type: none"> <li>• Dark frames at different CCD temperatures <b>-20°C, +20°C, +40°C</b> vs. VMC exposure time</li> </ul>	<p>Mission-like dark frames  Dark signal linearity vs. exposure time  Dark signal vs. CCD temperature</p>	<p><b>CAL 5</b></p>	<p>Cooling Limb</p>
<p><b>Purpose</b></p>	<p><b>Set-up</b></p>	<p><b>Proposed Activity</b></p>	<p><b>Data Product</b></p>	<p><b>CAL ID</b></p>	<p><b>VMC Mode</b></p>

<b>Spectral Responsivity</b>	Geometric set-up using monochromator with multi-mode fiber and with xenon lamp  No external cooling,  No external heating,  Peltier cooling.  Vacuum	<ul style="list-style-type: none"> <li>• Spectral scan of monochromator continuously from 340 nm to 1030 nm in steps of 1 nm inside of a channel and in steps of 10 nm outside of a channel</li> <li>• Peltier is switched on</li> </ul>	Spectral profile per channel  Spectral cross talk and stray-light  Spectral leakage and out-of band illumination	<b>CAL 6</b>	Cooling Limb
<b>PSF</b>	Geometric set-up using big collimator directly equipped with xenon lamp  No external cooling,  No external heating,  Peltier cooling.  Vacuum	<ul style="list-style-type: none"> <li>• Single pixel illumination in the center of all four channels by pinhole</li> <li>• Sub-pixel sampling in x and in y direction in steps of 1/10 pixel</li> <li>• Peltier is switched on</li> </ul>	Spatial resolution at center of all channels	<b>CAL 7</b>	Cooling Limb
<b>Purpose</b>	<b>Set-up</b>	<b>Proposed Activity</b>	<b>Data Product</b>	<b>CAL ID</b>	<b>VMC Mode</b>
<b>Ghosts</b>	Geometric set-up us-	<ul style="list-style-type: none"> <li>• Position of the bright xenon spot (w/o target)</li> </ul>	Check of the ghost suppression design	<b>CAL 8</b>	Cooling

	<p>ing bright spot of xenon lamp</p> <p>No external cooling,</p> <p>No external heating,</p> <p>Peltier cooling.</p> <p>Vacuum</p>	<p>in collimator focus) inside of FoV using turn table and collimator x-y stage</p> <ul style="list-style-type: none"> <li>• Try to provoke ghost spots in the non-illuminated part of field</li> </ul>	<p>of VIS, NIR1 and NIR2 channel</p>		<p>Limb</p>
<p><b>Integral stray-light</b></p>	<p>Radio-metric set-up</p> <p>No external cooling,</p> <p>No external heating,</p> <p>Peltier cooling.</p> <p>Vacuum</p>	<ul style="list-style-type: none"> <li>• A black obscuration will be arranged in the center of aperture of the integrating sphere additionally.</li> <li>• Illumination with bright flat-field including dark area</li> </ul>	<p>The intensity ratio between bright and dark areas (not in the transition zones) in the images gives the level of integral stray-light.</p>	<p><b>CAL 9</b></p>	<p>Cooling Limb</p>

## 4 Setups for Laboratory Calibration

### 4.1 CCD characterization setup

The CRE electronics consists of four functional units placed on 3 printed circuit boards.

- CCD head including pre-amplifier and CCD biasing (PCB1)
- CCD clock driver and analogue signal chain (PCB2)
- CCD controller and interface circuit (PCB3)

On PCB3 also located the connectors for signal and power. The selected technology for PCB3 and PCB2 is a rigid-flex technique. A pigtail connects PCB2 with the CCD head. Details are seen in figure 4.1.1.

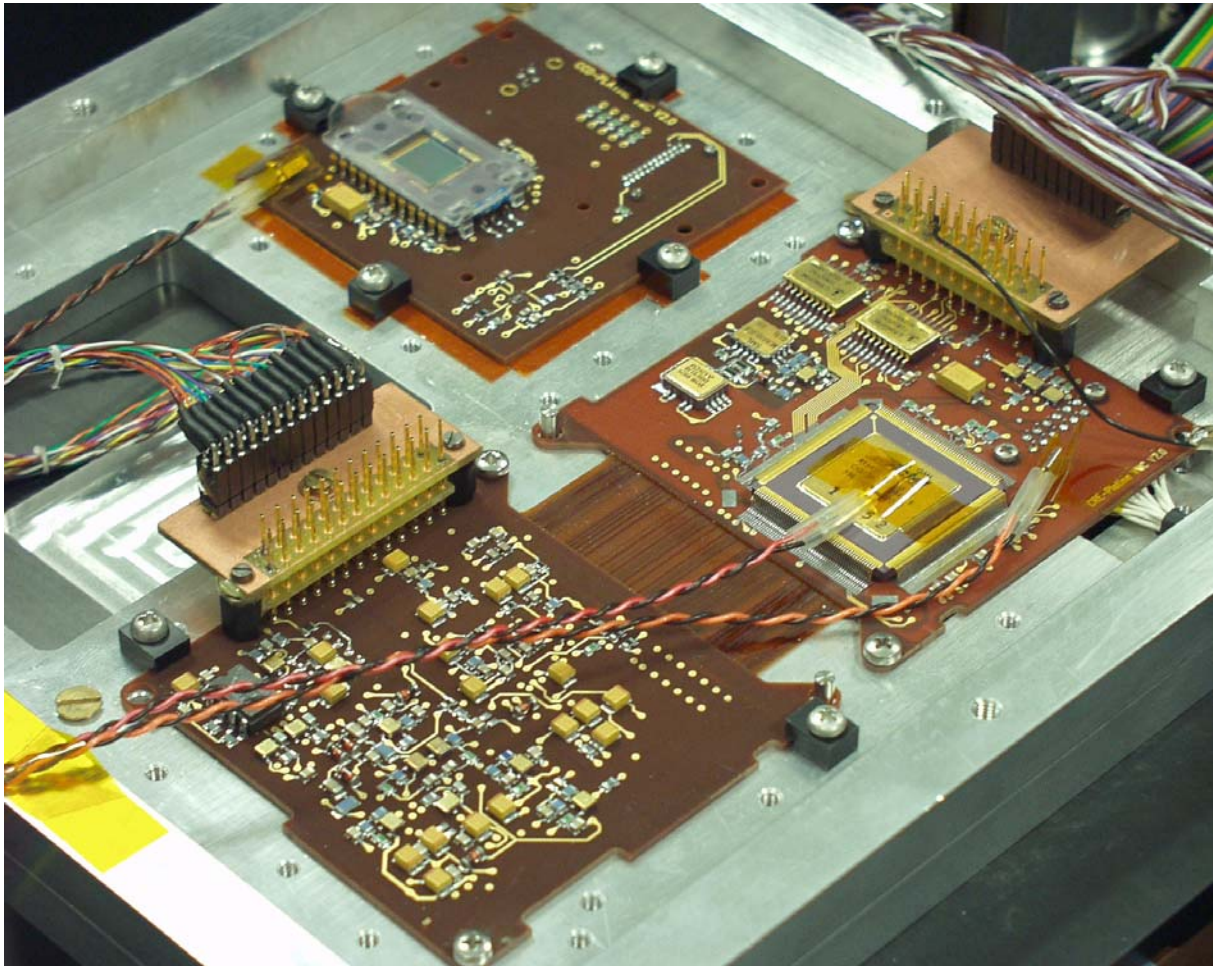


**Figure 4.1** FS CCD and CRE electronics during TV test

For assembly, integration and test (AIT) an EGSE was build up to operate CRE electronics without VMC DPU and VMC power supply. The implemented frame grabber inside the EGSE PC meets all interface condition reflected to timing, command sequences and signal level. During AIT more than 1000 images are taken.

Test procedures and data handling programs are written in IDL. For optical stimulation a diffuse shined reflector based on red LEDs (650nm) was used.

The setup was used to evaluate the electro-optical performance of the CCD including readout electronics. Further investigation was done on instrument level with the complete hardware including optic and housing.



**Figure 4.2 View of the complete CRE EGSE @ DLR**

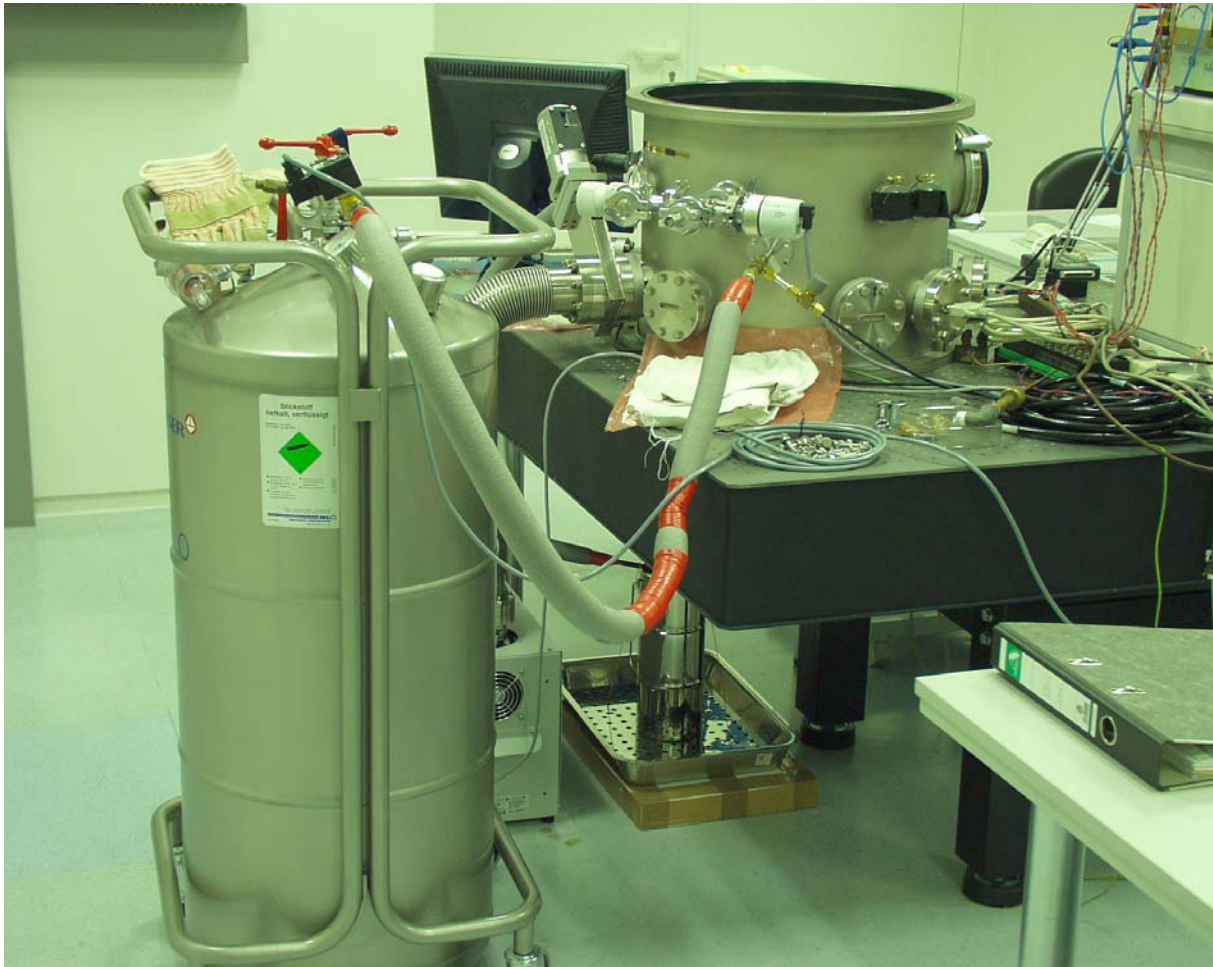


**Figure 4.3 Test setup during TV test (CRE and CCD sub-system level) @ DLR**

## 4.2 Focus Set-up

A special focus set-up (see figure 4.2-1) consisting of defocus-able collimator, pinhole and halogen lamp was implemented at MPAA clean bench of class 100. All VMC focus setting was done in clean room class 100 or better at ambient.

The VMC focus approach consists of four basic steps:

- **Step 1: Microscope Measurements of CCD Position** Meas-  
ure the orientation of the CCD assembled on its board at center and four corners wrt. optics mounting surface on camera front plate using 3D Zeiss microscope.
- **Step 2: Initial Shims Determination**  
Define the initial thickness of the shims in order to compensate CCD orientation wrt. optics focal plane orientation. Position the CCD using shims to its nominal position.
- **Step 3: Lateral Optics Spots Positioning on CCD**  
Position the spots of the optical channels symmetrically to CCD center using the lateral attachment screws of the mechanical ring.
- **Step 4: Optical Focusing in VIS channel using focus set-up (see figure 4.2-1)**  
Perform the optical focus measurement using illuminated “Siemensstar” target in focus of collimator.

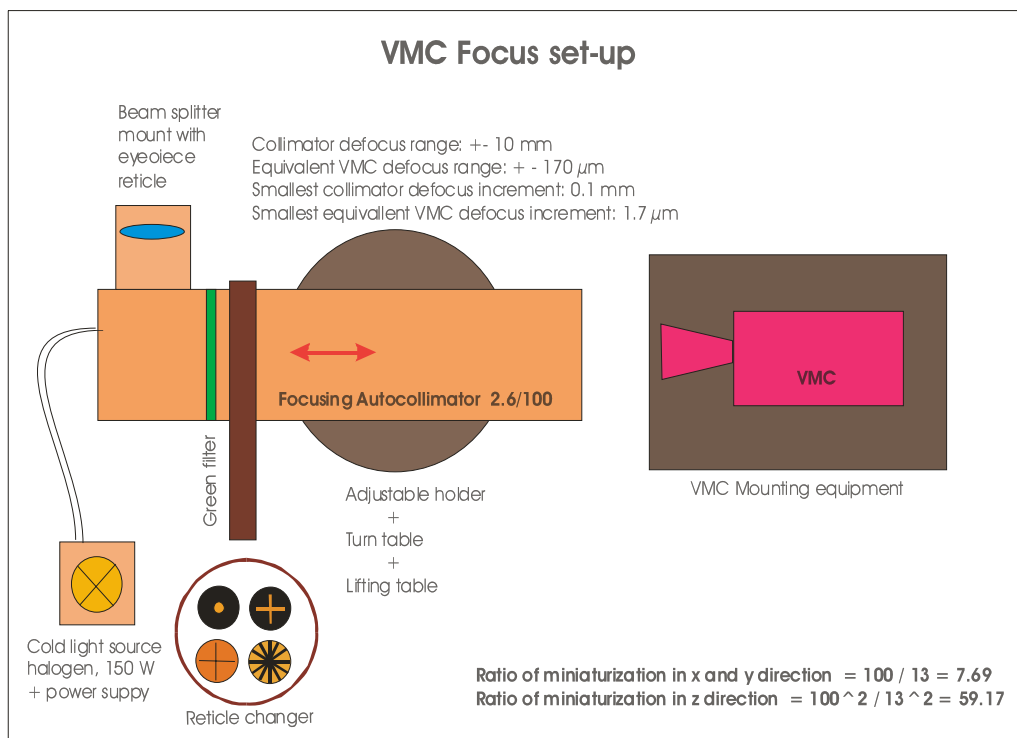


**Figure 4.4 Overview of VMC Focus Set-up**

### **4.3 Geometrical, Spectral and Radiometric Set-up for Camera Calibration**

The calibration of VMC FS was done at closest-to-flight environmental conditions in the MP Ae clean room using the Optical Ground Support Equipment (OGSE) of the OSIRIS cameras on ROSETTA.

For calibration the VMC FS was located in the TV chamber with a large front window for optical adjustment in the parallel beam of collimator (see figure 4.3-3 geometrical / spectral set-up). In a later stage the collimator will be replaced in an absolutely calibrated integrating sphere (see figure 4.3-4 radiometric set-up).

The calibration of VMC was separated in a geometric and in a radiometric part each following different measurement procedures. The calibration topics are presented in table 3-1 of this document describing the purpose, the proposed activity and the data products. Each topic is provided with a level of priority given by the CAL identifier in column 5. Due to the simultaneous imaging of the four VMC channels the calibration activity flow could be optimized sometimes.

In order to archive the calibration data products the operation of VMC EGSE and OGSE will be combined such that the separate OGSE header which contains the facility set-up status is stored together with the appropriate VMC image and image header. The calibration data products shall be stored in two parallel archives in terms of EGSE recorder files and PDS files.

The geometric calibration of VMC FM will characterize:

- Focus per channel at room temperature in vacuum
- Focus per channel as function of temperature in vacuum
- Relative channel alignment with respect to VIS channel
- Stray-light, channel cross talk and ghosts
- Point Spread Function (PSF) on axis / off-axis per channel

The radiometric calibration will determine /evaluate:

- Set of dark (and bias) frames depended on temperature and on exposure time
- Spectral range which is covered per channel, out-of-band illumination
- Flat-field per channel
- Absolute calibration per channel in units of spectral radiance ( $W/m^2 \mu m sr$  per DN)
- Linearity and Saturation

## Calibration Set-up in MPAe clean room



**Figure 4.5** Calibration Set-up (side view) used for geometrical and spectral calibration @ MPS

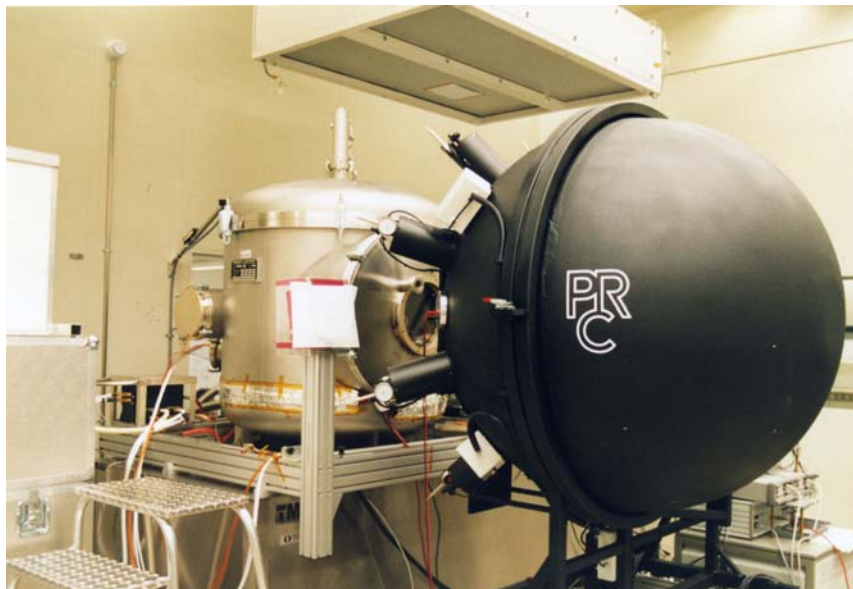


**Figure 4.6** Calibration Set-up (side view) used for radiometric calibration @ MPS

## Geometrical and Spectral Set-up for VMC

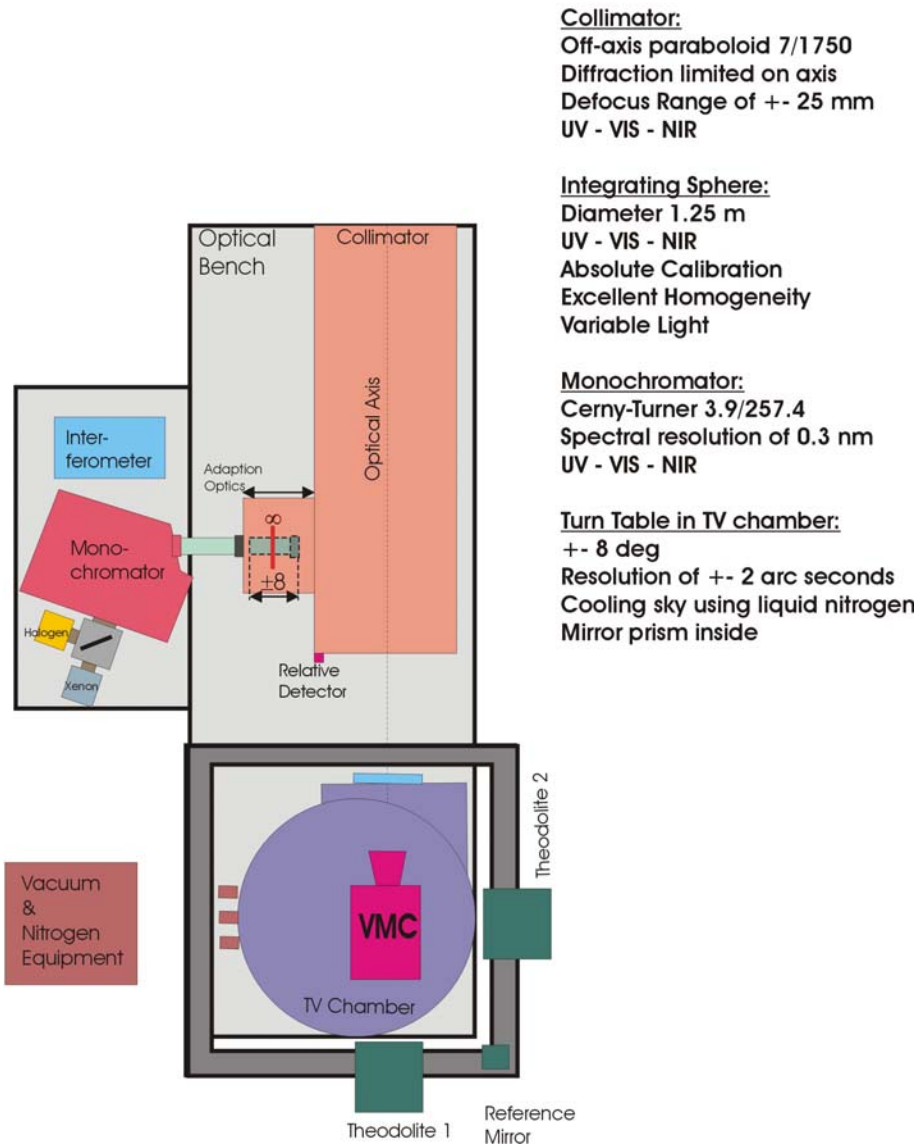


Figure 4.7 Geometric and Spectral set-up (top view)

## Radiometric Set-up for VMC

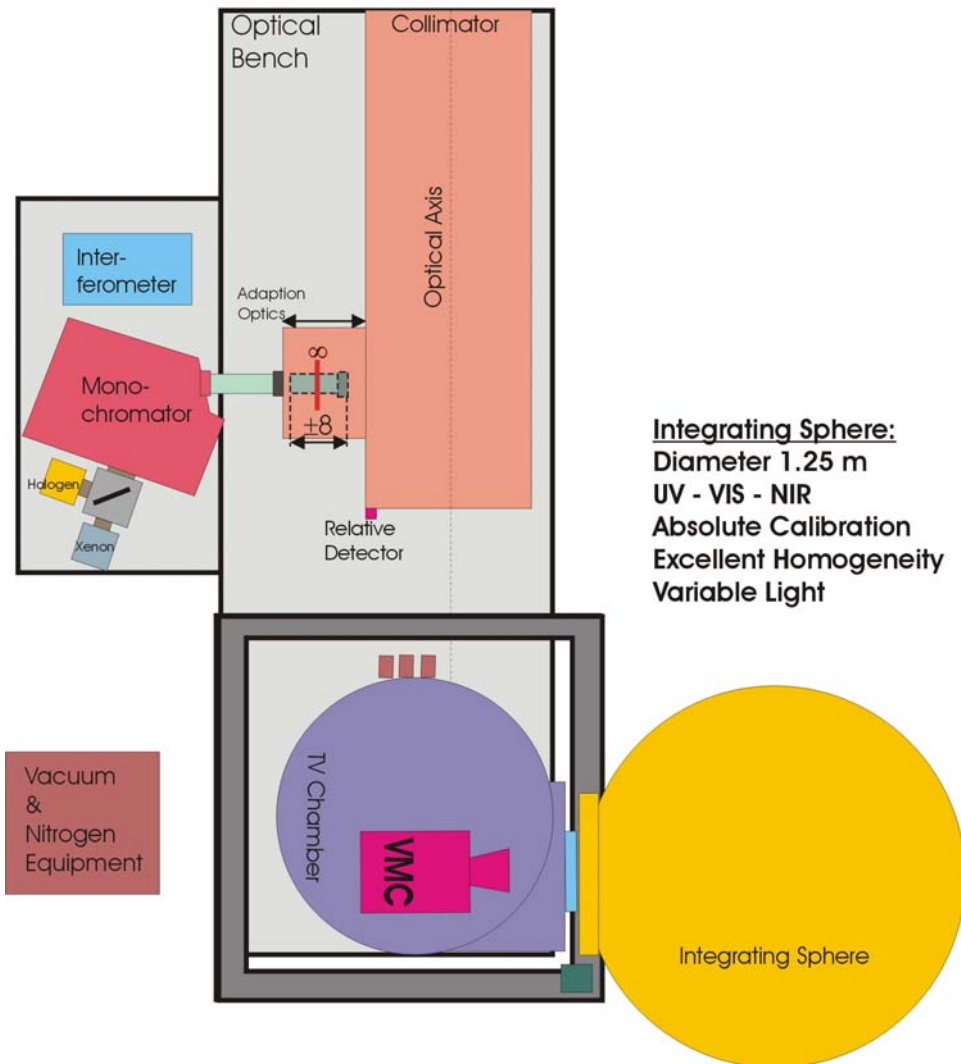


Figure 4.8 Radiometric set-up (top view)

#### 4.4 VMC Assembly under Calibration

The VMC FS including FS Harness was adjusted on instrument mounting platform equipped to the turn table in the TV chamber. VMC FS was electrically connected via test harness with the VMC EGSE located in the check-out room in front of the clean room.

During calibration the VMC FS was equipped in an analogous manner to S/C mounting under mission-like thermal environment allowing imaging as realistic as possible. Therefore the VMC (up to half of its baffle) was covered by test MLI to simulate the later S/C wrapping. The VMC itself was assembled on its instrument platform within the TV chamber. The instrument platform simulates the later S/C mounting surface thermally. Instrument (CCD) cooling under vacuum was done via cooling sky upside VMC instrument platform using liquid nitrogen. The instrument platform for VMC mounting was additionally equipped with external heaters (6 x 39  $\Omega$ ) in the area around VMC feet allowing up to 15 Watt heat entry.

Figure 4.4-1 illustrates the VMC (gray) mounted on instrument platform (green) on turn table (green) under the cooling sky (purple) facing the large optical window (red) in the TV chamber during calibration.



Figure 4.9 VMC mounted in TV chamber during calibration

## 4.5 VMC Image Header

The VMC image header (ASCII) used for calibration contains file naming, image ID, camera parameters, externally measured temperatures and set-up parameters. For example:

PDS\_VERSION\_ID    = PDS3  
RECORD\_TYPE       = FIXED\_LENGTH  
RECORD\_BYTES      = 80  
FILE\_RECORDS      = 36  
PRODUCT\_ID       = "VMC\_FS\_CAL04\_20050421\_164744\_03093.pds"

DESCRIPTION       = Flatfield integrating sphere Halogen medium case

H\_TIME:            = 04/21/2005 16:47:37.058 UTC

H\_IMAGE\_ID:       = 03093

H\_IMAGEMODE:      = Limb

H\_CAMERA\_ID:      = FS

H\_OPTICS\_ID:      = FS

H\_PELTIER\_ID:     = FS

H\_CCD\_ID:         = FS

H\_CCD\_LINES:      = 1024

H\_CCD\_COLUMNS:   = 1024

H\_CCD\_LINES\_ACTIVE: = 1018

H\_CCD\_COLUMNS\_ACTIVE: = 1008

H\_CCD\_FIRST\_ACTIVE\_LINE: = 5

H\_CCD\_FIRST\_ACTIVE\_COLUMN: = 7

H\_EXPTIME:        = 29999.8 ms

H\_NUMBER\_LINES:   = 00093

H\_NUMBER\_FRAMES:   = 00057

H\_CCD\_TEMP:       = 20.0 °C

H\_PELTIER\_STATUS:   = OFF

H\_HARD\_BINNING:    = 0

H\_SOFT\_BINNING\_ALL: = 0

H\_SOFT\_BINNING\_VIS: = 0

H\_SOFT\_BINNING\_NIR1: = 0

H\_SOFT\_BINNING\_NIR2: = 0

H\_SOFT\_BINNING\_UV: = 0

H\_COMPRESSION\_ID:   = OFF

H\_COMPRESSION\_FACTOR: = 0

H\_COMPRESSION\_QUALITY: = 0

H\_MAX\_DNVALUE:     = 012687

H\_MIN\_DNVALUE:     = 001788

H\_AVERAGE\_DNVALUE: = 8970.2

H\_SATURATION\_FLAG: = 0

[STATUS]

STATUS = OK

[ENVIRONMENT]

TIME\_STAMP = "04:42:39 PM 04/21/2005"

BAROMETRIC = 1001.400000

TEMP °C = 20.800000

HUMIDY % = 0.300000

[PRESSURE\_IN\_TV\_CHAMBER]

TIME\_STAMP = "04:42:40 PM 04/21/2005"

VAC\_PRESSURE = "1.7 X 10<sup>-5</sup> mbar"

[TV\_CAMERA\_MOUNTING]

TIME\_STAMP = "09:52:50 AM 04/13/2005"

CAMERA\_MOUNT = horizontally

[MOTORTV\_M2]

TIME\_STAMP = "09:57:18 AM 04/13/2005"

POS\_M2 = 11700

[MOTORTV\_M1]

TIME\_STAMP = "09:56:57 AM 04/13/2005"

POS\_M1 = 11500

[INTEGRATING\_SPHERE]

TIME\_STAMP = "04:42:09 PM 04/21/2005"

VIS\_DETECTOR = +2.5144E-07O0R4

NIR\_DETECTOR = +1.8228E-05O0R2

UV\_DETECTOR = +2.5406E-09O0R4

ABSOLUTE\_RELATIV\_DETECTOR = +2.0776E-07O0R4

[COLLM\_MOT\_POSITION]

TIME\_STAMP = "01:09:21 PM 04/21/2005"

COLLM\_ID = 0

MOT\_X = -11830

MOT\_Y = -71942

MOT\_Z = -8074

[MONOCHROMATOR]

TIME\_STAMP = "10:52:32 AM 04/21/2005"

WIDTH\_SLIT\_ENTR = 1000.000000

WIDTH\_SLIT\_EXIT = 1000.000000

ID = 1

WAVELENGTH = 179.972840

SHUTTER = 1

[MONO\_FILTER\_ID]

TIME\_STAMP = "10:52:32 AM 04/21/2005"

FILTER\_GG385 = 0

FILTER\_RG610 = 0

FILTER\_GE1600 = 0

FILTER\_EMPTY = 1  
FILTER\_CLOSED = 0  
[MONO\_GRATING\_ID]  
TIME\_STAMP = "10:52:32 AM 04/21/2005"  
GRATING\_1 = 1  
GRATING\_2 = 0  
GRATING\_3 = 0  
[TV\_TEMP]  
TIME\_STAMP = "04:38:36 PM 04/21/2005"  
TEMP\_1 = -21.600000  
TEMP\_2 = 0.000000  
TEMP\_3 = -19.240000  
TEMP\_4 = -21.250000  
TEMP\_5 = -19.240000  
TEMP\_6 = -17.460000  
TEMP\_7 = -10.420000  
TEMP\_8 = -2.070000  
TEMP\_9 = -1.760000  
TEMP\_10 = 3.750000  
TEMP\_11 = -0.760000  
TEMP\_12 = -0.910000  
TEMP\_13 = -185.780000  
TEMP\_14 = -184.530000  
TEMP\_15 = -184.690000  
TEMP\_16 = -187.930000

^IMAGE = "VMC\_FS\_CAL04\_20050421\_164744\_03093.bin"

OBJECT = IMAGE  
INTERCHANGE\_FORMAT = BINARY  
LINES = 1024  
LINE\_SAMPLES = 1024  
SAMPLE\_TYPE = LSB\_UNSIGNED\_INTEGER  
SAMPLE\_BITS = 16  
END\_OBJECT = IMAGE  
END

## 5 Laboratory Activity

The calibration of the VMC FS was performed at MPS within two weeks starting from 11.04.2005 until 22.04.2005. The involved people were I. Sebastian, M. Tschimmel, D. Belyaev and A. Dannenberg. Each step of calibration activity was documented in the logbook which is attached to the Calibration report (section 8). Table 5.1 gives a brief summary of the calibration activity.

Some general explanations of the usage of the calibration logbook are necessary:

- The naming convention for the calibration data (binary images, PDS files and EGSE recorder files) are given by the VMC Calibration Plan VMC-MPAE-PL-SF000-001\_D\_ - as follows (cf. chapter 6).
- An ASCII header file of identical name belongs to each PDS calibration data file taken during calibration (see also chapter 4.5).
- The calibration image and header files are stored in the VMC calibration archive on sun2 server at Max-Planck-Institute. The EGSE recorder files are also available at IDA.
- All calibration activity of VMC FS is covered by entries in the logbook.
- Logbook overview (section 8): On the left side of the pages is written: recorder file names, general remarks about the test conditions, unusual occurrences. On the right side of the pages is written: log of the calibration activities, sometimes with notes of unusual occurrences. The abbreviations are: Exp.T – exposure time [milliseconds or seconds], CCDtemp – temperature of CCD chip [°C], ID – image file number. If in the rightmost column an image ID with ‘error’ is written this means that the EGSE has delivered an error message (see page 46 left side).
- Temperature ranges: three main temperature ranges were covered: cold case (CCD Temperature in the range of -20 to -5 °C), medium case (CCD Temperature around +20 °C), and hot case (CCD Temperature around + 45 ° C). Focus and flat field measurements were performed at these temperature ranges.
- The addressed calibration topics are: VIS focus (CAL 1), all channel focus (CAL 2), flat field (CAL 4), dark signal (CAL 5), spectral responsivity (CAL 6), stray light measurements (CAL 9), tests (CAL 99). Note that three illuminated images are nominally combined with three dark images at same CCD temperature for flat field and spectral responsivity measurement.

**Table 5.1 VMC Calibration Activity Log**

<b>Date</b>	<b>Page</b>	<b>Calibration activity</b>	<b>Log entries</b>
13.04.2005	3-6	dark signal (CAL 5) in <i>hot</i> case	Exp.T, the real exposure time [ms], the mean value [DN], CCDtemp, ID
14.04.2005	7-8	VIS focus (CAL 1) in <i>hot</i> case	the small collimator position [+10 to -10], the number of unresolved pixels in Siemensstar image, Exp.T, mean value [DN], CCDtemp, ID
14.04.2005	8-9	all channel focus (CAL 2)	Exp.T, CCDtemp, ID
14.04.2005	10-12	Flat field (CAL 4) with corresponding dark signal (CAL 5) in <i>hot</i> case	Exp.T, CCDtemp, the lamp position, the CAL number [4/5], ID
15.04.2005	13-16	dark signal (CAL 5) in <i>cold</i> case	Exp.T, the mean value [DN], CCDtemp, ID
15.04.2005	16-18	Flat field (CAL 4) with corresponding dark signal (CAL 5) in <i>cold</i> case	Exp.T, CCDtemp, the lamp position, the CAL number [4/5], ID
16.04.2005	19-20	dark signal (CAL 5) in (very) <i>cold</i> case	Exp.T, the mean value [DN], CCDtemp, ID
16.04.2005	21-23	VIS focus (CAL 1) in <i>cold</i> case	collimator position [+10 to -10], the number of pixels in Siemensstar image , Exp.T, CCDtemp, frontplate and baseplate temperature [°C], ID
16.04.2005	23-27	dark signal (CAL 5) in <i>medium</i> case	Exp.T, the mean value [DN], CCDtemp, ID
18.04.2005	28-33	spectral responsivity (CAL 6) of NIR1 channel	the lamp, the slit width of the monochromator, the used grating and filter; the wavelength [nm], Exp.T, maximum value [DN], CCDtemp, ID
19.04.2005	34-38	spectral responsivity (CAL 6) of VIS channel	the lamp, the slit width of the monochromator, the used grating and filter; the wavelength [nm], Exp.T, CCDtemp, ID
20.04.2005	38-44	spectral responsivity (CAL 6) of UV, NIR1, NIR2 channel	the lamp, the slit width of the monochromator, the used grating and filter; the wavelength [nm], Exp.T, CCDtemp, ID
21.04.2005	44-45	spectral responsivity (CAL 6) of the blocking range between VIS and NIR1, UV	the lamp, the slit width of the monochromator, the used grating and filter; the wavelength [nm], Exp.T, CCDtemp,

		short-wavelength edge	ID
21.04.2005	47-48	Stray light measurements (CAL 9)	Exp.T, CCDtemp, the lamp position, the CAL number [4/5], ID
21.04.2005	49-51	Flat field (CAL 4) with corresponding dark signal (CAL 5) in <i>medium</i> case	Exp.T, CCDtemp, the lamp position, the CAL number [4/5], ID
22.04.2005	extra 1-3	VIS focus (CAL 1) for off-axis positions at ambient	collimator position, the number of unresolved pixels in the Siemensstar , ID

## 6 Data Archiving

The following chapter explains the file naming convention, the necessary IDL software tools and the data archive structure of the recorded files.

The naming convention for the calibration data (PDS files, images and EGSE recorder files) are given by the VMC Calibration Plan VMC-MPAE-PL-SF000-001\_D\_ - as follows:

1. EGSE recorder files: FS\_Calibration\_CALID\_yyyymmdd.\*
2. PDS format with separate binary image file:  
VMC\_FS\_CALID\_yyyymmdd\_hhmiss\_count.ext

The used abbreviations are:

CALID	calibration ID given in table 3-1 (CAL01 ... CAL 09, CAL99)
yyyy	year
mm	month
dd	dd
hh	hour
mi	minute
ss	second
count	image counter (1 ... 99 999); start on 1 <sup>st</sup> day of calibrations and continued until end (FS calibration covers ID 771 until ID 4157)
ext	Extension (pds, bin)

**Table 6-1 VMC file naming convention**

The necessary IDL software routines to work with the PDS and binary image files are located on the sun2-server in the folder “VMC\_FM\_Calibration\IDL\_Software”.

## 7 Results of the Calibration and Performance Study

### 7.1 CCD Performance

#### 7.1.1 CCD Quantum Efficiency

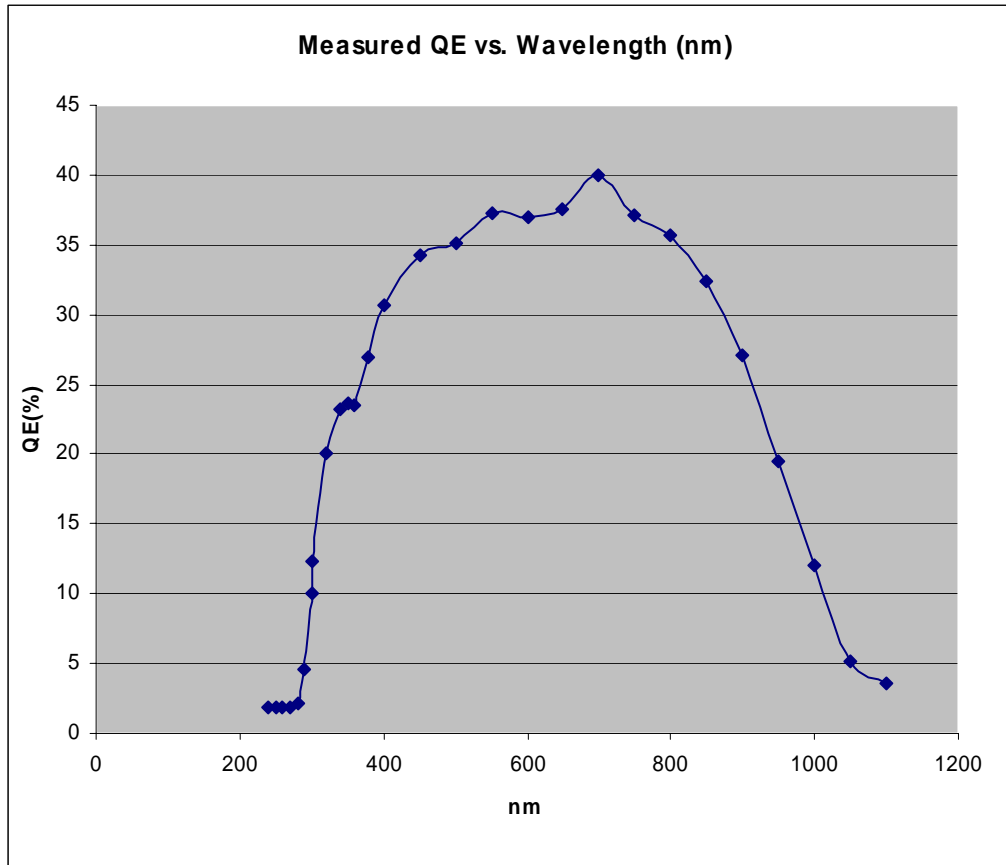
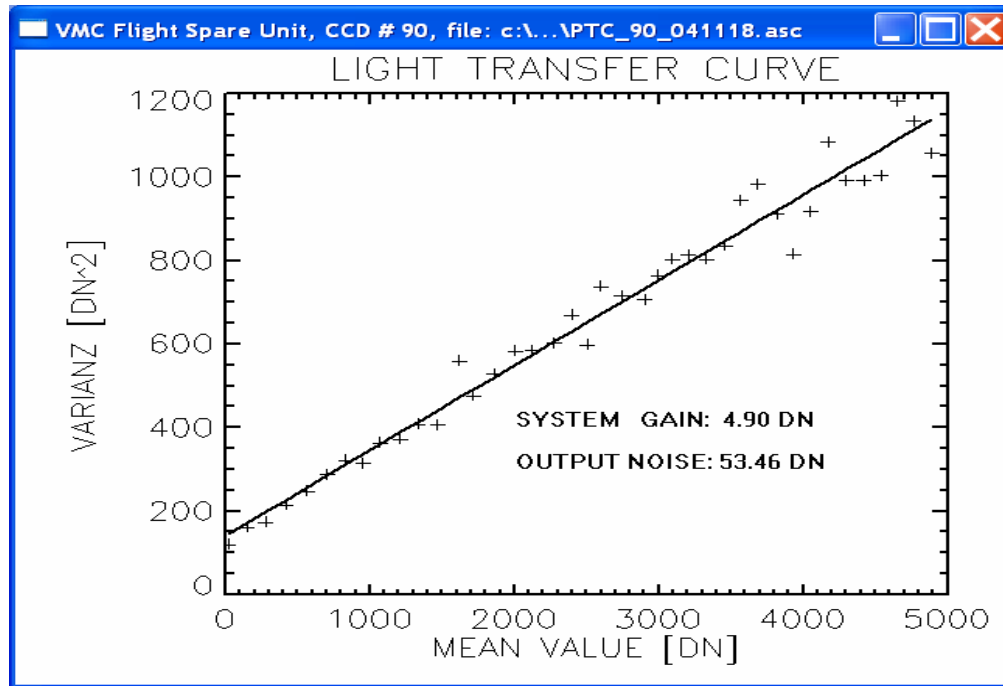


Figure 7.1 The measured Quantum Efficiency of the Kodak KAI-1010 CCD

#### 7.1.2 Performance Test

To verify the electro-optical performance of the detector including readout electronics the photon-transfer-technique is used to specify total noise in darkness and system gain. At different exposure times images are acquired with and without light. Illumination is performed with light from a diffuse shined radiator based on red LEDs. The exposure is controlled via the EGSE PC (on/off of the LEDs).

The linearity error is in the range less than 1% (see also CRE FS ADP). Figure 7.1-2 shows the light transfer curve of the CCD90.



**Figure 7.2 Photon Transfer Curve @ ~ 24 °C Thermo-vacuum test**

CRE (unit level) was TV tested to demonstrate correct function over the specified temperature range. All measurements were done in darkness. At different exposure levels images were acquired and saved.

**Figure 7.1-3** shows the averaged dark current behavior at two different exposure times (250ms and 4s) in the hot case. The noise is calculated at min exposure time (1 line equal to about 500 $\mu$ s).

**Figure 7.1-4** shows the averaged dark current behavior at two different exposure times (250ms and 4s) in the cold case. The noise is calculated at min exposure time (1 line equal to about 500 $\mu$ s).

**Figure 7.1-5** presents the noise at very large exposure time in the hot and cold case. At temperature beyond 25°C the noise increased rapidly.

To separate the noise performance of the detector from the readout electronics also the CRE electronics was TV tested without CCD. In this configuration the CRE electronics input was grounded (no CCD). **Figure 7.1-6** shows the behavior of the electronics offset (without CCD) and the noise performance of the electronics separately.

The noise of the readout electronics is in the range of 5 electrons at 2 MHz pixel frequency. As expected the exposure time control has no influence.

### Conclusions:

1. The electronic noise is very stable over temperature at about 5 electrons
2. The main contribution of noise comes from the CCD.
3. At large exposure time cooling must be used to set the temperature operation range to max 22°C

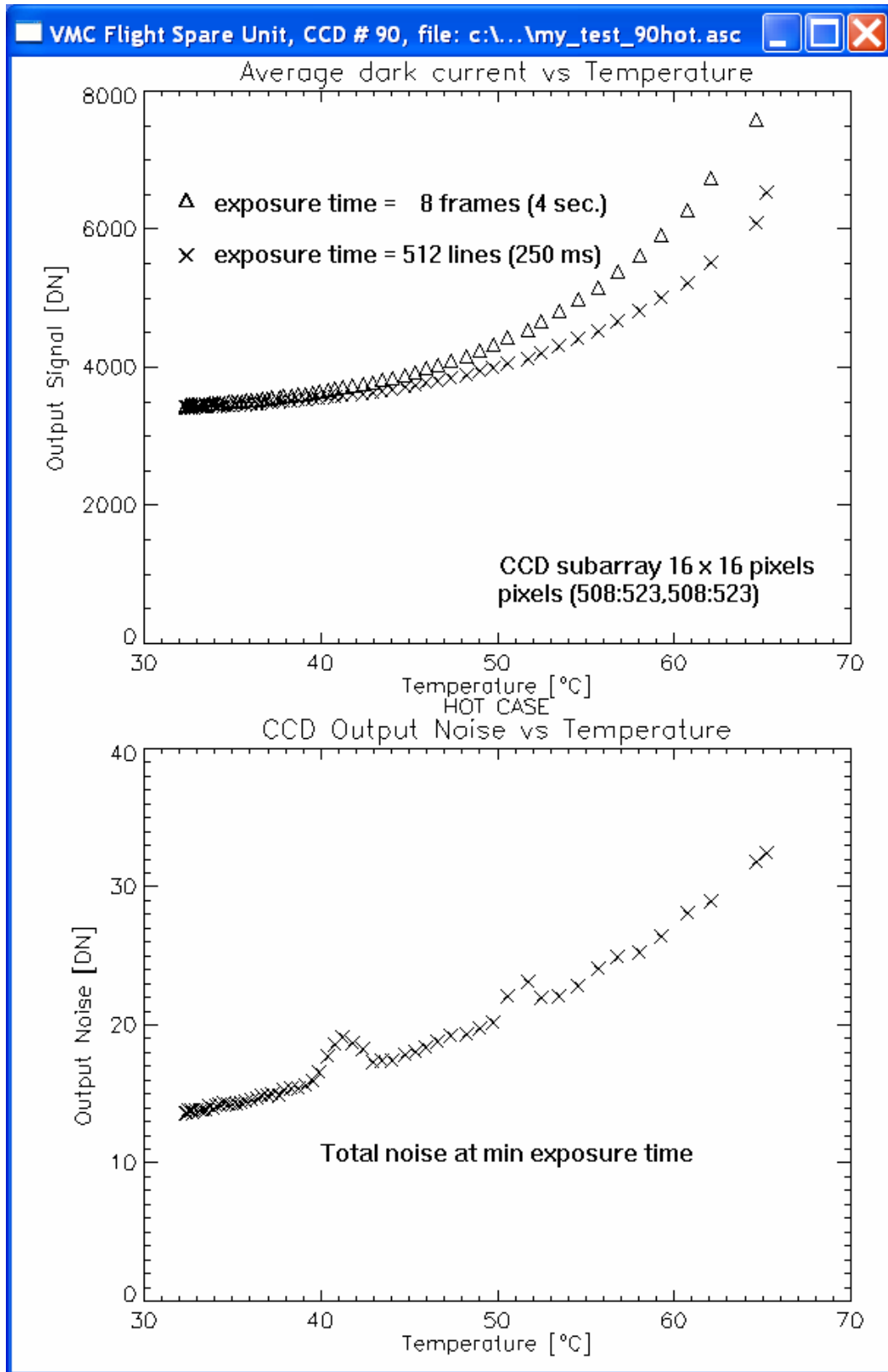


Figure 7.3 FS CCD 90 hot case

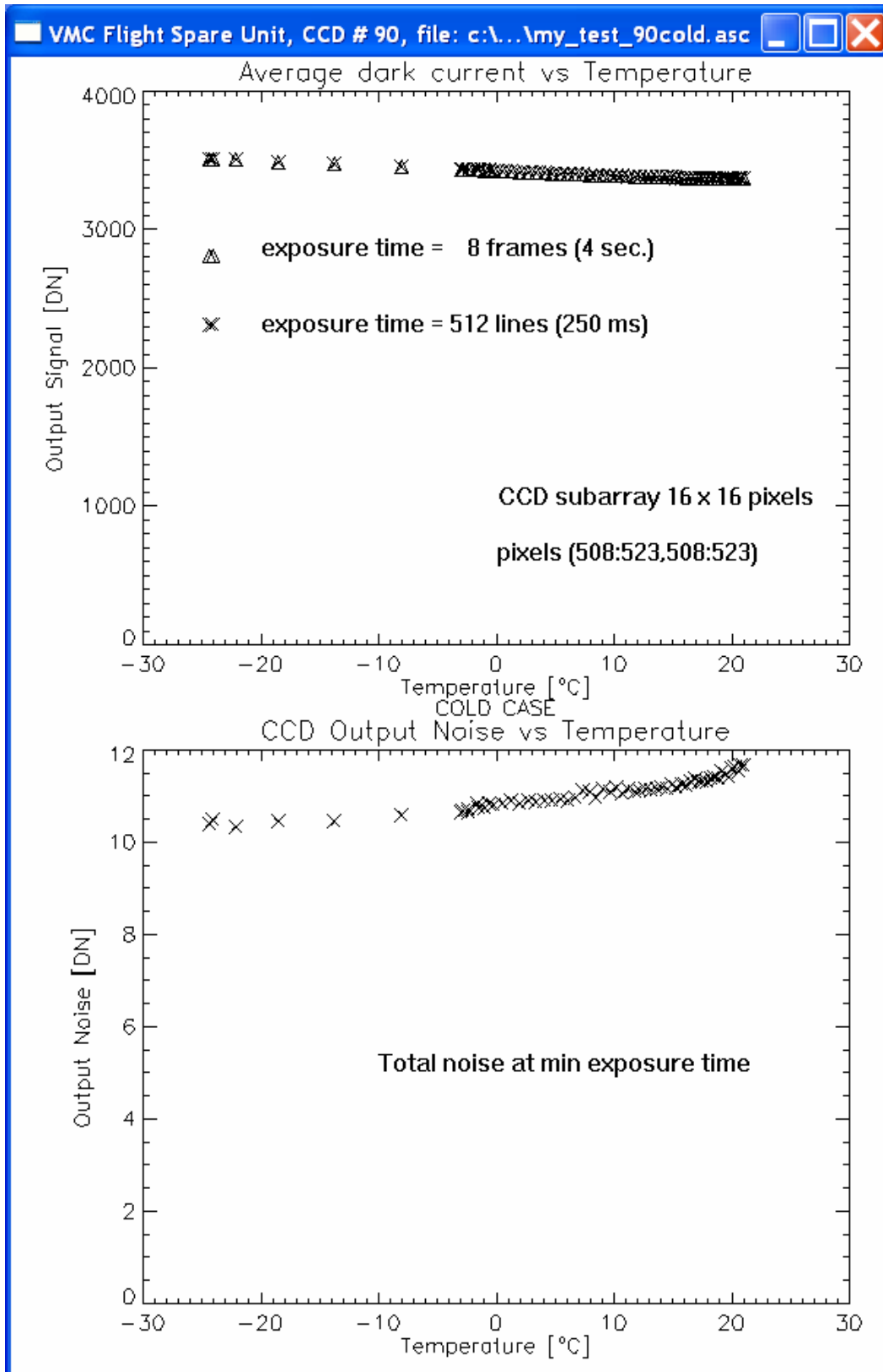


Figure 7.4 FS CCD 90 cold case

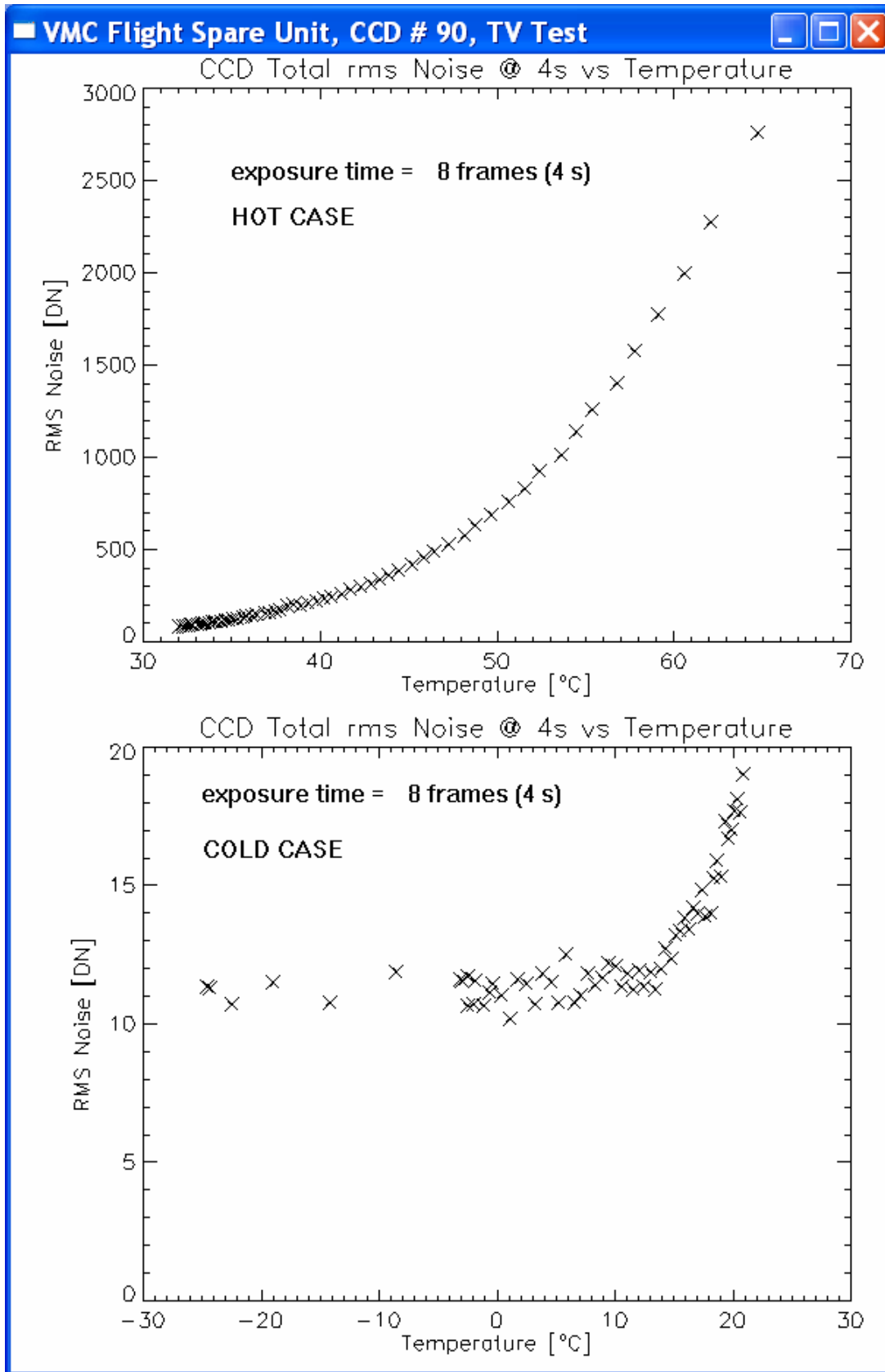


Figure 7.5 FS CCD 90 cold case

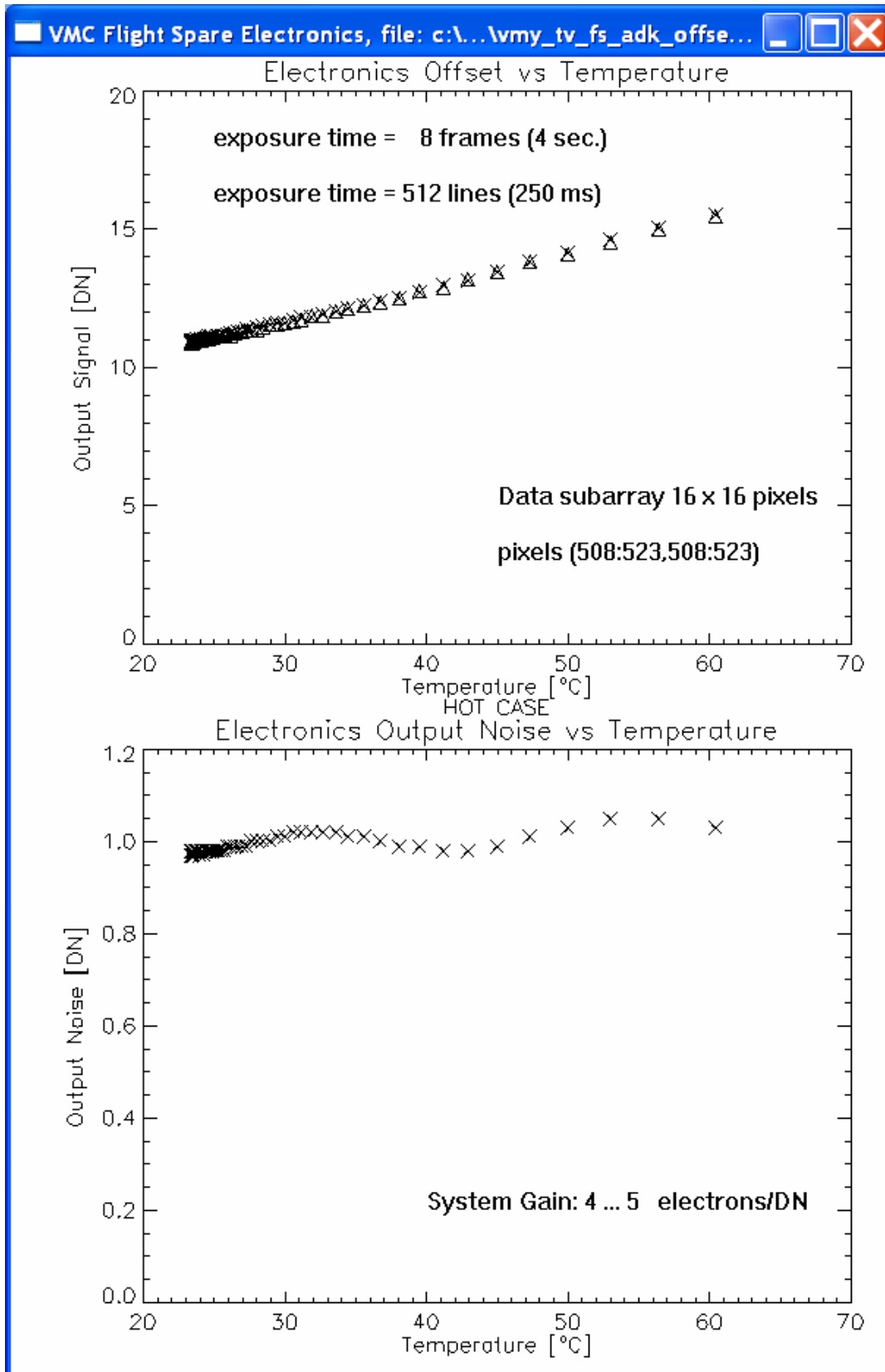


Figure 7.6 FS Electronics Offset hot case

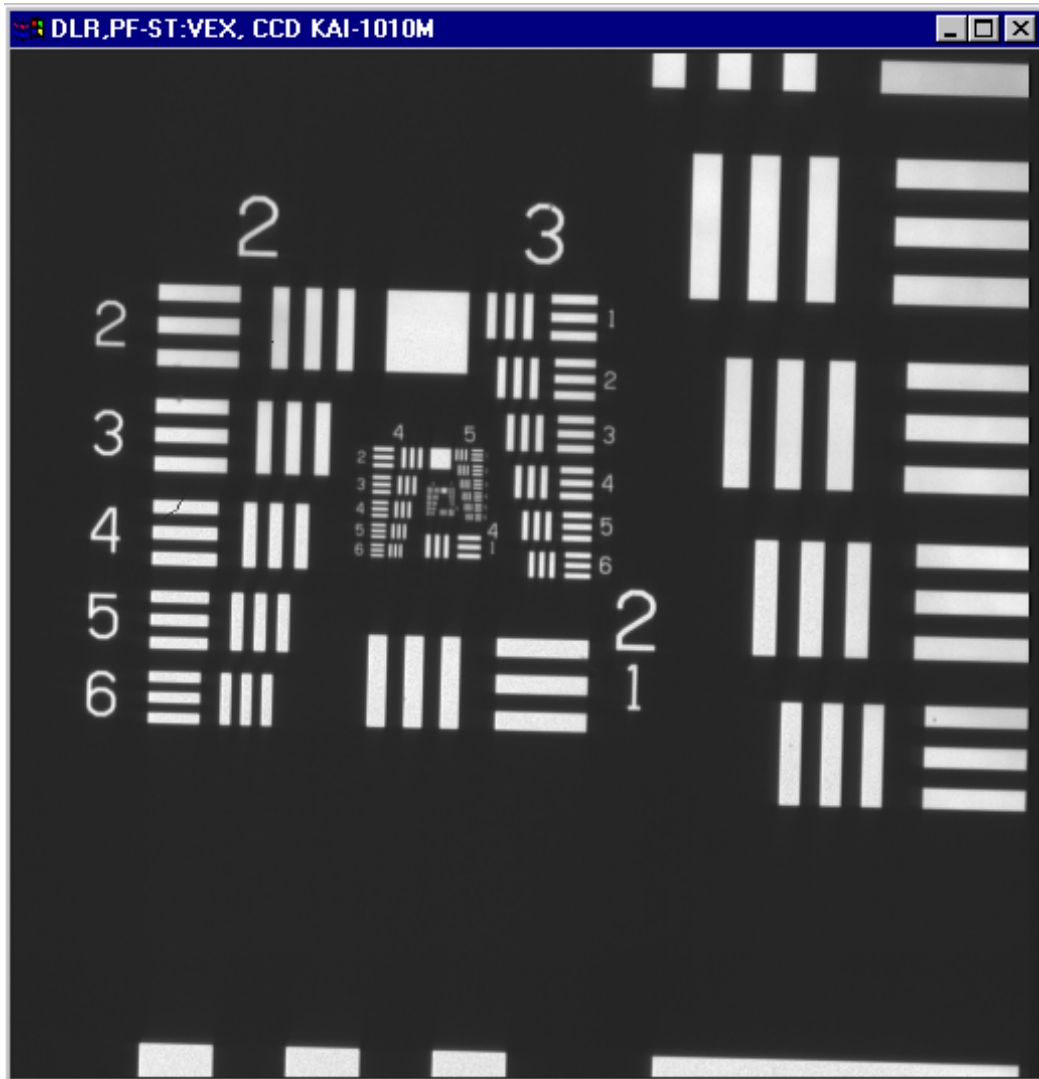


Figure 7.7 CCD 90 Test Image (row data) (IDL binning 2 by 2, image PF090433.05x)

### 7.1.3 Functional Tests

**Figure 7.1-7** shows a test images taken with CCD 90. A vertical and horizontal plot is seen in **Figure 7.1-8**. To demonstrate dark signal non uniformity

**Figure 7.1-9** shows a dark image at room temperature with a corresponding horizontal cut.

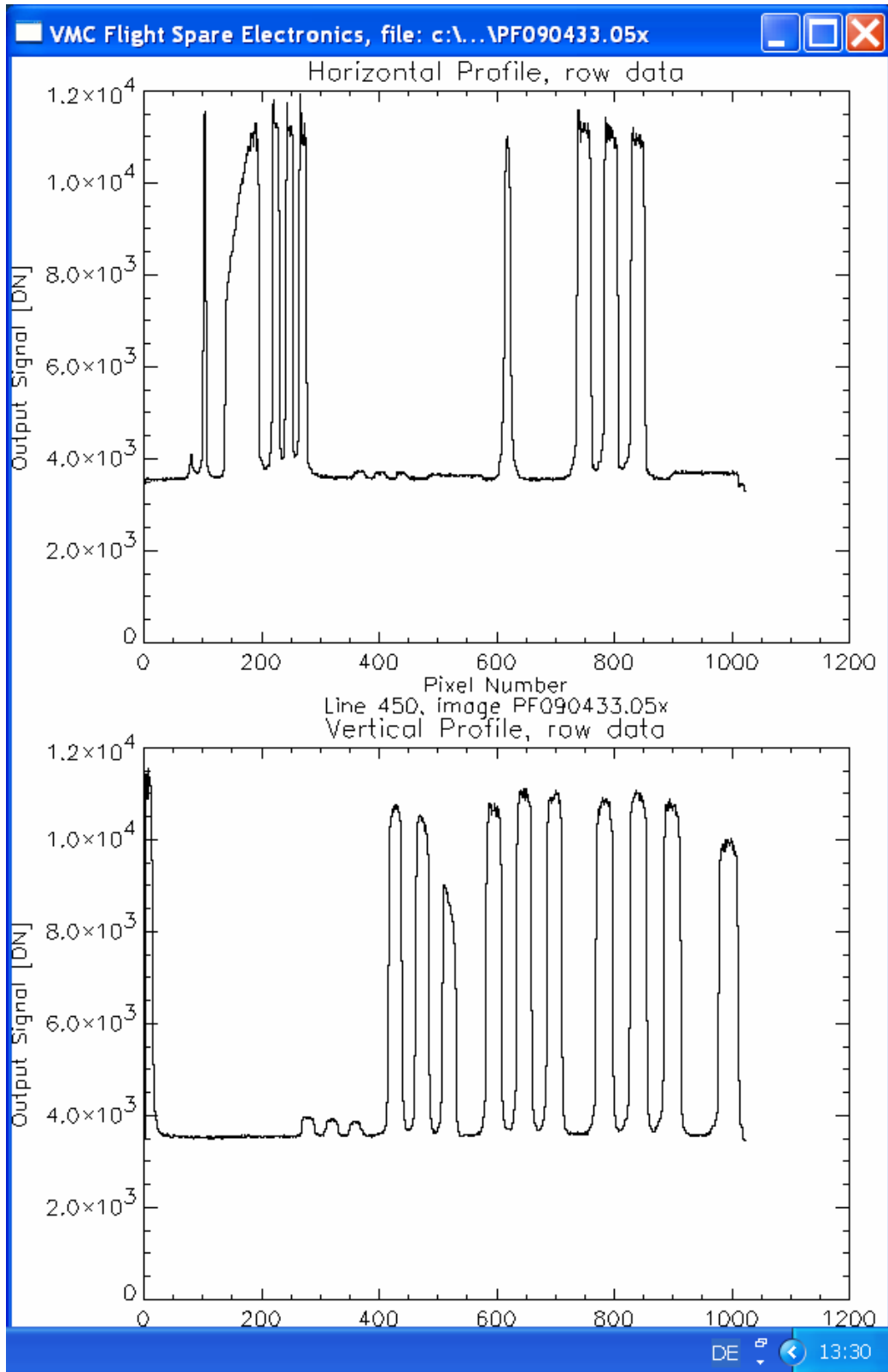


Figure 7.8 Horizontal and vertical profile of image PF090433.05x

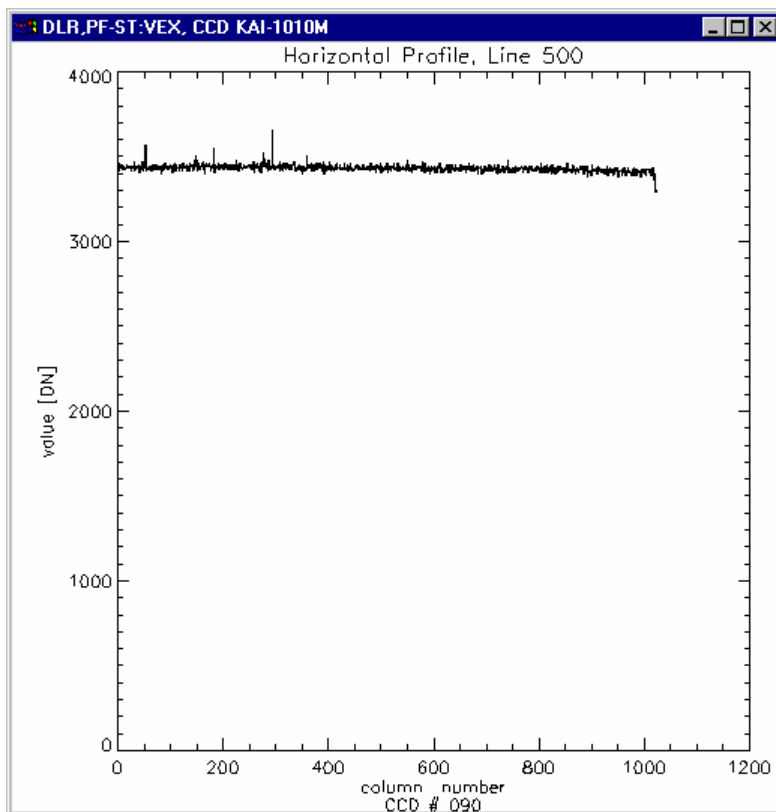
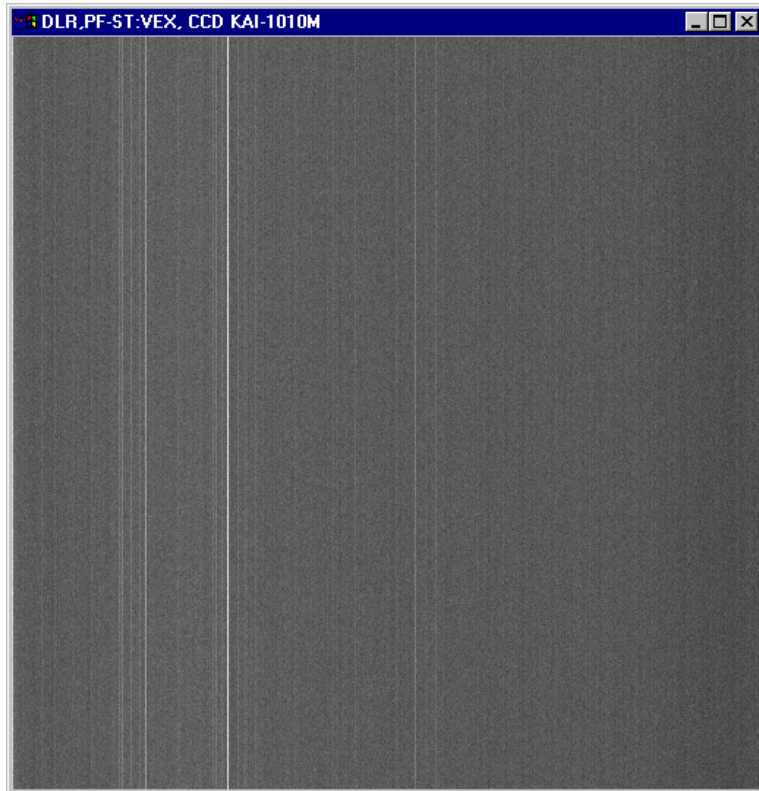
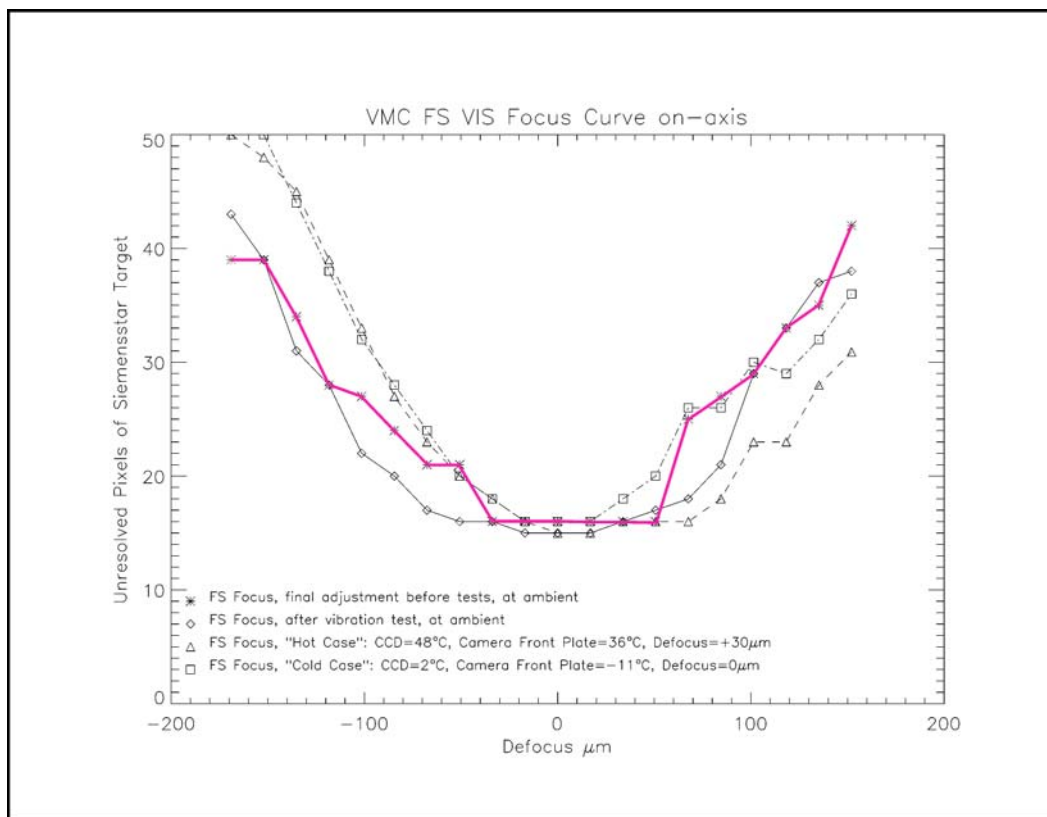


Figure 7.9 CCD Dark image with horizontal plot

## 7.2 Geometric Properties

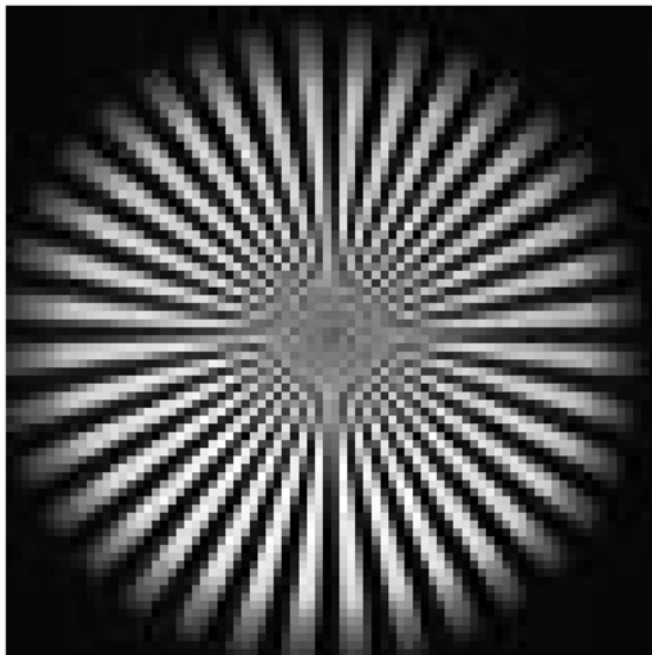
### 7.2.1 Focus Measurements

The focusing of VMC was done using the laboratory set-up described in section 4.2. The best focus curve for final adjustment prior to environmental tests (purple) is shown in figure 7.2-1. This focus check within VIS channel on-axis was performed several times between environmental tests in order to confirm that vibrations or TV tests had not distorted the focus status. Full focus test for all 4 channels was performed during laboratory calibration at three temperatures: room, +40C, and -20C. In all cases defocusing was not detectable or was low and within the range of depth of field of  $\pm 25 \mu\text{m}$ . Hot temperature case with camera temperature of + 36°C and CCD temperature of + 48°C results in just acceptable camera defocus of + 30  $\mu\text{m}$ .

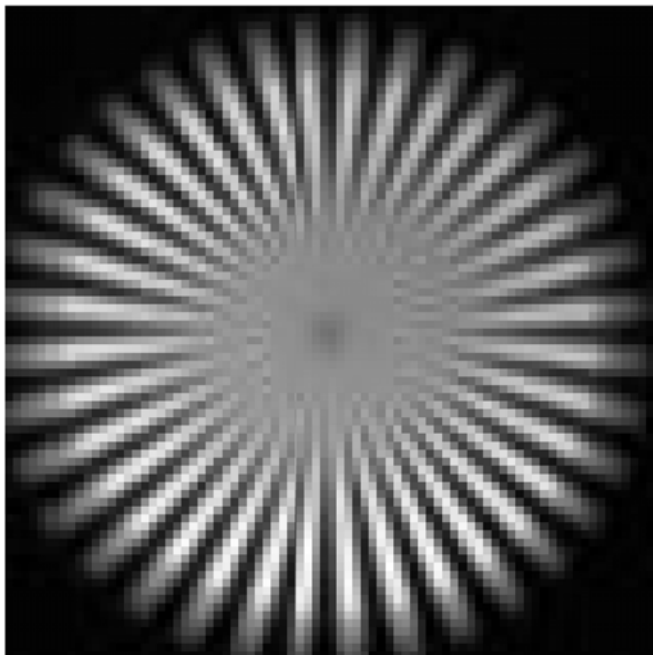


**Figure 7.10** Measurements of the best focus position for VIS channel on-axis during integration and between environmental tests.

Figure 7.2-2 shows two VMC images of VIS channel center (on-axis). In both cases the “Siemensstar” target in collimator focus illuminates approximately half of the FoV of VIS channel. Focus status at infinity (best focus) and defocus were simulated by the collimator that faces the camera frontally. The number of non-resolved pixels in the center of the VMC Siemensstar image is used to quantitatively characterize the focus. Minimum number of non-resolved center pixels stands for best focus adjustment as identified by focus curve minimum given in figure 7.2-1. The near-Earth commissioning proved that the VMC focus had not degraded during the launch and in space (see section 9).



VMC FS VIS Channel  
on-axis  
Image of Siemensstar  
@ infinity  
Best Focus



VMC FS VIS Channel  
on-axis  
Image of Siemensstar  
Defocus: -100  $\mu\text{m}$

**Figure 7.11** VMC image of the “Siemensstar” target for best focus and -100  $\mu\text{m}$  defocus on-axis.

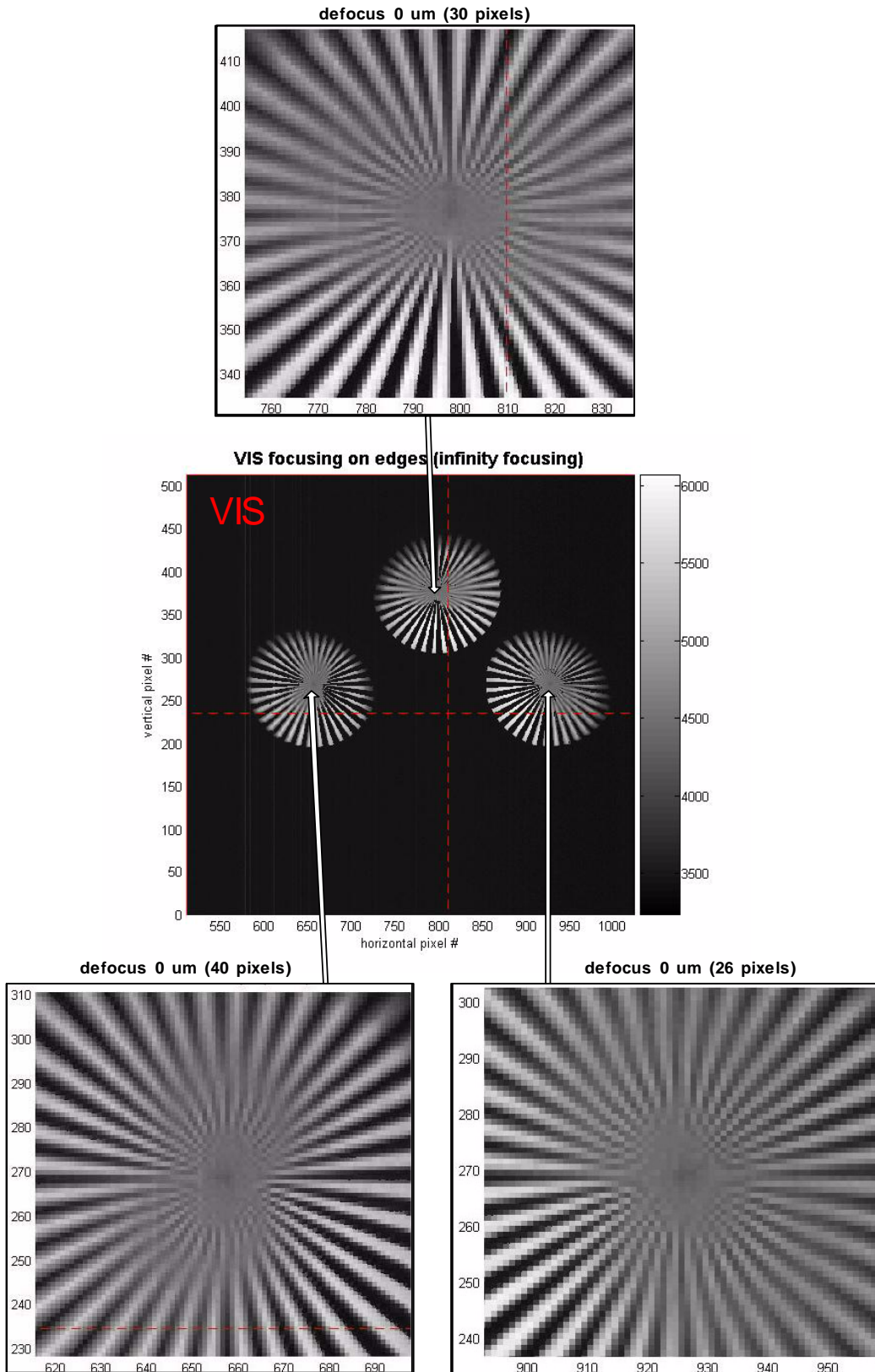


Figure 7.2-3 VMC images of the “Siemensstar” target for infinity focus at non-axis case.

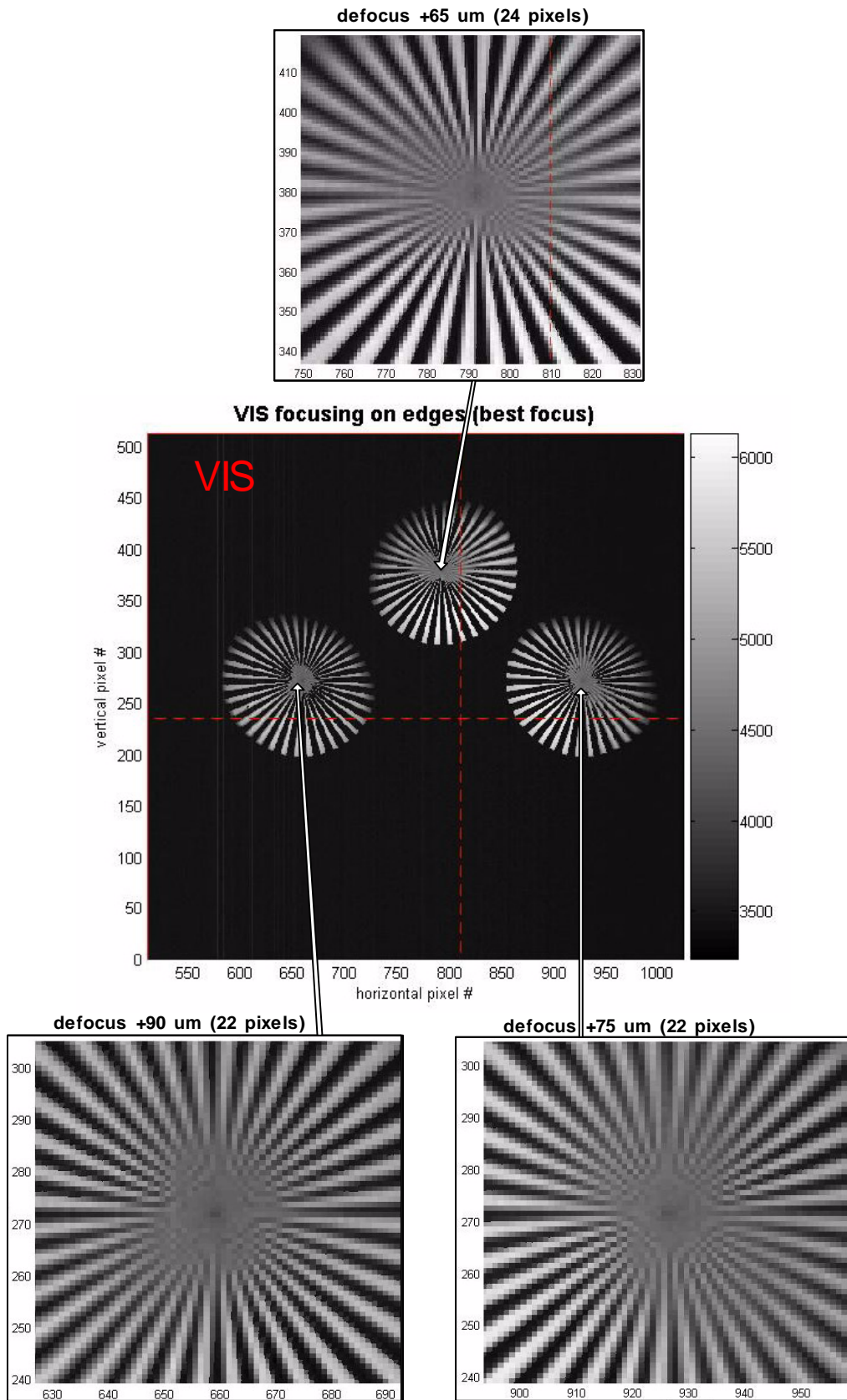
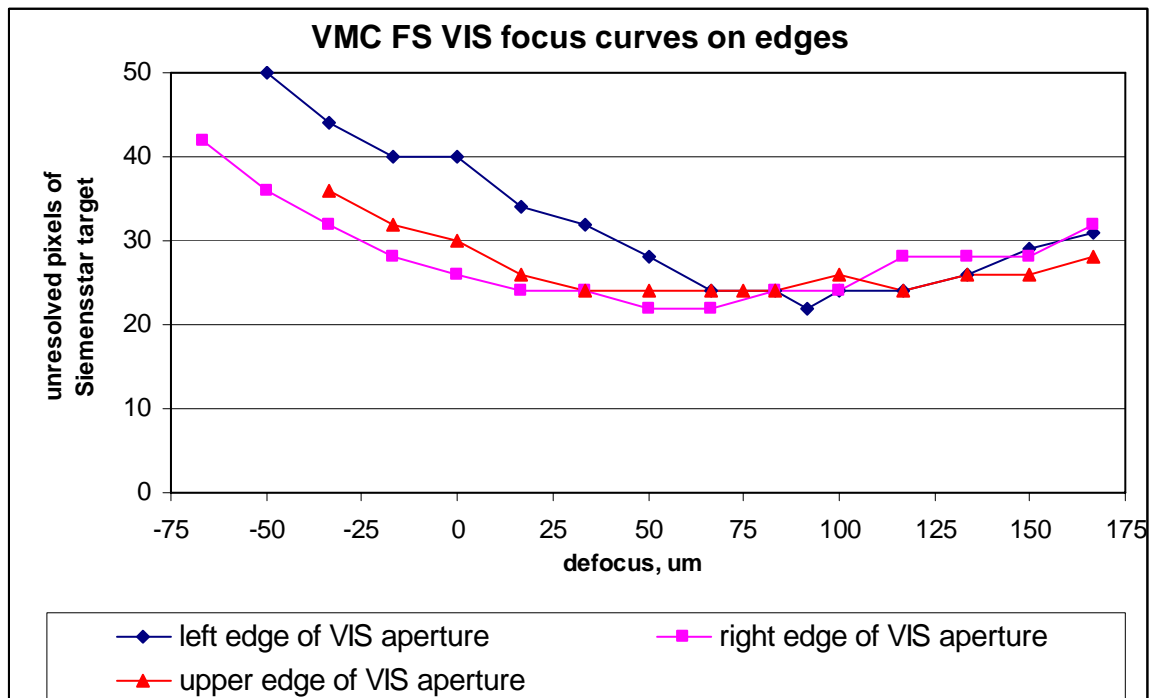


Figure 7.2-3 VMC images of the “Siemensstar” target for the best focus at non-axis case.

Several VMC images of the “Siemensstar” target were taken on edges of the VIS channel for non-axis focus check. In this case infinity focusing (defocus position 0  $\mu\text{m}$ ) doesn't provide for best focus and gives more than 26 unresolved center pixels (figure 7.2-3). Moreover, distribution shape of unresolved pixels looks like “8” on left and right edges and like “ $\infty$ ” on upper edge while this distribution is circular for on-axis case (see figure 7.2-2; -100  $\mu\text{m}$  defocus). Unresolved pixels were counted along axis that is perpendicular to the axis of the sign “8”. In figure 7.2-4 non-axis VIS focusing at minimum number of unresolved center pixels is shown (the best focus in this case).

Figure 7.2-5 shows dependence of unresolved pixels number on defocus position.



**Figure 7.2-5** Measurements of the best focus position for VIS channel on edges of the aperture.

### 7.2.2 Field of View (FOV).

Figures 7.2-6 – 7.2-9 demonstrate VMC images of regular grid with step 1 cm. The distance from the VMC optics to the grid target was 230 cm. Grid image was taken for every corner of channels aperture and everywhere one grid step takes 6 pixels for every coordinate. Therefore, FOV of individual pixel is  $1/6\text{cm}$  that corresponds to  $7.25 * 10^{-4}\text{radian}$  ( $\sim 2'30''$ ). There are no any distortions in all the channels but there is some image unsharpness on edges of VIS channel FOV.

channel	VIS		NIR1		NIR2		UV	
	horizontal	vertical	horizontal	vertical	horizontal	vertical	horizontal	vertical
linear FOV, pixels	461+3	467+3	473+3	479+3	478+3	462+3	445+3	468+3
angular FOV, radian	0.331	0.335	0.339	0.344	0.343	0.332	0.32	0.336

**Table 7.2-1** Linear and angular FOV for every channel.

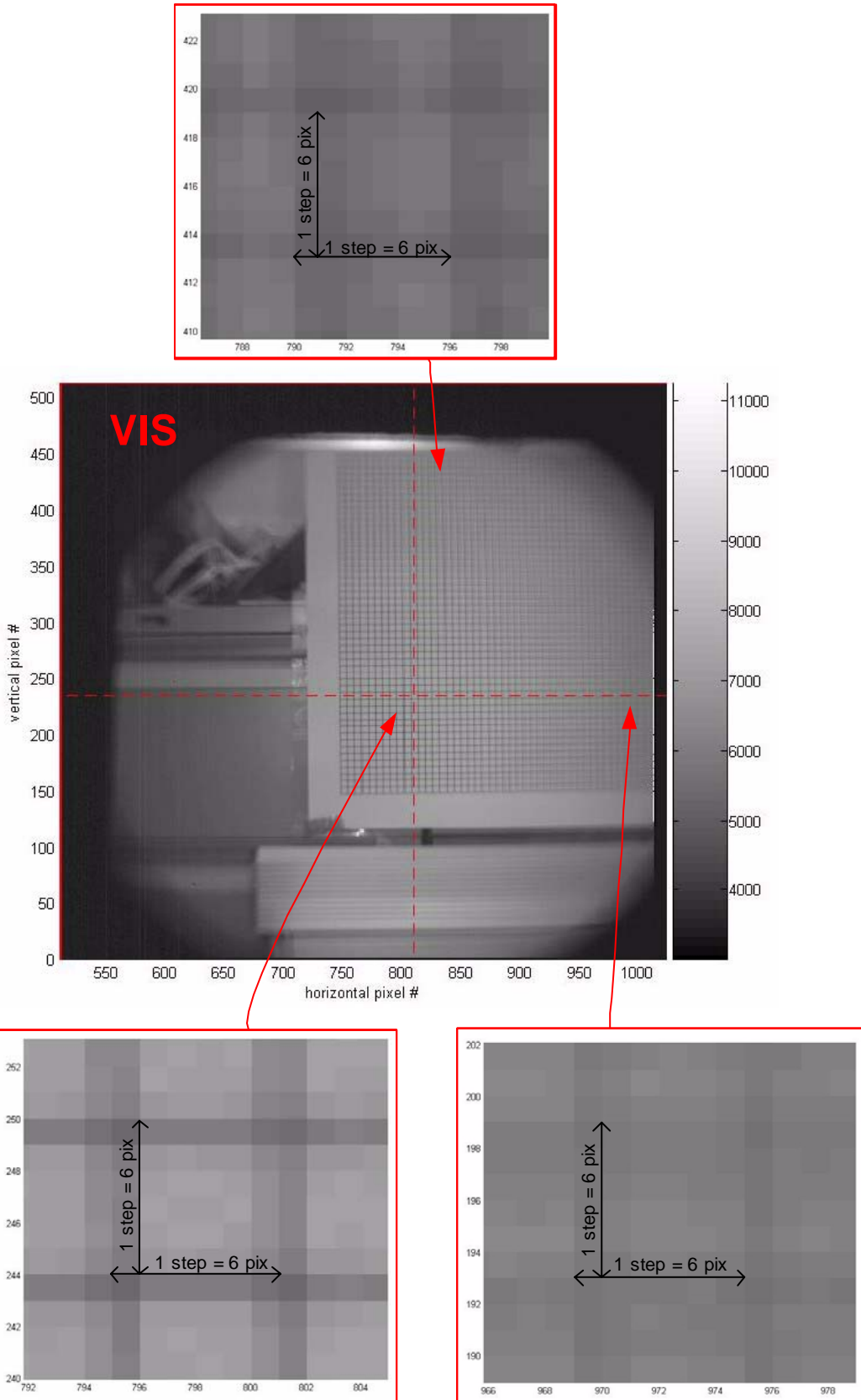
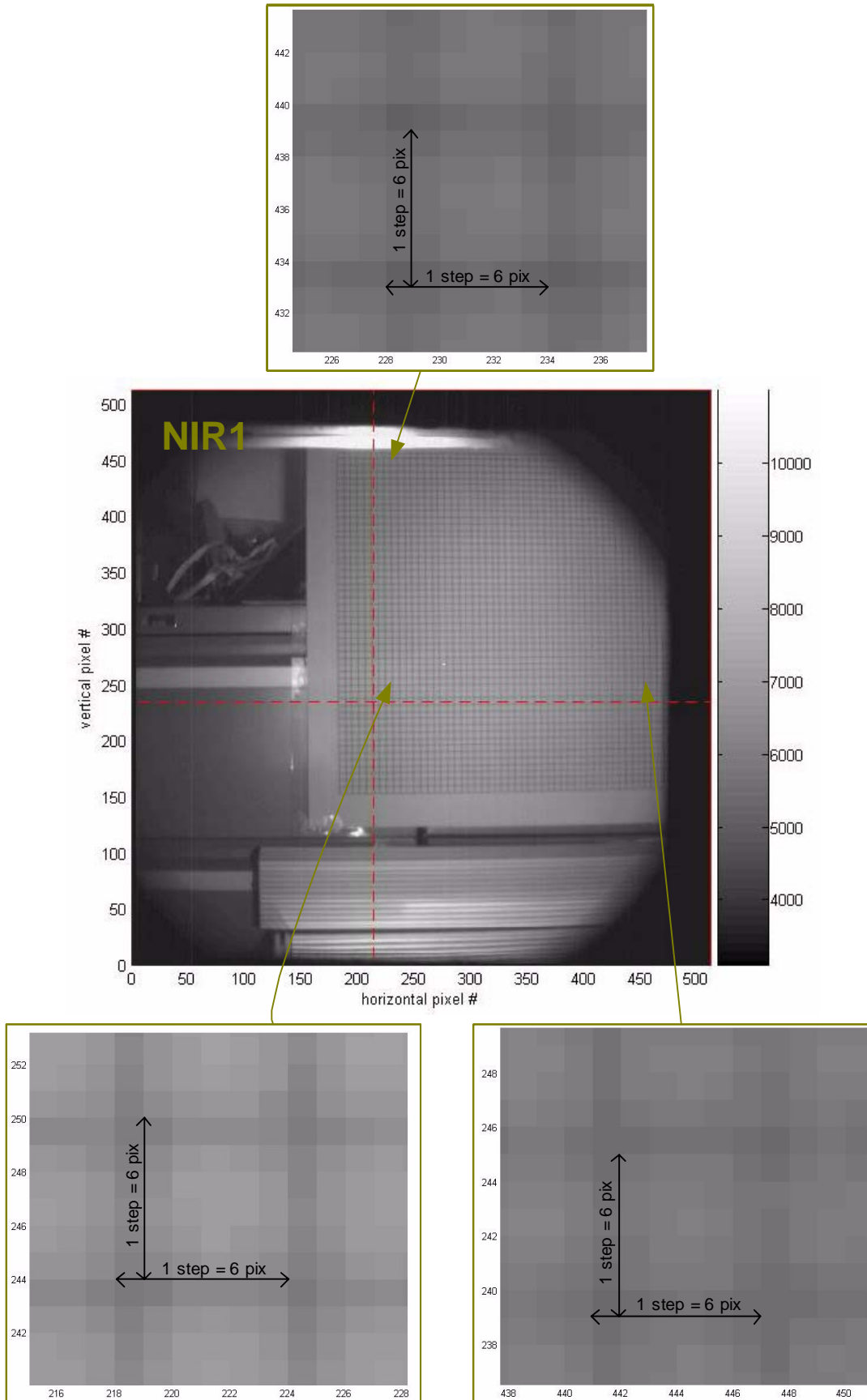
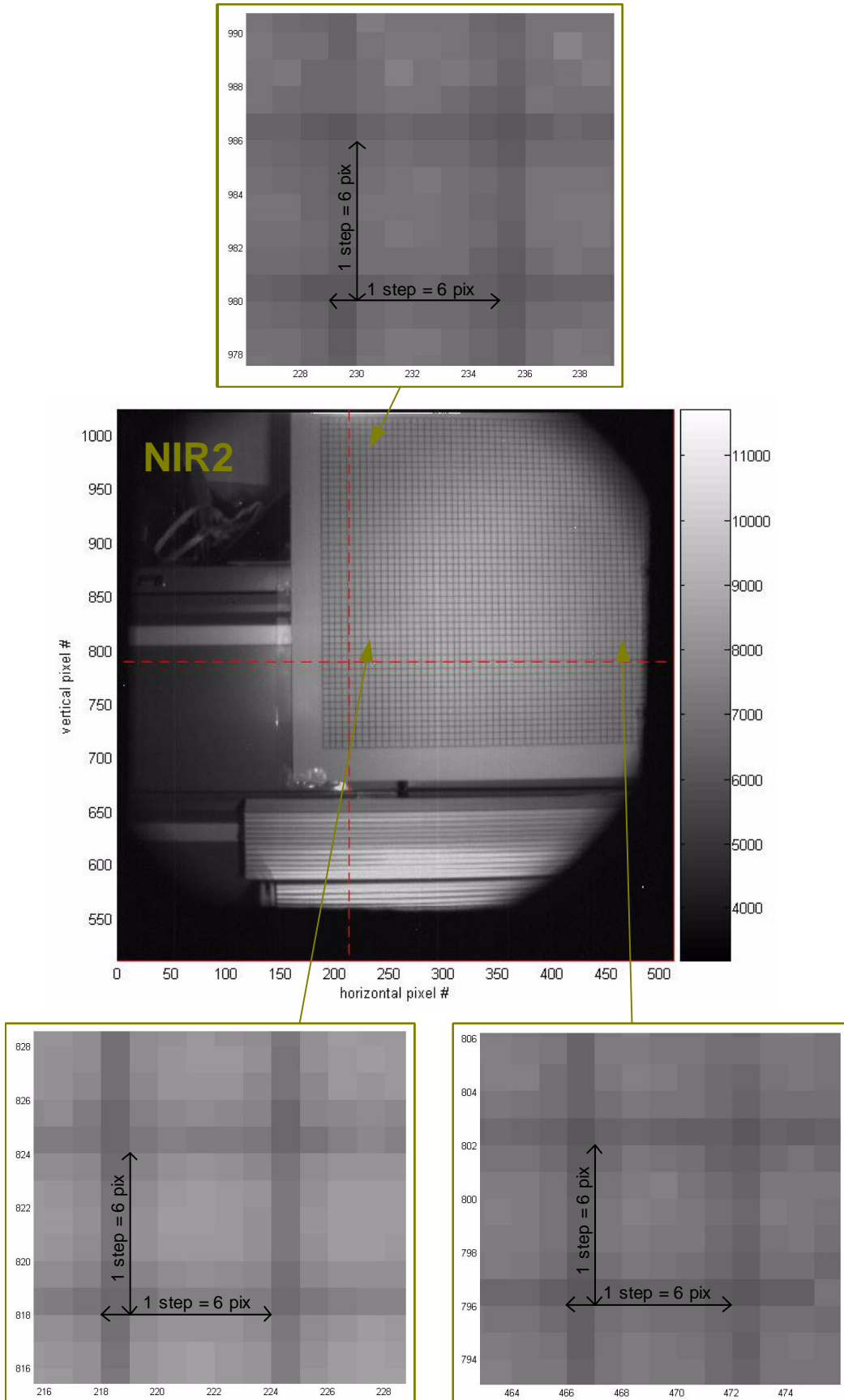


Figure 7.2-6 VMC image of regular grid in VIS channel.



**Figure 7.2-7** VMC image of regular grid in NIR1 channel.



**Figure 7.2-8** VMC image of regular grid in NIR2 channel.

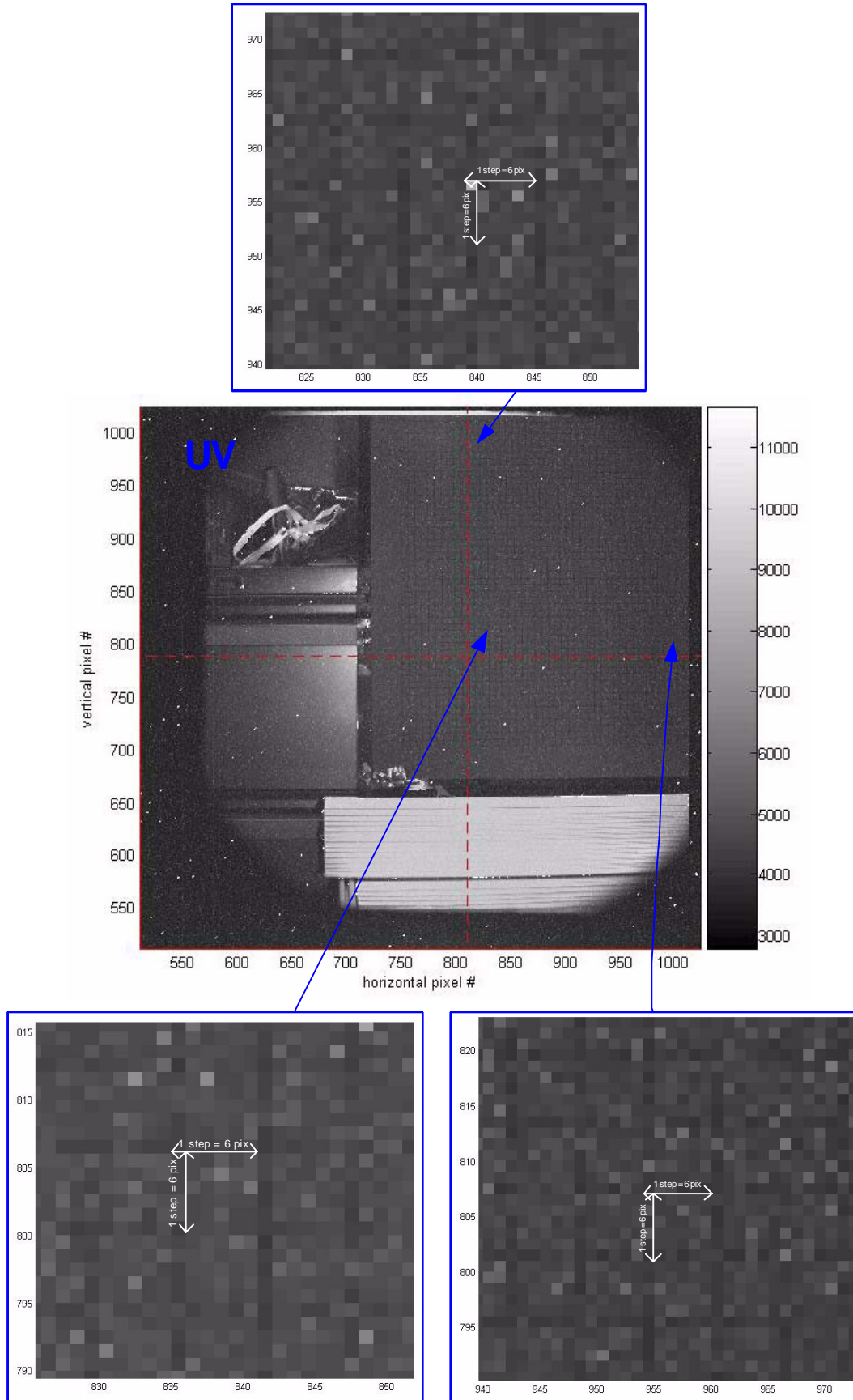


**Figure 7.2-9** VMC image of regular grid in UV channel.

In order to investigate point spread function of the VMC optics, images of pin-hole aperture were taken. Figures 7.2-10 and 7.2-11 show these images with suitable exposure time for every channel (VIS – 0.5 ms, NIR1 – 2.5 ms, NIR2 – 7.6 ms, UV – 1.5 ms). One can see that such image as a point source occupies 1 pixel of VMC CCD matrix. In figure 7.2-11 location of VMC channels and pixel numbering are the same as for IDL image processing (see figure 2.2-7) with theoretical center of VIS channel (811; 209) and others (yellow daggers). In VIS channel crossing of red dashed lines denotes actual position of pin-hole image. These lines are symmetrically transformed to others channels. Here, some misalignment between the channels is evident.

Figure 7.2-12 demonstrates relative location of pin-hole images on a background of flat-field image. All the marks are the same as in figure 7.2-11. Using such flat-field image it is possible to investigate FOV shape (see table 7.2-1).

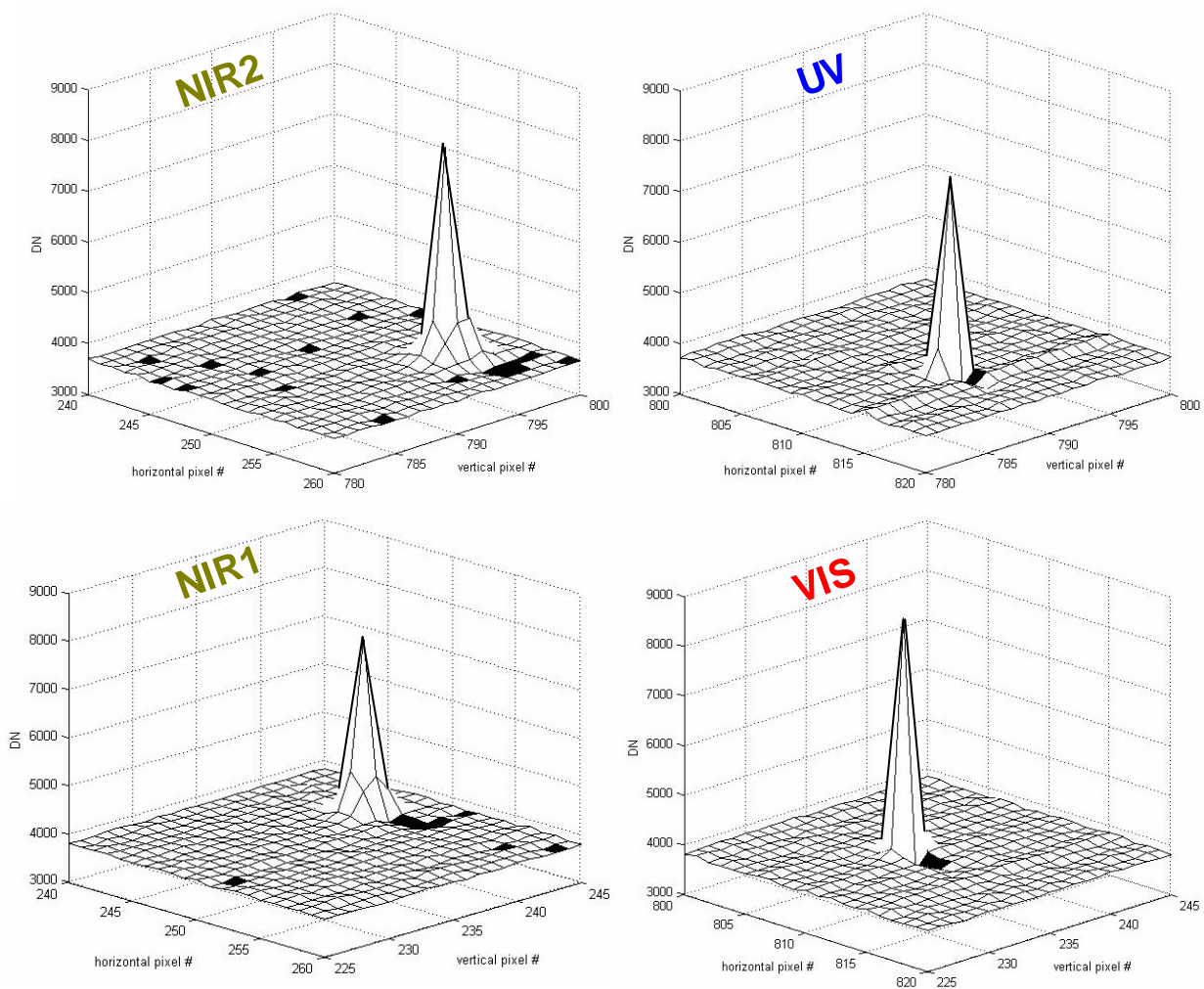


**Figure 7.2-10** Curves of point spread function for every channel.

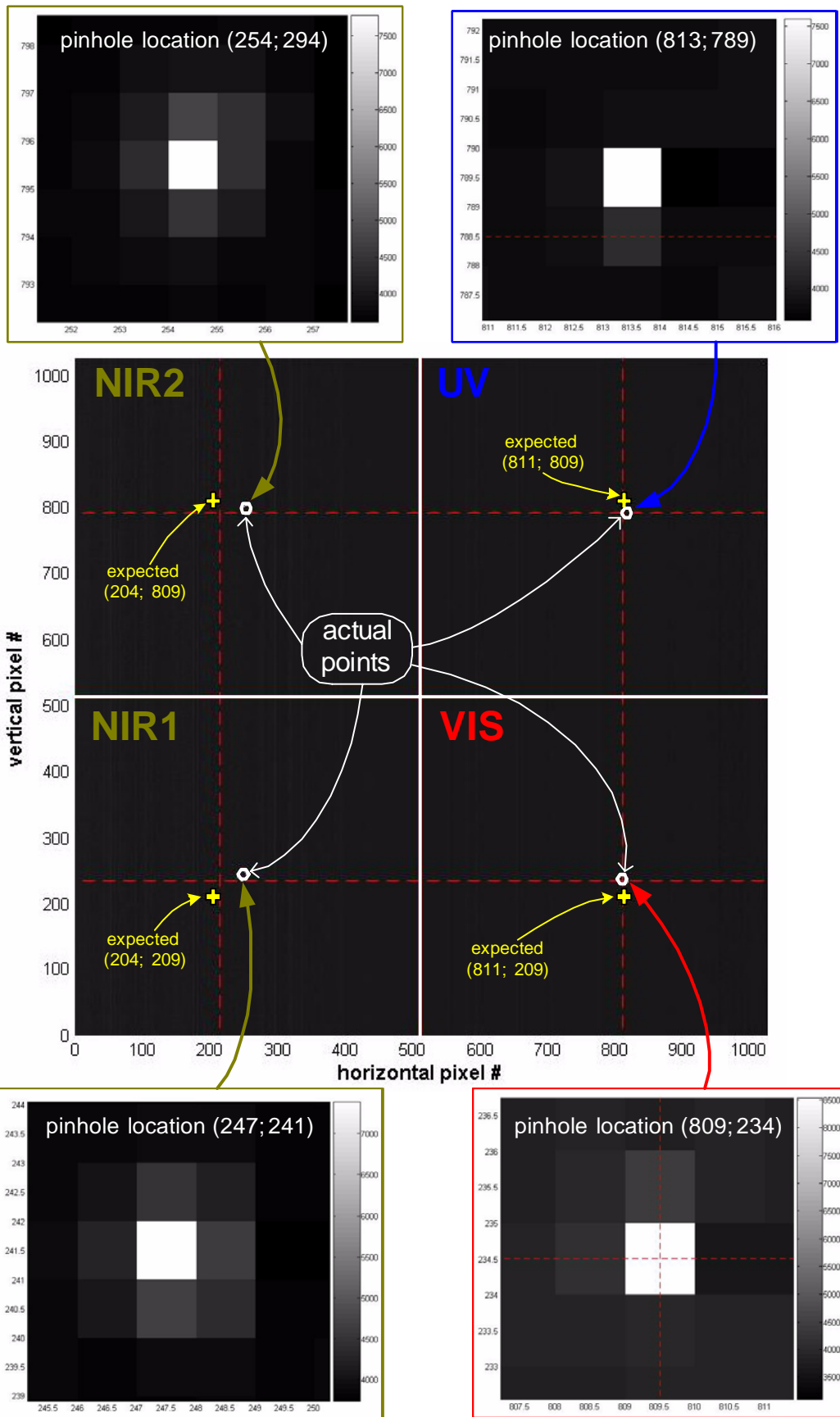
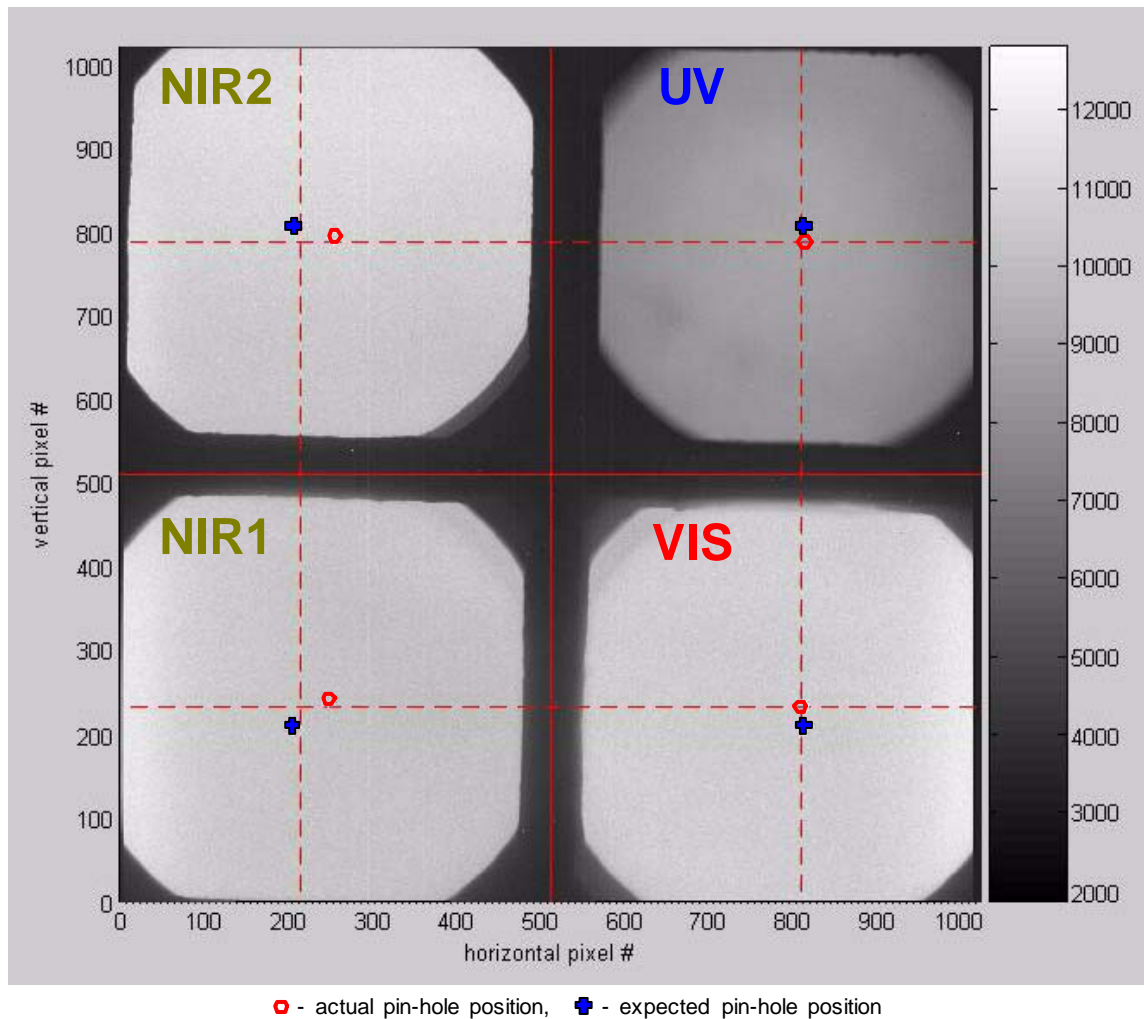


Figure 7.2-11 General view of pin-hole images.



**Figure 7.2-12** Location of pin-hole images on a background of flat-field image.

- Width and shape of the FOV
- FOV of individual pixel
- Point spread function (laboratory and in-flight)
- In FOV distortions (using regular grid images)

### 7.2.3 Channels co-alignment

- Reference to chapter 9: In flight observations of point sources (Venus, stars)

### 7.2.4 Stray Light Characterization

- Reference to chapter 9: In flight stray light characterization

## 7.3 Dark Signal Properties

### 7.3.1 Dark Signal Behavior with Temperature and Exposure

The VMC dark signal is a sum of dark current that is a function of temperature and exposure time and a bias – constant electronics offset which is about 3300-3400 DN. The figure 7.3-1 shows the covered behaviour of the dark signal with temperature and exposure time.

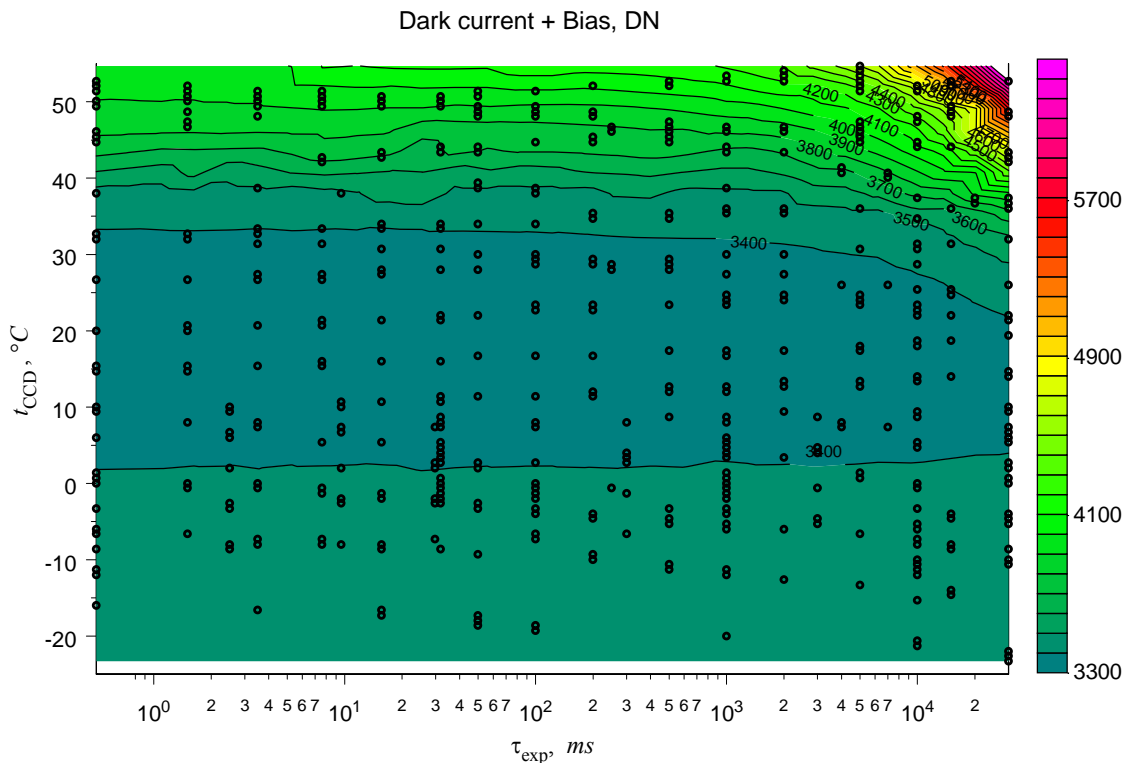


**Figure 7.12.** Dark signal as a function of the exposure time and CCD temperature, average over whole matrix except hot pixels and shaded boundary frame. Measured points are shown with the black circles.

For the temperatures below  $\sim 35^{\circ}\text{C}$  and all available exposures (0.5ms-30s) the dark signal is mainly equal to the electronics offset. At  $t > 40^{\circ}\text{C}$  the increase of dark current with temperature becomes dominant.

Figure 7.1-9 shows bright columns that are characteristic features of the CCD. Their behaviour with temperature and exposure differs from that of the rest of CCD (Figure 7.3-2). The figure 7.3-2 shows brightness cross section through the CCD for the images taken at about constant temperature but with different exposure times. The dark signal in surrounding CCD pixels increases faster with exposure than that in dark columns.

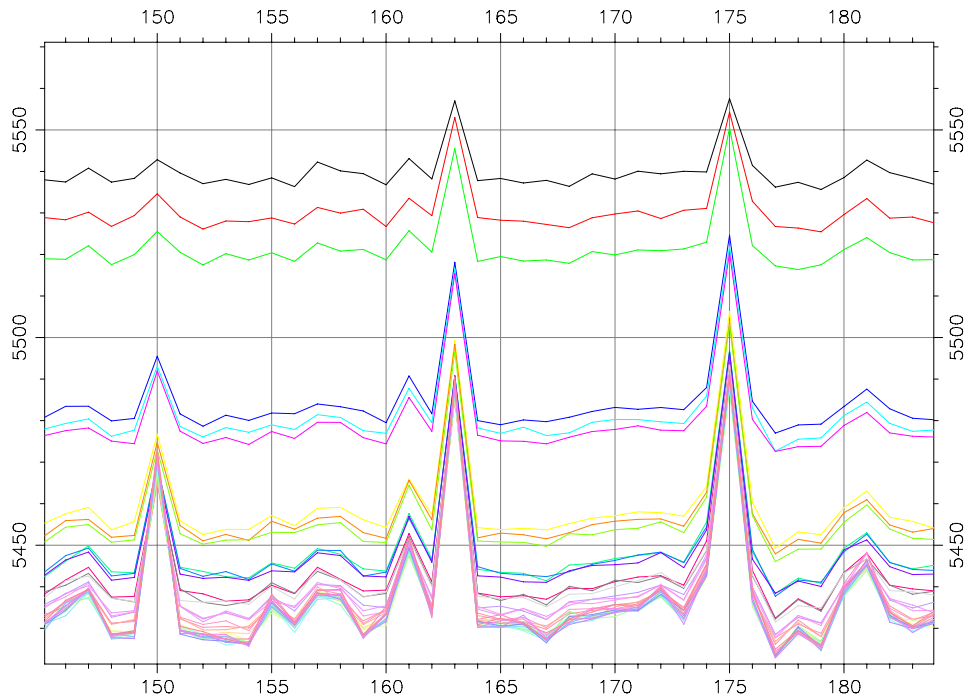


**Figure 7.13** Behaviour of the dark signal in the vicinity of the bright columns with exposure time. Exposure time increases from bottom to top of the plot.

### 7.3.2 Dark Signal Noise

The figure 7.3-3 shows the field of dark signal noise as function of exposure time and CCD temperature. This plot represents standard deviation of the CCD counts obtained by subtraction of two subsequent images. Except for the region of high temperatures and high exposures the dark noise is below 25 DN that is close to the standalone CCD noise. Note that the standard deviation of the dark signal in each single image is much higher that indicates that each CCD pixels behaves individually and that a matrix of dark current noise instead of a single value should be used for dark current correction.

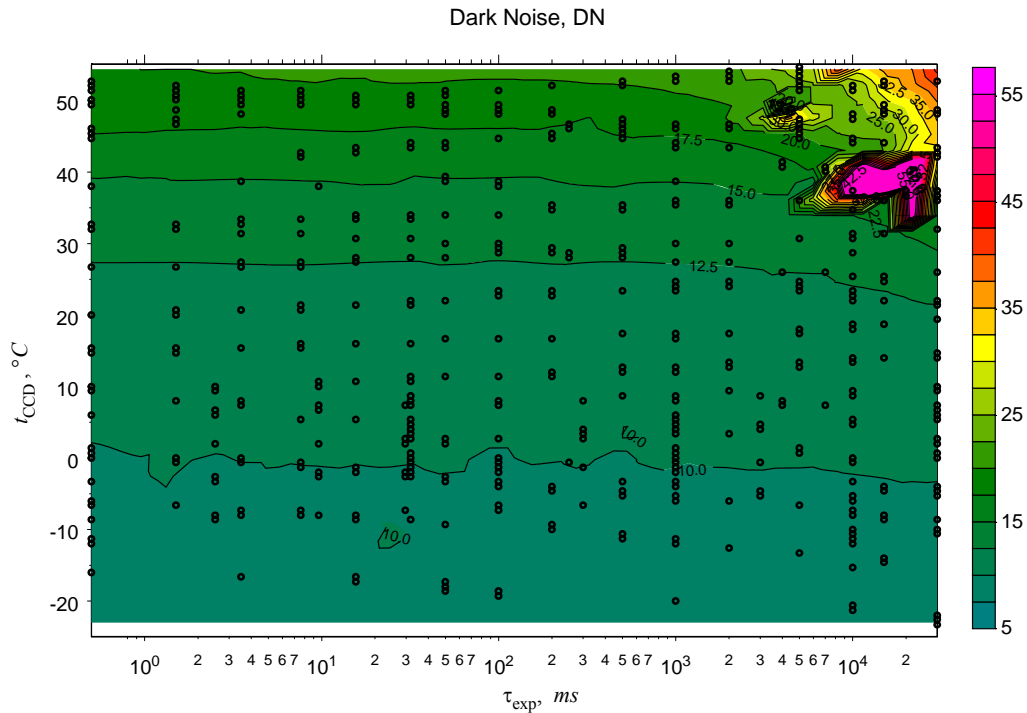


**Figure 7.14** Dark signal noise as a function of the exposure time and CCD temperature, average over whole matrix except hot pixels and shaded boundary frame. Measured points are shown with the black circles.

#### 7.4 Radiometric Properties

Figure 7.4-1 shows a set of exposure times and CCD temperatures for the laboratory measurements carried out for flat field and absolute radiometric calibration. During the calibration, the exposure time and CCD temperature were continuously changed, and for every condition point  $\{\tau_{\text{exp}}, t_{\text{CCD}}\}$ , 3 measurements were taken at the same exposure time and nearly the same temperatures of CCD. It is evident that no one image satisfies simultaneously in all 4 channels to the two requirements: 1) signal is sufficiently high, and 2) image is not saturated. An example of the image is given in Fig 7.4.-2. The intensity of the calibration source — integrating sphere — was not constant during the calibration, the measurements were taken with halogen lamps of the sphere, and at 2 positions of dial gauges: 30 and 45. The absolute calibration of the sphere was made in 2001 for dial gauges position of 12. The spectral shape of the sphere has been changed, although very little. To account for those changes and define the absolute spectrum, the three detectors inside the sphere are to be used: UV, VIS, and NIR. Vacuum chamber window transmission must be also taken into account. Spectral sensitivities of the channels must be known for exact calibration.

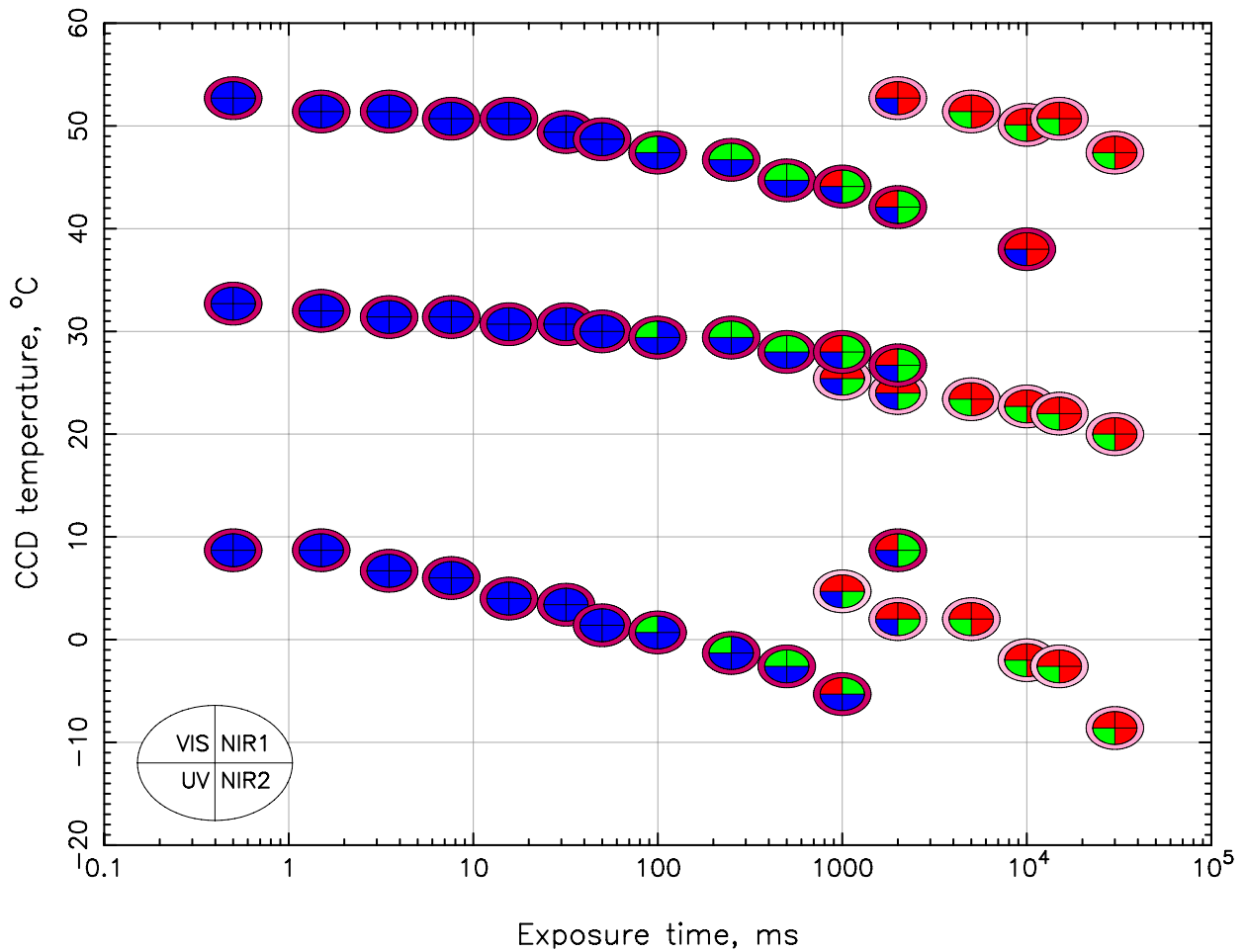


**Figure 7.4-1** Laboratory measurements with integrating sphere. Colors designate, by channels, the average signal level in the central part (300x300 pixels) of the channel field of view: blue — low signal noisy images ( $S - \text{DARK} < 500$ ), red — saturated images ( $S > 9300$ ), and green — images that are not fit into any of the two groups, i.e. images suitable for calibration. Color from dark to light magenta on of the outer ring designate the intensity of the sphere set for the measurements: in the visible channel it was varied from  $8.2 \cdot 10^2$  to  $3.5 \cdot 10^2 \text{ erg}/(\text{s cm}^2 \text{ sr } \mu\text{m})$ .

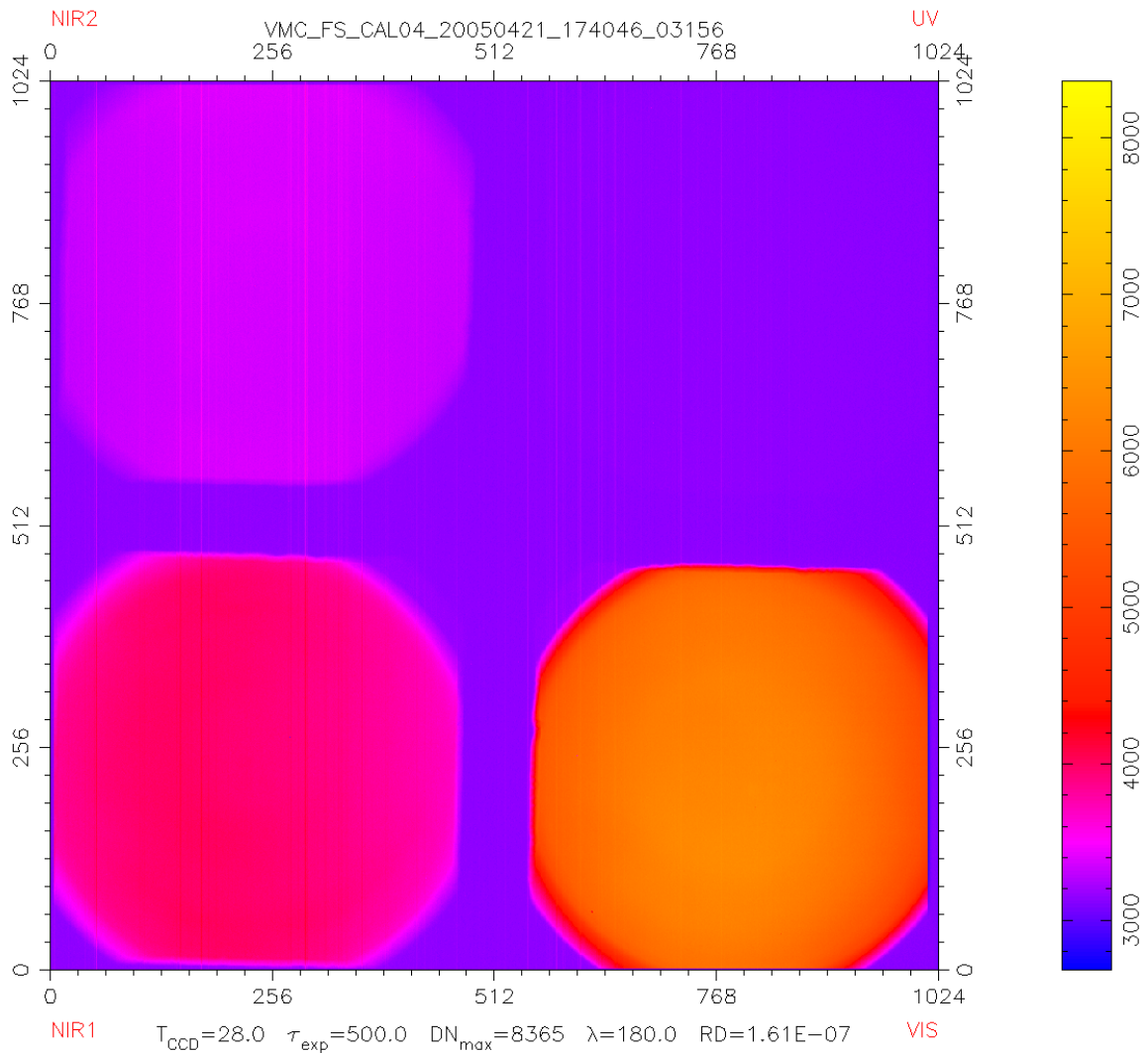


**Figure 7.4-2** Example of the integrating sphere image taken for the flat field and absolute radiometric calibration.

Let us consider the values measured by the camera and those to be defined during the calibration. As far as the calibration source – the integrating sphere – has its own spectrum, we have to consider the spectral properties of the source and the camera also for the radiometric calibrations, although they will be defined in the next section.

The CCD signal is equal to the number of photons incident on the CCD times quantum efficiency

$$DN \equiv DN_{RAW} - DN_{DARK} = \beta N_{ph} Q \cdot \tau; \quad DN = \frac{DN}{e} \frac{\text{photon}}{s} \frac{e}{\text{photon}} s,$$

where  $\beta$  is some constant coefficient (electronics gain,  $[\frac{DN}{e}]$ ),  $N_{ph}$  is the number of photon flux (photons per second),  $Q$  is the quantum efficiency of the CCD, and  $\tau$  is the exposure time. To make the dimensions clear we keep the units of electrons and photons, although they are dimensionless as numbers of particles.

When the photon flux and quantum efficiency are wavelength dependent, we consider the photon flux per unit wavelength and integrate over wavelength

$$DN = \beta\tau \int N_{ph}(\lambda)Q(\lambda) d\lambda; \quad DN = \frac{DN}{e} s \frac{photon}{s \text{ cm}} \frac{e}{photon} cm.$$

Number of photons is equal to the ratio of the flux to the energy of one photon.

$$N_{ph}(\lambda) = \frac{F_1(\lambda)}{hc/\lambda} \quad \frac{photon}{s \text{ cm}} = \frac{erg / s / cm}{erg / photon}$$

Flux is affected by the optics transmission

$$F_1(\lambda) = F'(\lambda)T(\lambda)$$

Thus, the CCD signal is expressed as follows:

$$DN = \beta\tau \int \frac{F'(\lambda)T(\lambda)\lambda}{hc} Q(\lambda)d\lambda; \quad DN = \frac{DN}{e} s \frac{(erg / s / cm) \text{ cm}}{(erg s)(cm / s) / photon} \frac{e}{photon} cm$$

If the spectral sensitivity is defined with respect to intensity, the field of view of a pixel  $\Omega$  and the area of the entrance window  $A$  must be added:

$$DN = \beta\tau \int \frac{I(\lambda) A \Omega T(\lambda)\lambda}{hc} Q(\lambda) d\lambda = \tau \int I(\lambda) S(\lambda) d\lambda \quad (7.4.1)$$

Thus the spectral sensitivity  $S(\lambda)$  with respect to the intensity of the incident radiation is equal to

$$S(\lambda) = \frac{\beta A \Omega T(\lambda) Q(\lambda)\lambda}{hc} \sim T(\lambda) Q(\lambda)\lambda \quad (7.4.2)$$

The last value (normalized) has to be compared with the normalized spectral sensitivity defined with respect to the intensity of the incident radiation. The spectral calibration will be considered in details in the next section.

The purpose of the radiometric calibration is to provide a quantity that can be compared with the theoretical simulations of the measurements. This quantity may be defined quite arbitrary, e.g. the intensity of the radiation taken with the spectral resolution of our instrument  $I_c$  :

$$I_c = \frac{\int I(\lambda) S(\lambda) d\lambda}{\int S(\lambda) d\lambda} \quad \left[ \frac{erg}{s \text{ cm}^2 \text{ sr cm}} \right] \quad (7.4.3)$$

For the camera,  $I_c$  a matrix  $I_c(i, j)$ .

Equations 7.4.1–7.4.3 assume the spectral sensitivity of the camera in general, or, in fact, the spectral sensitivity of an individual pixel. This would be an ideal case, which is not feasible both due to calibration difficulties and huge informational content of that multidimensional value. We assume that the spectral sensitivity  $S_c(\lambda)$  characterizes channels and it is common to all the pixels of the channel, so that variations other than spectral ones are given by the flat field  $S_{FF}(i, j)$ . Thus, Eq. 7.4.1 should be re-written as follows:

$$DN = \tau \tilde{S}_{FF}(i, j) \int I(\lambda) S_c(\lambda) d\lambda \quad , \quad (7.4.4)$$

where the matrix  $\tilde{S}_{FF}(i, j) \left[ \frac{DN}{s(\text{erg} / s / \text{cm}^2 / \text{sr})} \right]$  is a function of temperature and, generally speaking, exposure time.

For convenience, dependence on the pixel  $(i, j)$  can be assigned to a dimensionless value  $S_{FF}(i, j)$ , which will represent just the heterogeneity of the CCD matrix, while radiometric properties are given by the scalar value  $S_R$ :

$$\tilde{S}_{FF}(i, j) = S_R S_{FF}(i, j) \quad (7.4.5)$$

Both components,  $S_R$  and  $S_{FF}$  are in principle functions of temperature, exposure time, and may be even intensity of radiation, if the CCD is nonlinear with respect to it.

It is convenient to normalize the spectral sensitivity:

$$\int S_c(\lambda) d\lambda = 1, \quad (7.4.6)$$

so we can write simply

$$I_c = \int I(\lambda) S_c(\lambda) d\lambda \quad (7.4.7)$$

The calibrated signal (Eq. 7.4.3) is therefore given by the following equation:

$$I_c(i, j) = \frac{DN(i, j)}{\tau \tilde{S}_{FF}(i, j)} \quad , \quad (7.4.8)$$

and the flat field can be defined by means of calibration measurements as

$$\tilde{S}_{FF}(i, j) = \frac{DN(i, j)}{\tau I_c(i, j)} = \frac{DN(i, j)}{\tau \int I(\lambda) S_c(\lambda) d\lambda} \quad (7.4.9)$$

The intensity  $I(\lambda)$  of the calibration source (integrating sphere) must be known, and the spectral sensitivities of the channels of the camera must be defined in advance during the spectral calibration. If the source spectrum is a smooth function, as a first approximation Eq. 7.4.9 can be simplified:

$$\tilde{S}_{FF}(i, j) = \frac{DN(i, j)}{\tau I(\lambda_c)} \quad , \quad (7.4.10)$$

where  $\lambda_c$  (strictly defined from the equation  $I(\lambda_c) = \int I(\lambda) S_c(\lambda) d\lambda$ ) is the mean wavelength of the channel (it is not equal to the maximum sensitivity wavelength).

Thus, the computational procedure for the radiometric calibration was the following:

- 1) Definition of the computational wavelength grid  $\lambda_j$  (0.001  $\mu\text{m}$  step) and interpolation to that grid of the following values:
  - a. Integrating sphere calibrated spectrum,
  - b. Spectral sensitivities of the channels,

c. Vacuum chamber window transmission.

2) Definition of the absolute value of the signal  $I_c$  as follows:

$$I_c = \frac{\sum_j I_S(\lambda_j) T_{VC}(\lambda_j) S_c(\lambda_j)}{\sum_j S(\lambda_j)} \frac{D_c}{D_{c0}},$$

where  $I_S$  is the calibrated radiance,  $T_{VC}$  is the vacuum chamber transmission,  $S_c$  is the spectral sensitivity of the channel,  $D_c/D_{c0}$  is the ratio of the sphere's appropriate detector signal to that measured during the sphere calibration in 2001 (average value is taken), corresponding to the channel: UV for VMC UV channel, VIS for VMC VIS, NIR for VMC NIR1 and VMC NIR2

3) Radiometric calibration according to Eq. 7.4.9 and 7.4.5.

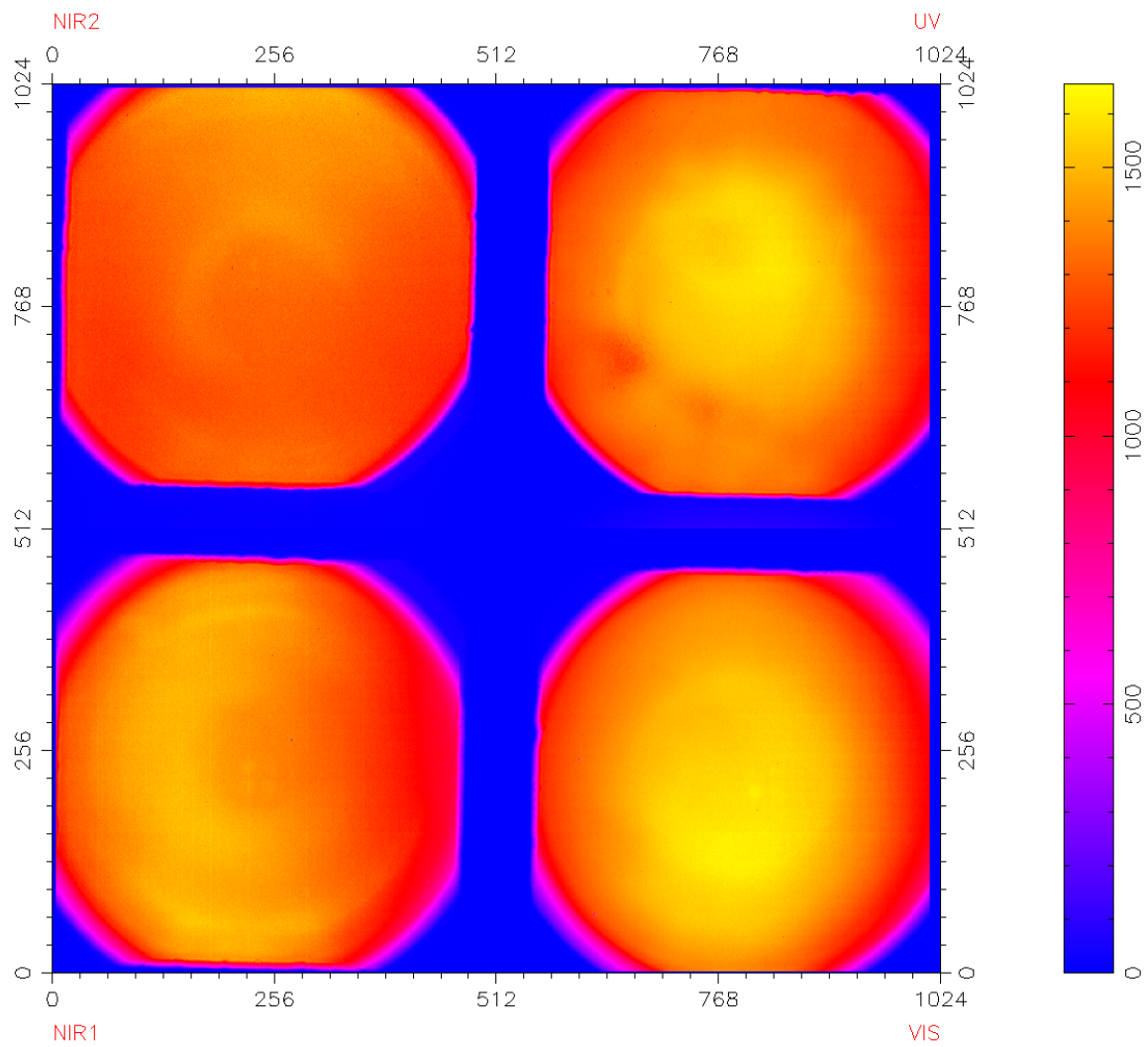


**Figure 7.4-3** *Dimensionless flat field of the VMC channels.*

	UV	VIS	NIR1	NIR2
Sensitivity DN/(erg/s/cm <sup>2</sup> /sr/μm)/ms	1.8E-3	1.1E-2	9.7E-4	2.6E-4
Exposure time required to achieve full well (6000 DN), ms, Venus <b>dayside</b> *	6.9	0.47	12	55
Exposure time required to achieve full well (6000 DN), ms, Venus <b>dayside</b> **	21	1.1	31	230
Exposure time required to achieve full well (6000 DN), ms, Venus <b>nightside</b> *	4.0E+9	4.0E+8	1.2E+6	4.6E+5
* Assuming the following values of the Venus brightness [erg/s/cm <sup>2</sup> /sr/μm]:				
Dayside	5.0E+05	1.2E+6	5.0E+5	4.2E+5
Nightside	8.7E-04	1.4E-3	5.0E+0	5.0E+1
** Assuming the following values of the Venus brightness [erg/s/cm <sup>2</sup> /sr/μm] (taken for theoretical VMC sensitivity estimations in 2002-2003):				
Dayside	1.6E+05	5.0E+5	2.0E+5	1.0E+5

**Table 7.4-1** Radiometric properties of the VMC. Sensitivity of the VMC channels averaged over 300x300 pixels in the centers of channels at  $t_{ccd} \approx 27^\circ$  and  $\tau_{exp} = 500$  ms.

- Linearity, i.e mean value of signal vs integrating sphere brightness

## 7.5 Spectral Properties

Spectral properties of four channels were determined in the laboratory calibrations. Figures 7.5-1 and 7.5-2 show comparison of the measured spectral properties with those specified in original VMC optics specification. The visible filter deviates from specification but that was agreed with optics manufacturer since this deviation does not reduce performance. The NIR1 filter is also shifted from its expected position. This resulted from a mistake of manufacturer. However it was decided to leave the filter as it is since there was no degradation of scientific performance.

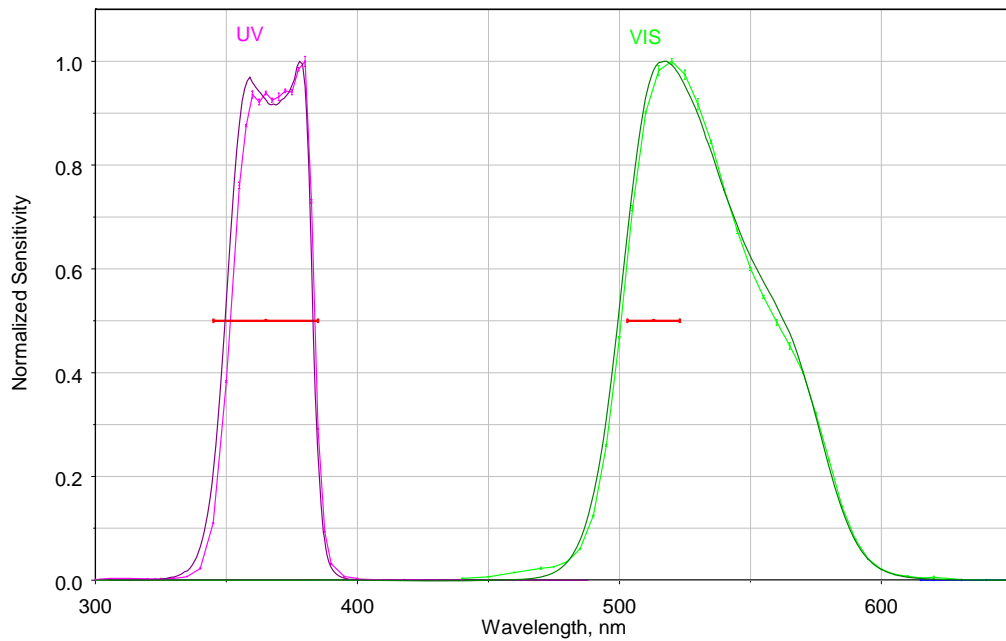


**Figure 7.15** Normalized spectral sensitivities of the VMC UV and VIS channels. Bright curves with error bars – measurements in MPS; dark curves — sensitivities derived from the CCD quantum efficiency and filter transmissions provided by manufacturers; red bars — original specification.

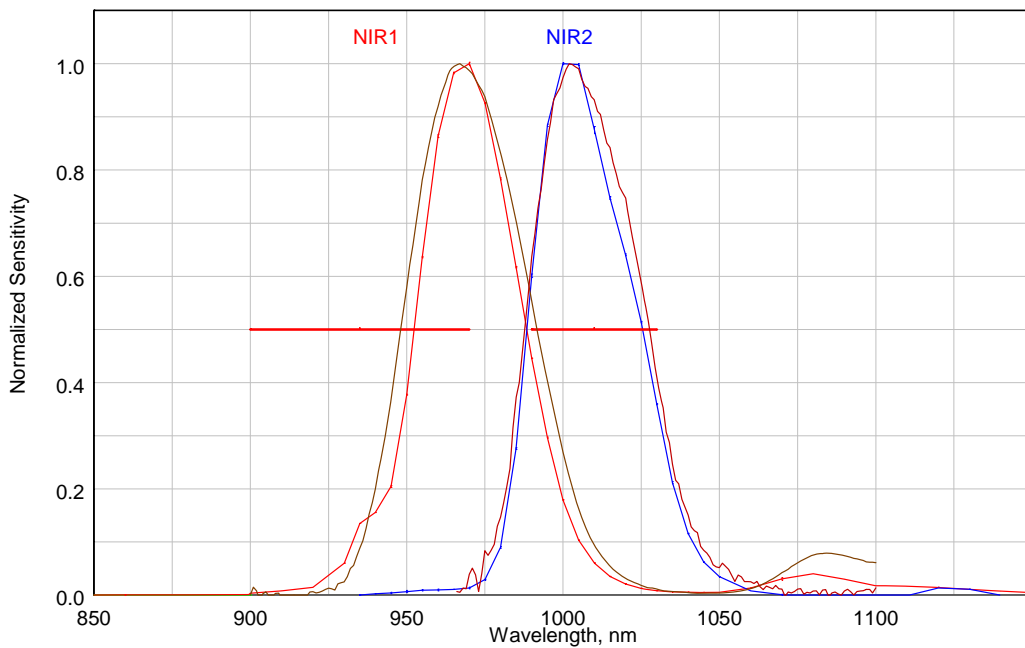


**Figure 7.16** The same as in figure 7.5-1 for NIR channels

During the calibrations, the current of the relative detector  $I_D [A]$  is proportional to the intensity of the incident radiation  $I(\lambda) \left[ \frac{\text{erg}}{\text{s cm}^2 \text{ cm sr}} \right]$  :

$$I_D = B \int I(\lambda) S_D(\lambda) d\lambda, \quad A = \text{cm}^2 \text{sr} \frac{\text{erg}}{\text{s cm}^2 \text{ cm sr}} \frac{A}{\text{erg/s}} \text{cm}, \quad (7.5.1)$$

where  $B [cm^2 sr]$  is some constant geometric coefficient.

Taking the ratio of Eq. (7.4.1) and (7.5.1), we have:

$$\frac{DN}{I_D} = \frac{\tau \int_{\Delta\lambda} I(\lambda) T_1(\lambda) S(\lambda) d\lambda}{B \int_{\Delta\lambda} I(\lambda) S_D(\lambda) d\lambda}$$

Here we introduced also additional transmission  $T_1(\lambda)$  of the optics between the relative detector and the camera, e.g. vacuum chamber window. Assuming that  $S(\lambda)$ ,  $T_1(\lambda)$ , and  $S_D(\lambda)$  change slowly with respect to the monochromator bandpass  $\Delta\lambda$  (note, there is no similar requirement to the source intensity), we may write:

$$\frac{DN}{I_D} \approx \frac{\tau T_1(\lambda) S(\lambda) \int I(\lambda') d\lambda'}{B S_D(\lambda) \int I(\lambda') d\lambda'} = \frac{\tau T_1(\lambda) S(\lambda)}{B S_D(\lambda)},$$

and

$$S(\lambda) \approx \frac{DN}{\tau} \frac{B S_D(\lambda)}{I_D T_1(\lambda)} \sim \frac{DN}{\tau} \frac{S_D(\lambda)}{I_D T_1(\lambda)}. \quad (7.5.2)$$

Without relative detector, Eq (7.4.1) is to be used:

$$DN = \tau \int_{\Delta\lambda} I(\lambda) S(\lambda) d\lambda \approx \tau S(\lambda) \int_{\Delta\lambda} I(\lambda) d\lambda.$$

and the sensitivity is defined as

$$S(\lambda) \approx \frac{DN}{\tau} \frac{1}{\int_{\Delta\lambda} I(\lambda) d\lambda} \quad (7.5.3)$$

If during the measurements the monochromator slitwidths were changing, the integral must include the changing monochromator transfer function  $S_{\Delta\lambda}(\lambda)$  :

$$S(\lambda) \approx \frac{DN}{\tau} \frac{1}{\int_{\Delta\lambda} I(\lambda) S_{\Delta\lambda}(\lambda) d\lambda} \quad (7.5.4)$$

If the source spectrum is also a slow function within the interval  $\Delta\lambda$  :

$$S(\lambda) \approx \frac{DN}{\tau} \frac{1}{\int_{\Delta\lambda} I(\lambda) S_{\Delta\lambda}(\lambda) d\lambda} \approx \frac{DN}{\tau} \frac{1}{I(\lambda) \int_{\Delta\lambda} S_{\Delta\lambda}(\lambda) d\lambda} \sim \frac{DN}{\tau} \frac{1}{I(\lambda) \Delta\lambda} \quad (7.5.5)$$

Thus, the theoretical and experimental spectral sensitivities (with respect to the intensity of the incident radiation) are defined as follows:

$$S_{theor}(\lambda) \sim T(\lambda) Q(\lambda) \lambda, \quad S_1(\lambda) \sim \frac{DN}{\tau} \frac{S_D(\lambda)}{I_D T_1(\lambda)}, \quad S_2(\lambda) \sim \frac{DN}{\tau} \frac{1}{\int_{\Delta\lambda} I(\lambda) S_{\Delta\lambda}(\lambda) d\lambda} \sim \frac{DN}{\tau} \frac{1}{I(\lambda) \Delta\lambda}$$

## 7.6 Thermal Behavior

### 7.6.1 Simulation of science operations in orbit

Simulation of the VMC thermal behavior in various scientific modes performed during the thermo-vacuum tests gives an opportunity to select an optimal regime for science operations in orbit. Dependences of the CCD, DPU and POC temperatures on observations timeline were obtained during TV tests. These dependences are shown in the following figures at different temperatures of the VMC environment (for the TV setup it is the base plate temperature of the TV chamber).

The VMC operation modes are marked in the figures in the following way:

- Limb mode (“**L**”): the regime of images acquisition, no cooling;
- Cooling mode (“**C**”): the regime of the CCD cooling by Peltier-cooler, no image acquisition;
- Standby mode (“**Stby**”): the regime the VMC “waiting” (Limb – OFF, Cooling – OFF, VMC - ON)
- VMC OFF: the regime when everything has been switched OFF.

Run 1. ( $T_{BP} = -40C$ )

Figure 1.1-1 shows ~110 minutes of VMC operated in Cooling and Limb modes in turn. Mean CCD temperature was slightly increasing. At t~97 min (vertical dotted line) the regime “L+C” (simultaneous image acquisition and cooling) was switched on. This stabilized the CCD temperature.

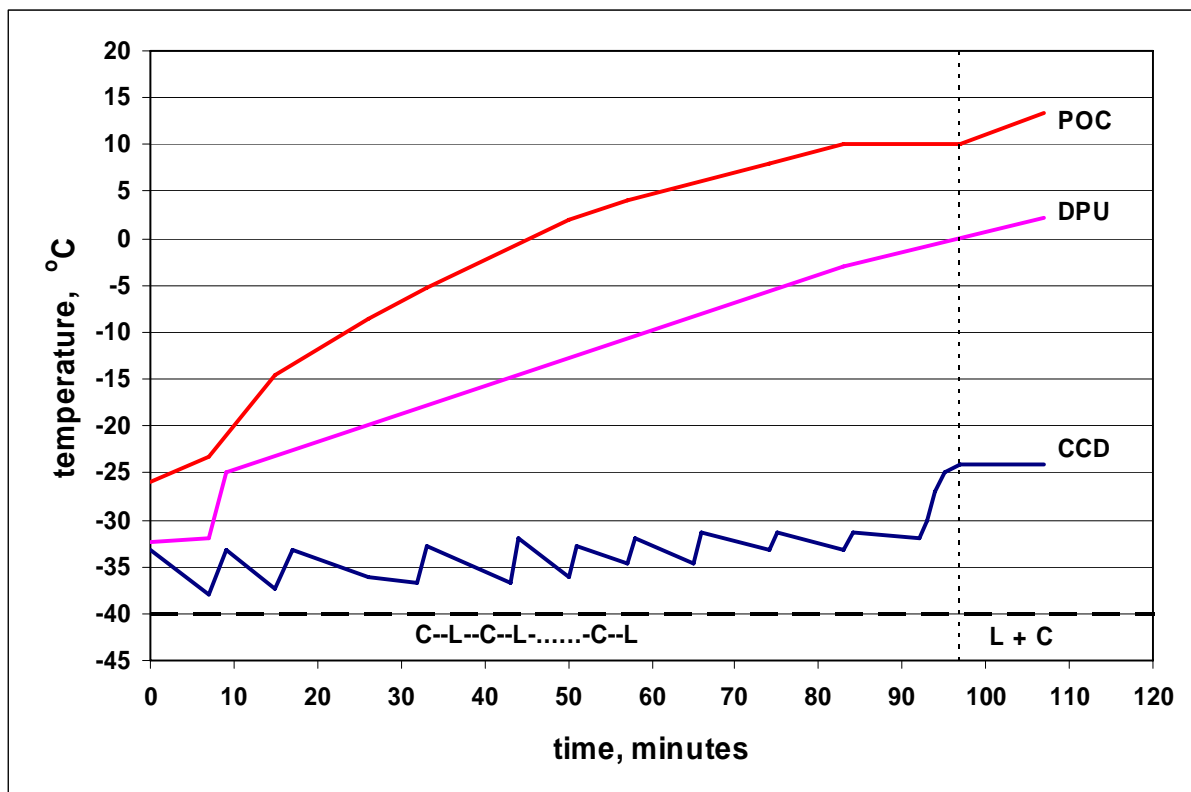


**Figure 7.17** Dependence of CCD, DPU and POC temperatures on the VMC operation time at the base plate temperature of  $-40^{\circ}C$  (“L + C” – Limb and Cooling modes simultaneously).

Run 2. ( $T_{BP} = -30C$ )

In the beginning VMC was in Standby mode for 15 minutes. Then, as in Run 1, VMC was operated in Cooling and Limb modes in turn. After ~65 min Standby mode was on that resulted 1). In stabilization of the POC and DPU temperature due to low dissipated power in these sub-units and 2). Significant raise of the CCD temperature because of heating by electronics.

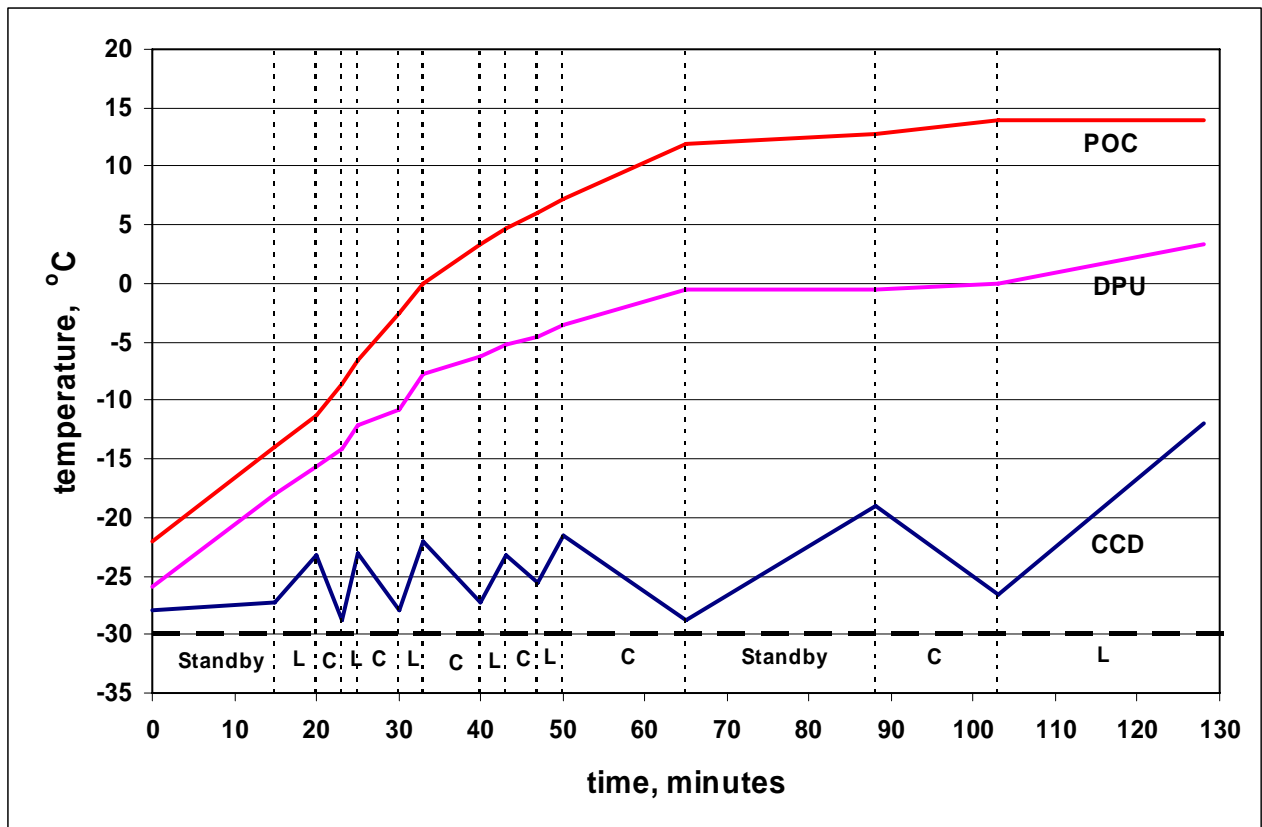


**Figure 7.18** Dependence of CCD, DPU and POC temperatures on the VMC operation time at the base plate temperature of  $-30^{\circ}C$ .

Run 3. ( $T_{BP} = -30C$ )

This run started with ~ 20 minutes of cooling that resulted in CCD temperature decrease by ~12 C. After that the Limb mode with continuous image acquisition ( $\tau=0.5$  ms,  $\Delta t=30s$ ) was on. The CCD temperature gradually increased with a rate of ~0.32C/min following the DPU and POC temperature increase. Mean temperature differences achieved and kept between the CCD and sub-units are ~30C with DPU and ~40C with POC.

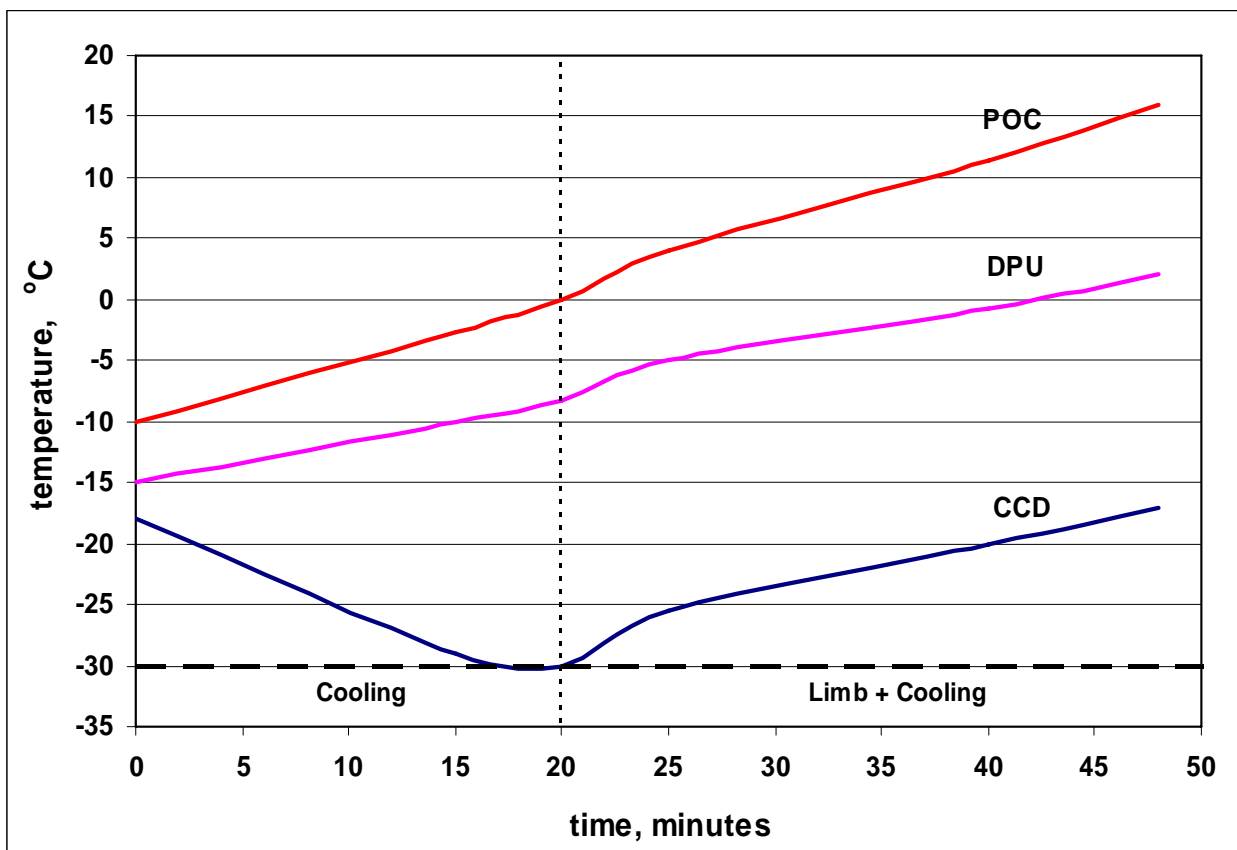


**Figure 7.19** Dependence of CCD, DPU and POC temperatures on the VMC operation time at the base plate temperature of  $-30^{\circ}C$  (“Limb + Cooling” – Limb and Cooling modes simultaneously).

Run 4. ( $T_{BP} = -20C$ )

This run had the timeline similar to that of Run 3. The difference was that on the minute 45 the cooling was off while VMC was still continuously taking images. This resulted in the CCD temperature rate increase from  $\sim 0.5C/min$  to  $\sim 1.5C/min$ .

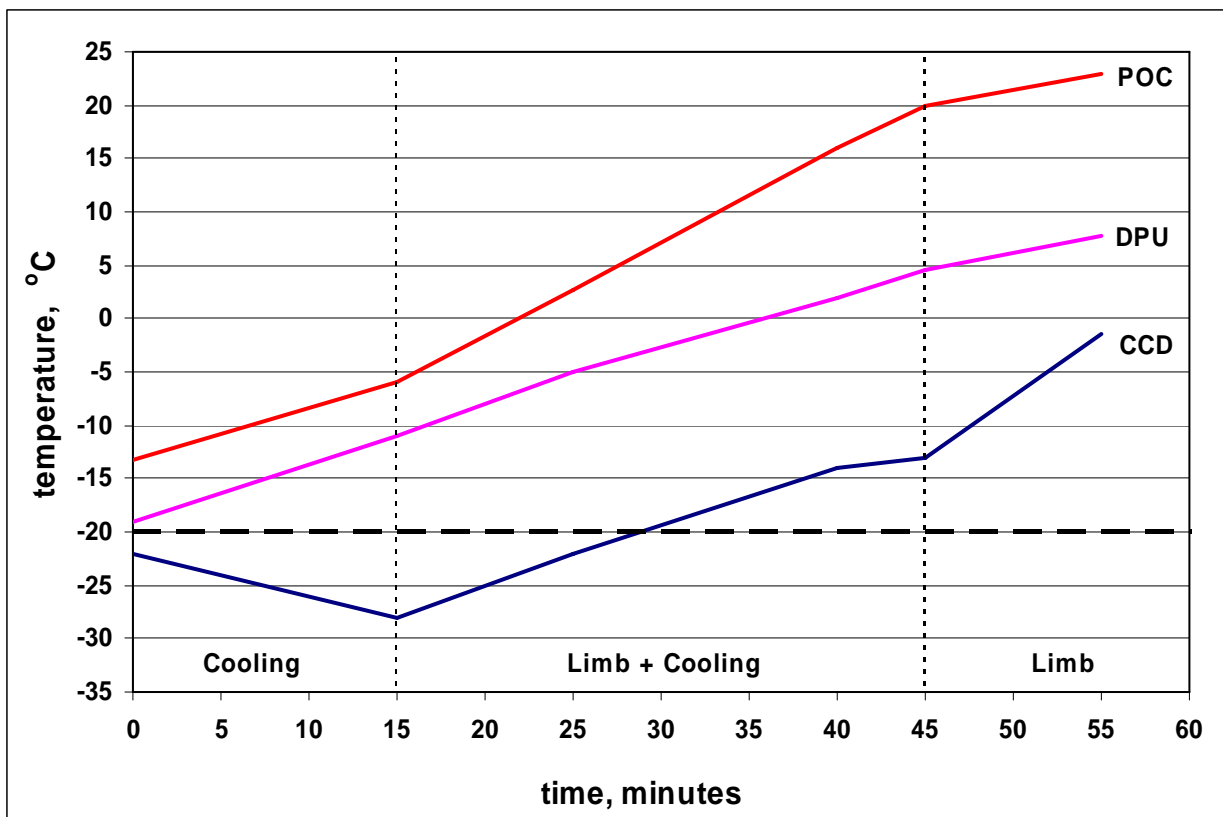


**Figure 7.20** Dependence of CCD, DPU and POC temperatures on the VMC operation time at the environment temperature  $-20^{\circ}C$  ("Limb + Cooling" – Limb and Cooling modes simultaneously).

Run 5. ( $T_{BP} = -10C$ )

In contrast to Runs 3 and 4 image acquisition (limb mode) was started right after VMC switch on together with cooling. 77 images were taken during first 40 minutes. In the first 10 minutes the peltier element managed to keep CCD temperature virtually constant ( $\sim 17C$ ). After that the CCD temperature started increasing with a rate of  $\sim 0.4 C/min$  following temperatures of electronics.

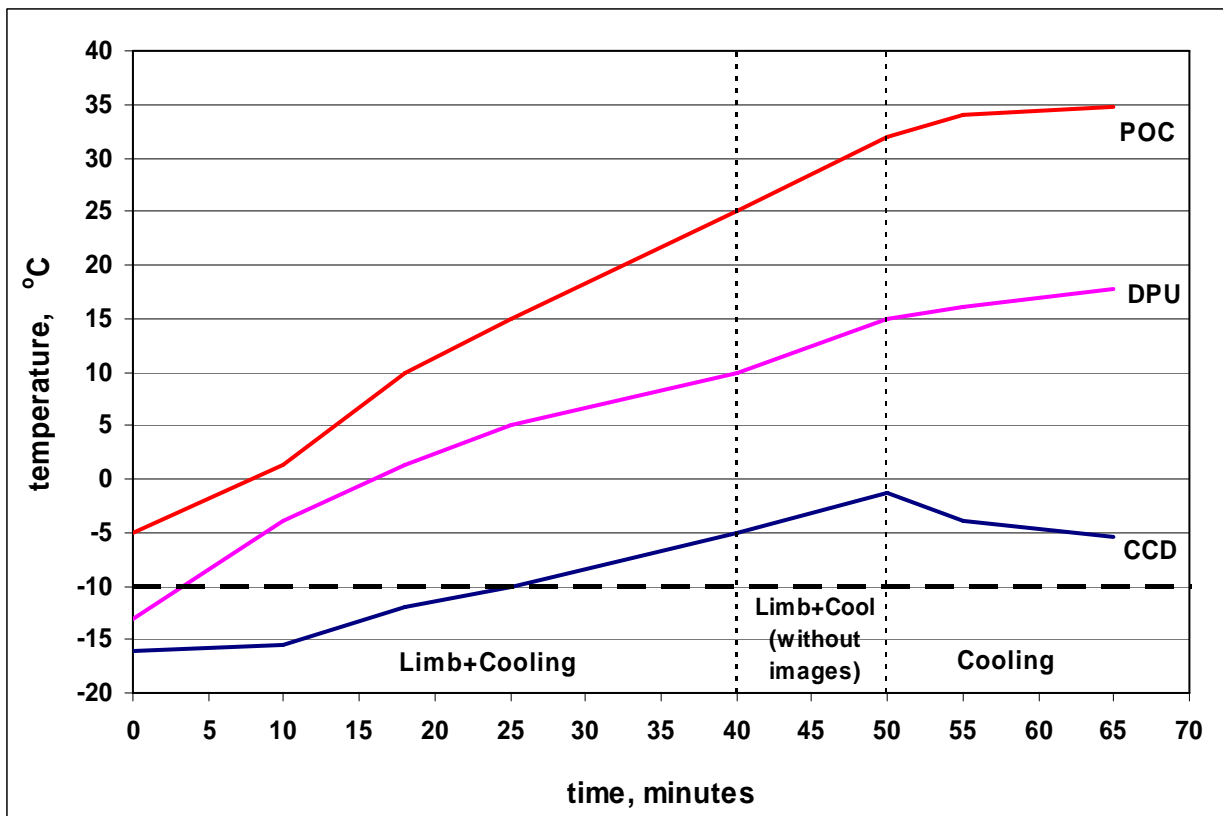


**Figure 7.21** Dependence of CCD, DPU and POC temperatures on the VMC operation time at the environment temperature  $-10^{\circ} C$  (“Limb + Cooling” – Limb and Cooling modes simultaneously).

“Limb without images” mode means Limb mode but without image acquisition. Thus, one can see that taking of images itself does not influence thermal behavior of the CCD, DPU and POC.

Run 6. ( $T_{BP} = +10C$ )

This run is similar to the Run 5: From the beginning the VMC was switched on in Limb+Cooling mode. First 20 minutes the images were acquired by manual commanding. After that continuous image acquisition was used. No significant differences in thermal behavior in these two regimes was found. At  $t \sim 37$  min image acquisition was stopped and VMC was kept in Cooling mode for about 25 minutes.

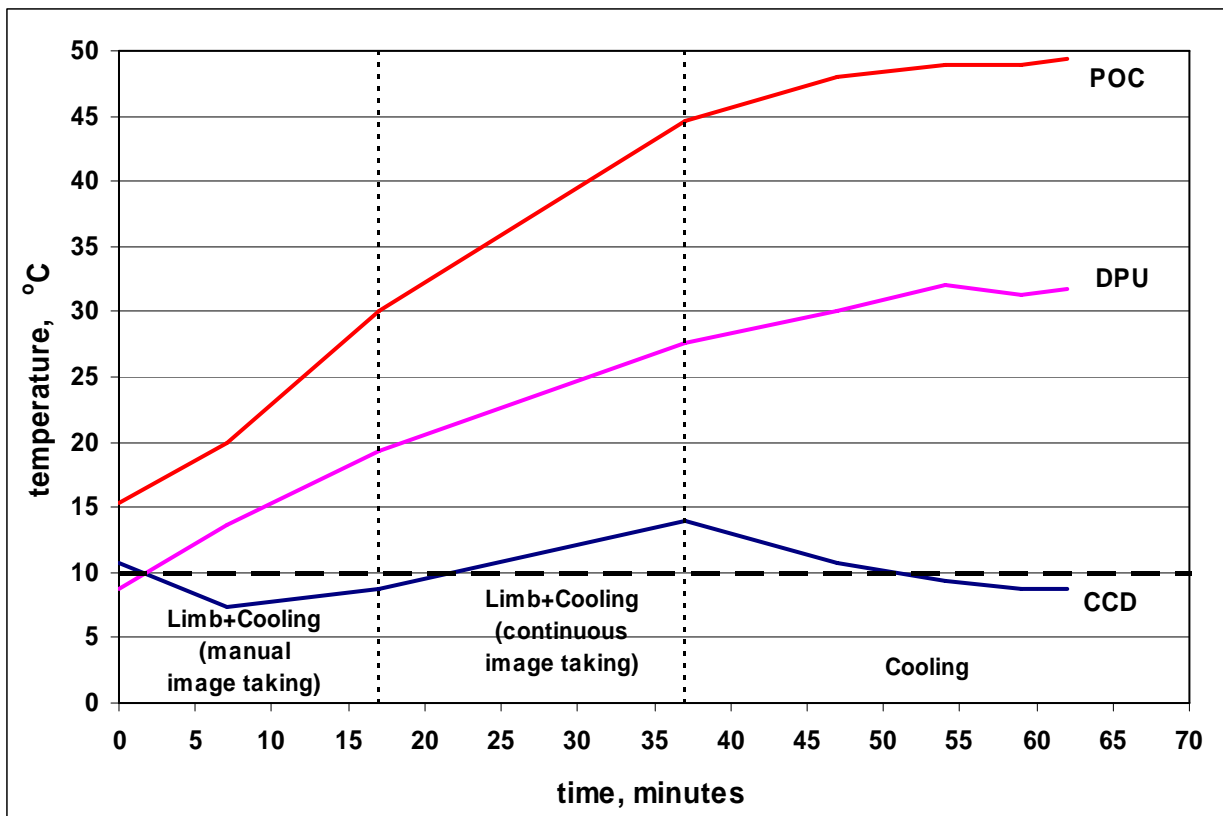


**Figure 7.22** Dependence of CCD, DPU and POC temperatures on the VMC operation time at the environment temperature  $+10^{\circ}C$  ("Limb + Cooling" – Limb and Cooling modes simultaneously).

Run 7. ( $T_{BP} = 0C$ )

In this run the off-pericenter (VEX case#2 and #3) timeline was simulated for the base plate temperature of 0C. During the first 50 minutes of this run approximately 10 min periods of continuous image acquisition (“L+C”) were interchanged with ~15 min of Cooling without imaging. This resulted in keeping the CCD temperature within 5C from that of base plate. Transition to the “standby” mode (i.e. cooling off) at t~50 min resulted in quick raise of CCD temperature due to conductive heat exchange with hot electronics. At t~70 min the VMC was OFF that resulted in decrease of POC and DPU temperatures. However at the same time the CCD temperature was going up.

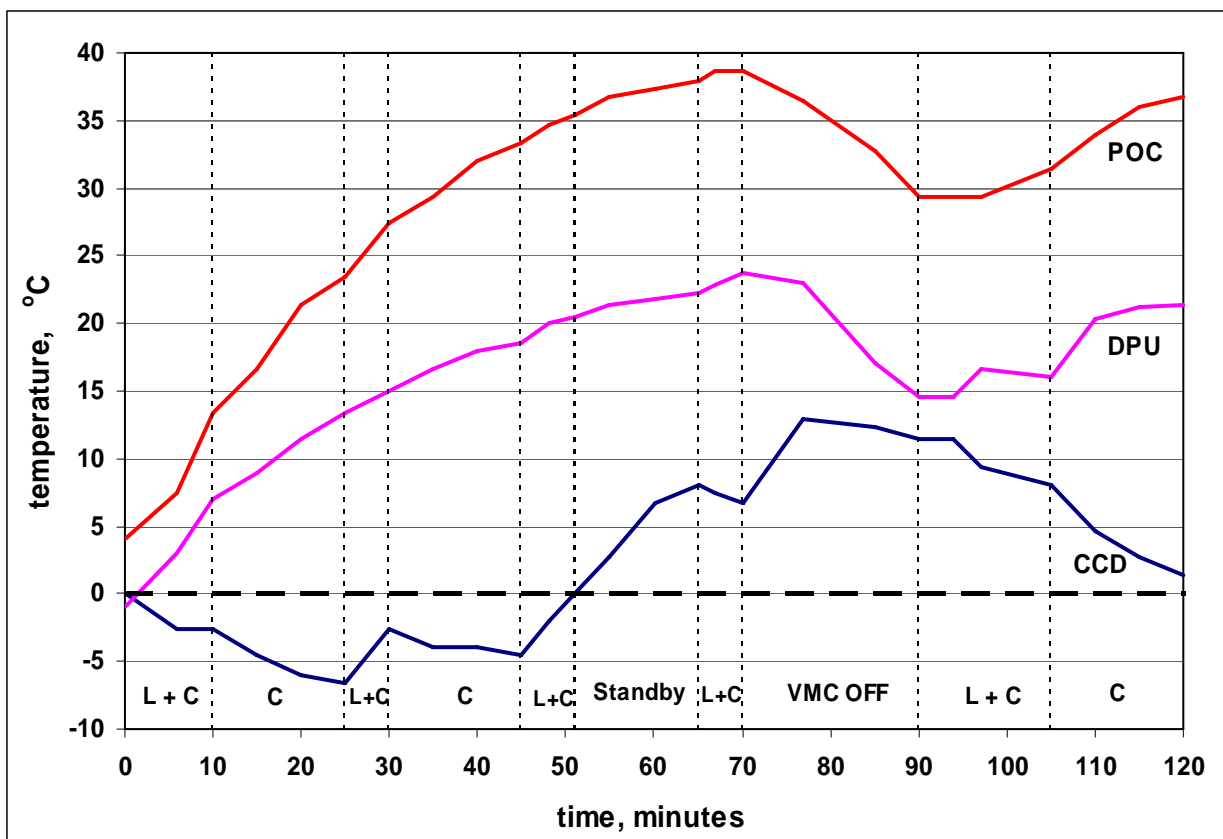


**Figure 7.23** Dependence of CCD, DPU and POC temperatures on the VMC operation time at the environment temperature 0° C (“L + C” – Limb and Cooling modes simultaneously).

Run 8. ( $T_{BP} = +20C$ )

This run also simulates the off-pericenter (VEX case#2 and #3) timeline for the base plate temperature of 20C. During the first 110 minutes ~10 min periods of continuous image acquisition (“L+C”) were interchanged with ~15 min of Cooling without imaging. This resulted in keeping the CCD temperature within 5C from that of base plate. Transition to the “standby” mode (i.e. cooling off) at  $t \sim 110$  min resulted in quick raise of CCD temperature due to conductive heat exchange with hot electronics. At  $t \sim 137$  min the VMC was OFF that resulted in decrease of POC and DPU temperatures. However at the same time the CCD temperature was going up.

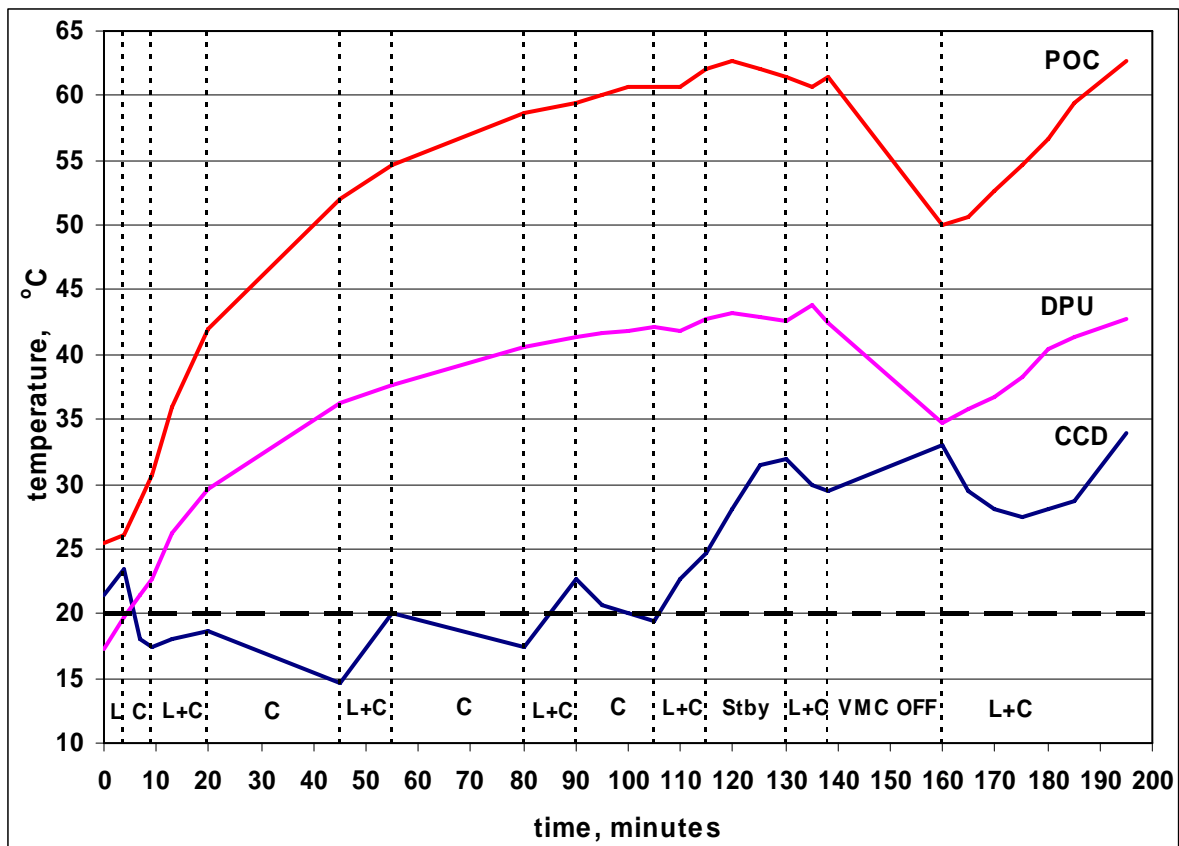


**Figure 7.24** Dependence of CCD, DPU and POC temperatures on the VMC operation time at the environment temperature  $+20^{\circ}C$  (“L + C” – Limb and Cooling modes simultaneously).

### 7.6.2 Expected in-flight performance

Simulation of in-flight operations during the VMC FS TV tests together with numerical modeling of the spacecraft thermal behaviour in typical orbital cases carried out by Astrium (CDR

study) allows one to predict CCD temperatures expected in flight. Figure 7.6-9 shows the dark signal as function of CCD temperature and exposure time (colored curves) as measured during VMC FS calibration. Red horizontal bars show ranges of CCD temperatures expected in flight for typical VEX observations (science cases) as follows from the Astrium thermal modeling and VMC FS performance during the TV tests. Important conclusion is that for all planned observations the CCD temperature falls in the optimal domain in which dark signal and dark noise are close to their minimal values and have weak dependence on CCD temperature and exposure time.

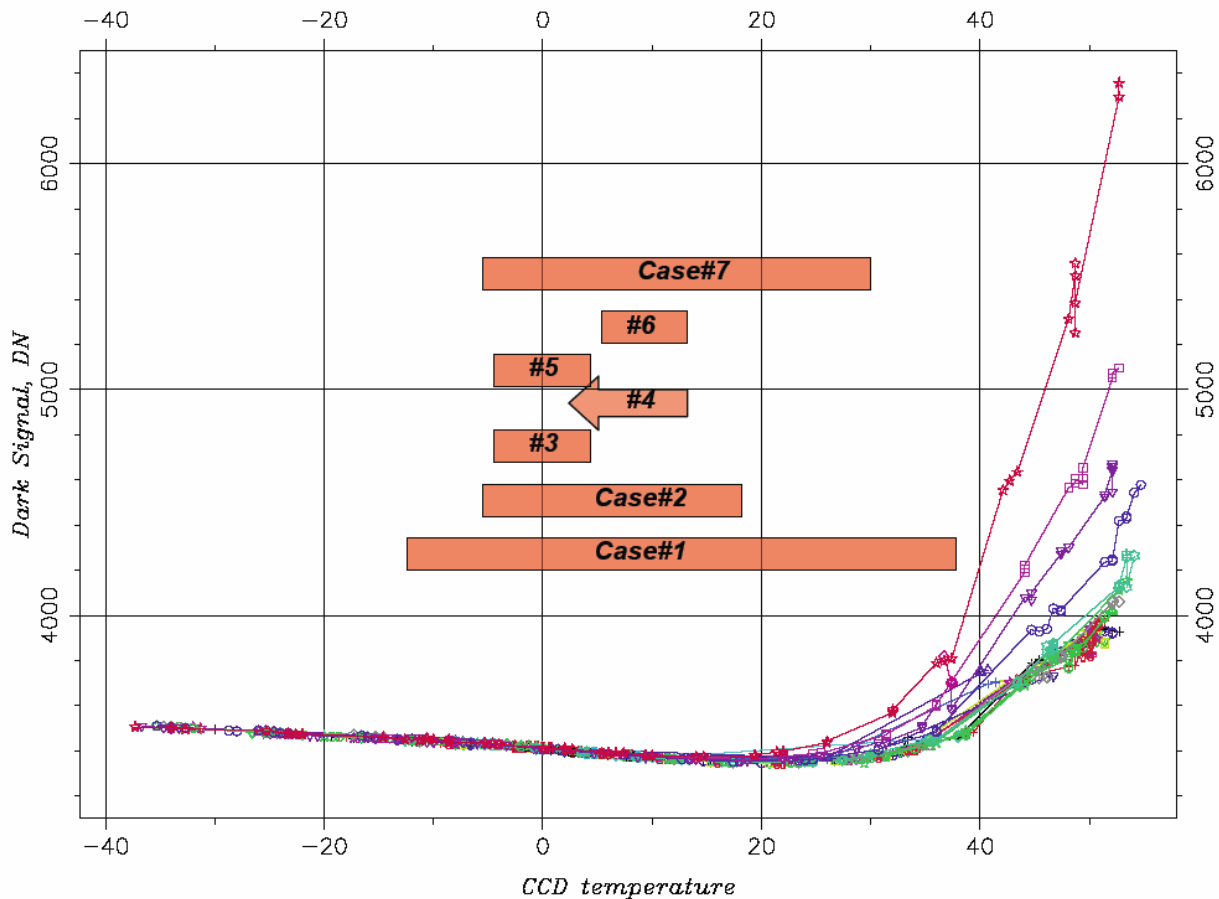


**Figure 7.25** Dependence of the VMC dark signal on the CCD temperature at different exposures (colored curves). Red horizontal bars show temperature ranges expected in flight in different science cases as follows from the Astrium thermal analysis (CDR study).

### 7.6.3 Conclusions and recommendation for in-flight operations

Analysis of the results of simulation of the VMC thermal behaviour performed as part of the VMC thermo-vacuum tests led to the following conclusions and recommendations for in-flight operations.

1. In cooling mode the Peltier element can provide about 10-12C cooling of the CCD.
2. Continuous image acquisition in Limb+Cooling mode result in that the CCD temperature increases with mean rate of 0.3-0.5 C/ min. Switch off the Peltier element results in 3 times higher rate (~1.5 C/min).
3. Thermal equilibrium conditions in Limb+Cooling mode are characterized by temperature difference wrt to base plate of: +30...40C for DPU and +40...50C for POC.
4. The Peltier element can keep the CCD temperature
  - within 10-15 C from that of base plate in continuous image acquisition mode. These are expected conditions in the Pericenter and Limb modes.
  - within 5 C from that of base plate in interrupted image acquisition mode (i.e. when each 10 min of imaging are followed by ~20 min of cooling). This is the recommender regime for Monitoring mode.
5. In the Pericenter and Limb modes it is recommended to simultaneously switch on cooling and image acquisition in order to prevent heating of electronics (DPU, POC) during preparatory phase.
6. According to the Astrium CDR study expected in-flight thermal conditions would result in CCD temperature between -15 and +35C. This is the CCD temperature domain in which VMC performance is optimal, i.e. dark signal and dark noise are close to their minimal values and have weak dependence on CCD temperature and exposure time.

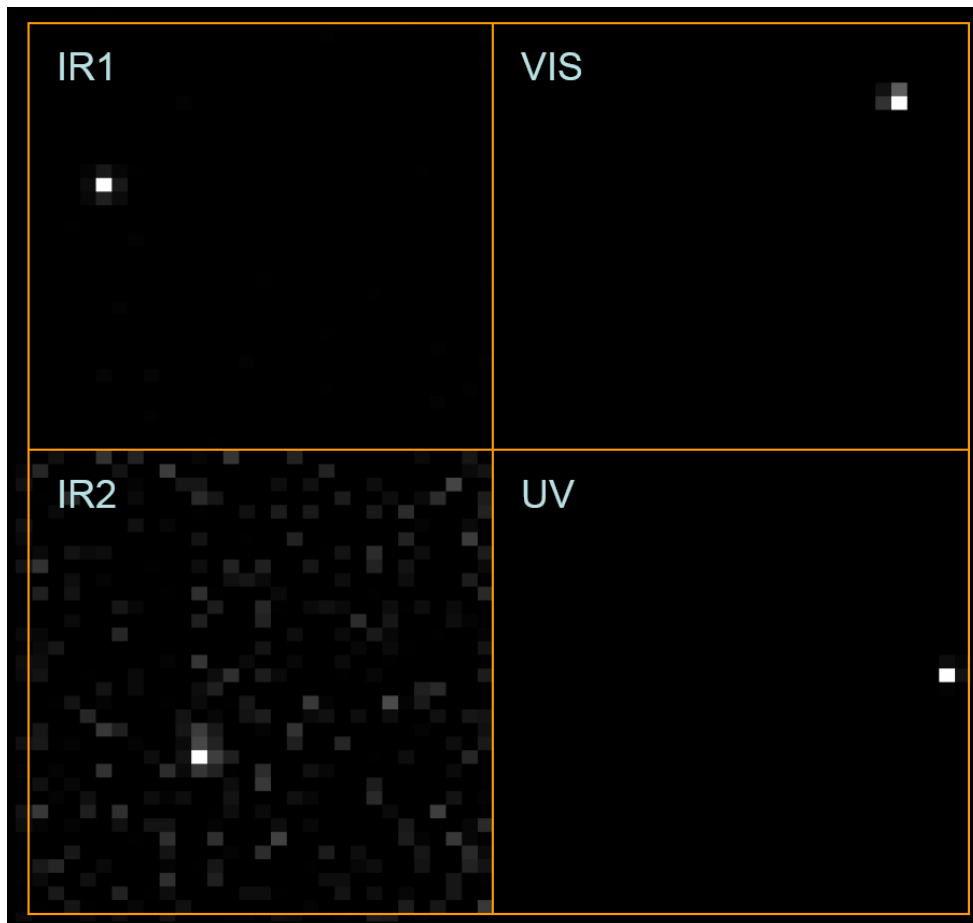
## 8 Annex 1. Calibration activity Log-book

## 9 VMC performance during the near-Earth commissioning

The near-Earth commissioning of the Venus Express instruments was performed in the first month of cruise in November-December 2005. The VMC commissioning included functional check, observations of point sources (Venus, stars) and extended sources (Earth and Moon), and stray light measurements. These observations allowed us to check the VMC performance in space.

### 9.1 In-flight focus check and channels misalignment

Observations of point sources (Venus, stars) gave a chance to check the VMC focus and point spread function in space.



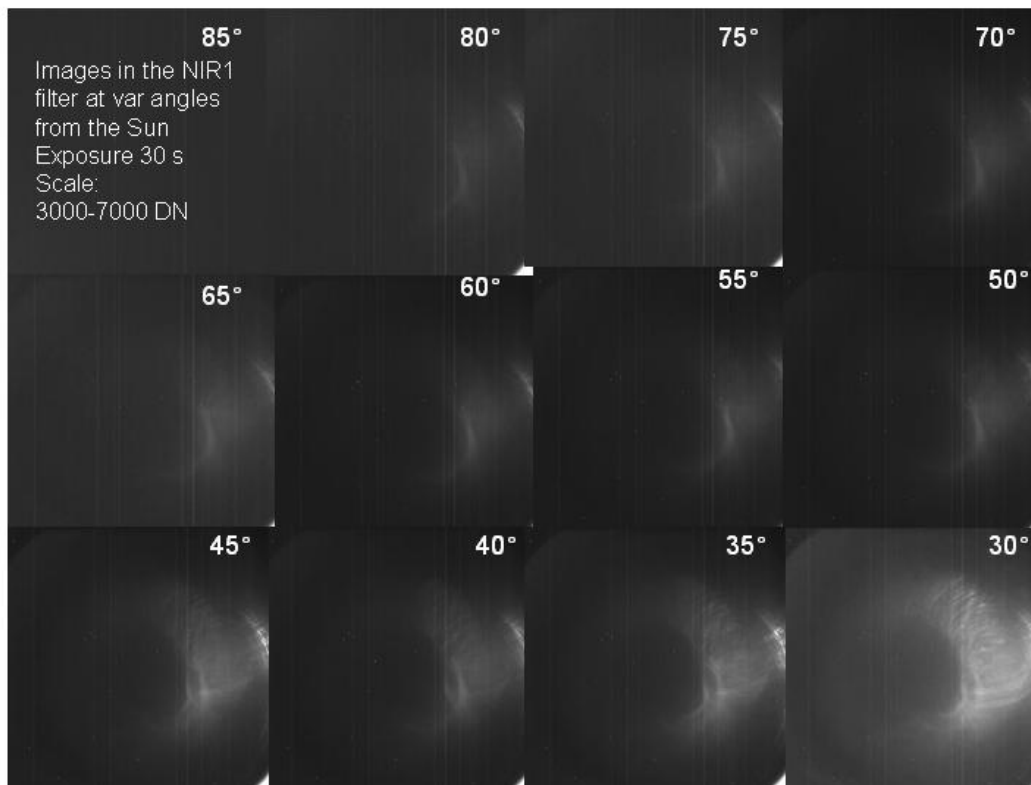
**Figure 9-1** Images of Venus taken by VMC during the near-Earth commissioning campaign

Figure 9-1 shows the images of Venus in four VMC channels taken during the near-Earth verification. These images allow one to make two conclusions. The first one is that the point spread function is about one pixel wide like it was during the on ground tests. Hence the instrument experienced no focus degradation during the launch and in space (see section 7.2.2).

The second conclusion is about the relative misalignment of VMC channels. In Figure 9.1 the Venus image is expected to be in the centre of the frame according to the data on spacecraft pointing. All four VMC images are shifted from this position by  $\sim 1.2$  degrees.

## 9.2 In-flight stray light characterization

A specific test to characterize the stray light originated from the Sun out of FOV was performed during the near-Earth commissioning. The spacecraft pointed its +Z axis (co-aligned with the VMC optical axis) at various angles (90-10 degrees) from the Sun. Figure 9-2 shows a set of images in the NIR1 channel taken at different angles from the Sun at maximum exposure of 30s. These tests showed that the contribution from the solar stray light becomes significant at long exposures and angles between the VMC optical axis and the Sun less than 70 degrees. Thus the stray light will mainly affect the observations of the night side. The images taken in space during the stray light measurement campaigns will be used to subtract the stray light pattern from the VMC images.



**Figure 9-2** Sequence of VMC NIR1 images taken during the near-Earth verification campaign at different angles (85-30 degrees) from the Sun. Exposure time is 30s.

## 10 Image calibration procedure

The calibration procedure of individual VMC images includes correction for hot pixels, black current and flat fielding. Since the VMC detector was damaged by direct solar illumination during cruise phase (see Technical Note VMC-MPAE-TN-SS010\_001\_Anomalous features in VMC images\_iss3\_1.doc), additional flat fielding procedure, that uses images taken in flight was introduced. The main steps of the calibration pipeline are described below.

Step 1. Correction of "hot" pixels (e.g. Cosmic ray events)

A pixel is declared as "hot" if its value is by at least 640DN higher than that of the surrounding pixels. The value of "hot" pixels is replaced by the mean of the surrounding pixels. Since "hot" pixels have a "dark tail" (i.e. the values of the next five pixels in the same line are too low) these values are replaced by the mean of the corresponding pixels of the upper and lower lines.

## Step 2. Dark current correction

- A dark current image is calculated from the laboratory calibration images taking into account current CCD temperature and Exposure time.
- Difference between the mean value of the "masked" part of the CCD in the current image and mean value of the dark image is added to the dark image (correction of the mean dark level). For the images with exposure time > 5000 msec the same adjustment of the dark image is performed for each CCD column separately.
- The resultant dark image is subtracted.

## Step 3. Standard flat field correction

- A flat field is calculated from the laboratory images taking into account current values of CCD temperature and Exposure time.
- A "radiance scaling factor" is determined to get an output image of type integer. The scaling factor is stored in the header. Note that despite the "scaling factor" has dimension of radiance, it can be used as radiance value with caution. Absolute radiometric calibration of VMC still needs verification.
- The current image is divided by the flat field image.

## Step 4. Stray light correction (not used in routine processing)

- Select an appropriate (from geometry and illumination conditions point of view) stray light image. It is taken either from the pre-flight calibration or from in-flight observations.
- The selected stray light image is subtracted from the current image.

## Step 5. Additional Flat-field correction (Version 01 only)

This step performs additional flat fielding and corrects the VMC images for the damages of the detector due to direct solar illumination during the cruise phase.

- Several images of the Northern polar regions are captured in every orbit if possible. Due to close distance (proximity to pericentre) and high uniformity of Venus clouds at high latitudes these image can be used for additional flat fielding.
- The images of clouds without terminator, limb, or saturated values are selected manually for this purpose. If it was not possible to take images in a particular orbit, appropriate images for the next or previous orbits are used.
- Flat field image is calculated using manually selected images from the current orbit (or interpolated from the adjacent orbits) (see Fig. 10-1) by the following:

- For each pixel calculate the mean value between selected images ignoring very low (<10 DN) and very high (>7500 DN) values. DN values of each pixel are converted in radiance using scaling factor. This gives a “mean flat field”.
- The “mean flat field” image is normalized by its MEDIAN. *Median*, not *mean* is used in order to reduce the influence of “hot” or anomalous pixels.
- Current image is divided by the normalized flat field image.
- Fill manually identified bad pixels (might be defective or non-linear pixels) with interpolated values of the neighbouring pixels.

### Step 6. Flag special pixels

Special pixels are:

- Masked pixels, Value= -1
- Defective pixels, Value= -4
- Non-linear pixels, Value= -16
- Saturated pixels, Value=MAX(valid\_pixels)+1

Some of these pixels might be filled before in step 5 and will not be flagged here.

The above described procedure is routinely applied to the images in all four channels.

Figure 10-2 shows examples of the VMC UV images before and after calibration and flat field correction.

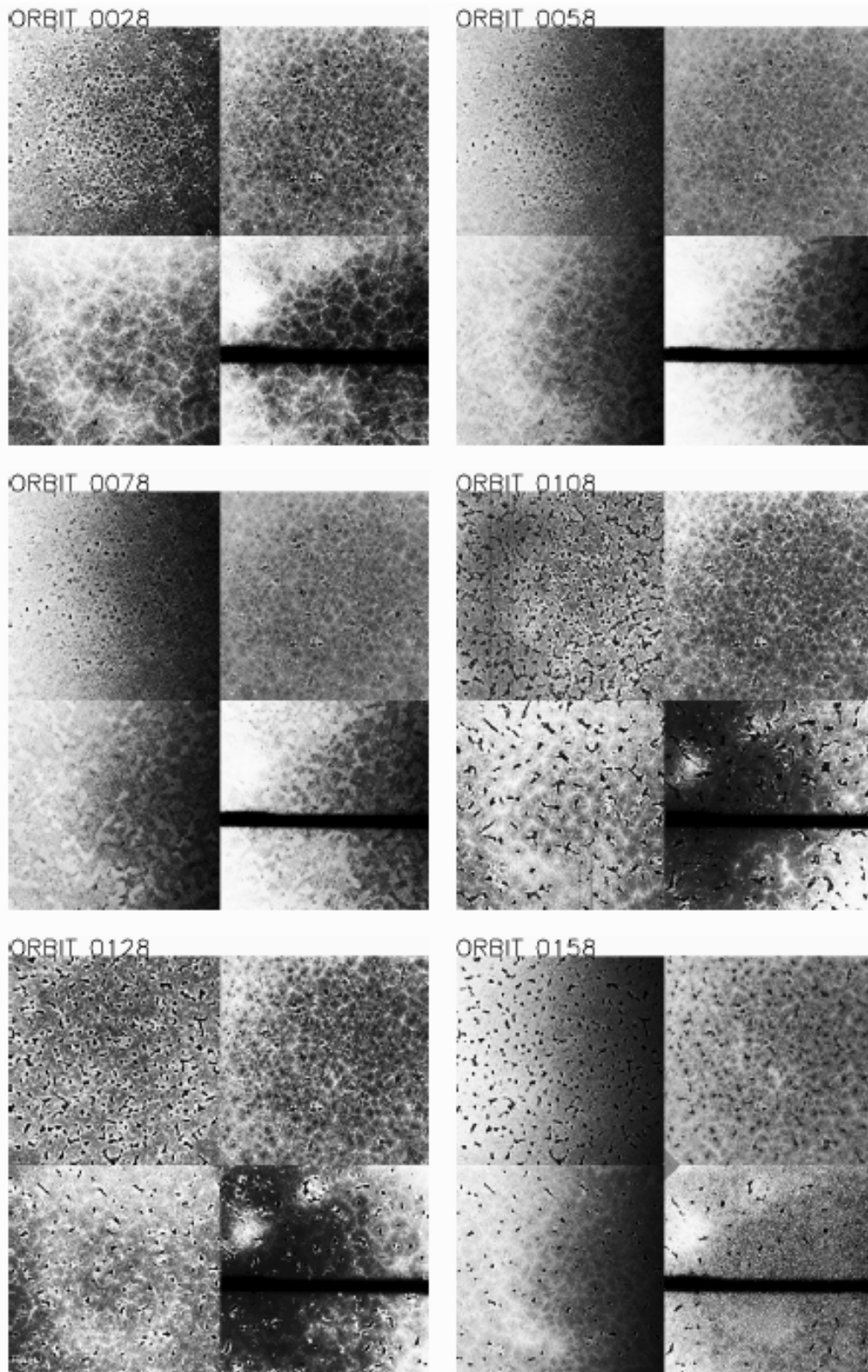


**Figure 10-1** *Examples of flat fields in four VMC channels derived in different orbits.*

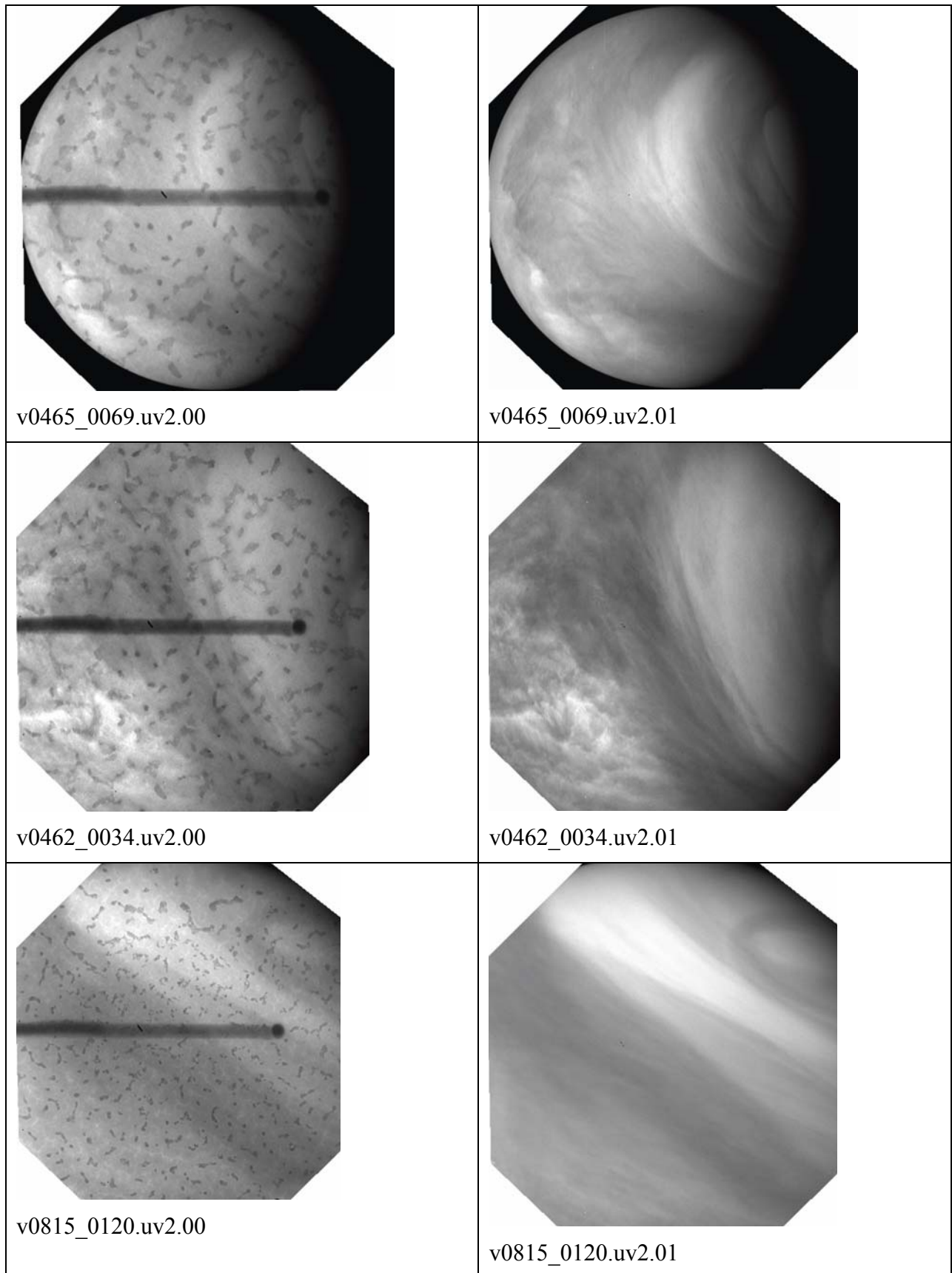


**Figure 10-2** Examples of raw(left) and flat fielded(right) VMC UV images.